No.623

Preferable Locational Area in a Single Facility Euclidean Minimax Location Problem

Y. OHSAWA, T. KOSHIZUKA

and A. IMAI

March 1995

Institute of Socio-Economic Planning, University of Tsukuba, Tsukuba 305, JAPAN,

phone: +81-298-53-5224, fax: +81-298-53-5070, e-mail: osawa@shako.sk.tsukuba.ac.jp.

1. Introduction

Since Weber's classic paper, a great deal of research has been done on single facility location models. The purpose of these models is to decide where to locate a facility in such a way that any social objective function is minimized. However, from a practical viewpoint, it is difficult to directly apply these models to urban facility planning. This is because decision-makers have to consider carefully many constraints such as land use regulations, traffic management and so on. In addition, they often have to incorporate subjective factors into the locational analysis.

In order to take the above considerations into account, the optimal location point, which is obtained by solving a single facility location model, has to be examined by employing a contour map. Contour lines (also called iso-cost lines) consist of a set of lines which give constant objective-function value on the plane. That is, locating a new facility at any point on a given contour line represents the same objective-function value. Consequently, the contour map expresses, at a glance, the cost penalty associated with the choice of a non-optimum location. That is, the contour map enables immediate comparison of alternative proposed sites. Therefore, a contour map assists decision-makers in choosing an appropriate location for the new facility.

Francis and White(1974) showed the procedure for constructing a contour map of the minisum model in which the travel cost is defined by the rectilinear distance and the squared Euclidean distance. However, it is known that exact methods for delineating contour maps are not available for the Euclidean distance minisum model except for the simplest cases where there are at most two facilities. Brady and Rosenthal(1980) and Love, Morris and Wesolowsky(1988) discussed briefly the contour map of the minimax model. But to our knowledge, there is no study to present the algorithm for constructing the

contour map of this model and to examine the characteristics of the contour lines.

The purpose of this paper is therefore two-folds: a) to show the procedure for constructing contour lines of the minimax model, b) to examine the properties of the degree of locational freedom. To draw contour lines, the Voronoi diagram, a classical mathematical object, is revived. The degree of locational freedom is defined as the area where the objective-function value is equal or less than constant value. The degree of locational freedom in a neighbourhood of the optimal point is important for decision-makers. This is because it represents the size of alternative sites which the decision-makers may select in place of the optimal point. The larger the size is, the easier for the decision-makers to make facility planning. Although the degree of locational freedom is data-dependent, we shall represent the lower and upper bounds on the degree of locational freedom. Also, we shall show that in general, the degree of locational freedom where the optimal point is determined by two demand points, is greater than the one where the optimal point is determined by two demand points.

This presentation is organized as follows. In section 2, a procedure for constructing contour lines of a single facility minimax model is described. The computational complexity of our method is $O(N \log N + KN)$, where N is the number of demand points, and K represents the number of contour lines. In section 3, first, the lower and upper bounds are developed. These bounds are represented by the diameter and the number of the demand points on the convex hull. Second, the approximation of the degree of locational freedom in a neighbourhood of the optimal point is shown. Section 4 is devoted to the applications of the degree of locational freedom to numerical examples using Japanese prefectural data. 47 problems are solved. In the final section, the paper concludes with several results obtained in this paper.

2. Contour lines and degree of locational freedom

2.1. Single facility minimax model

Suppose that a set of $N(< \infty)$ demand points $P_1 = (x_1, y_1), \cdots, P_N = (x_N, y_N)$ are distributed in the Euclidean plane. The transportation cost is given by an increasing and continuous function of the Euclidean distance. Then, the single facility minimax model is introduced to find the location of a facility so as to minimize the maximum transportation cost from demands points to the facility. Minimax formulation implies equity consideration since the poorest service is made to be as good as possible. Therefore, this kind of model is sometimes encountered in the determination of the location of emergency services such as hospitals, fire and police stations, as well as television and radio transmitters.

Mathematically, this model is to minimize the following objective function with respect to $P = (x, y)$:

$$F(P) = \max_{i \in I} C(\|P - P_i\|), \tag{2.1}$$

where $I = \{1, \cdots, N\}$, $C(\cdot)$ is the transportation cost function, and $\|\cdot\|$ is the Euclidean norm.

This model is also familiar in Computational Geometry as a enclosing circle problem: see Shamos and Hoey (1975). It is obvious that the optimal solution is the center of the minimum-radius disk containing points $P_1, \cdots, P_N$. We shall denote the boundary of the disk by $SEC\{P_1, \cdots, P_N\}$. So, the optimal location point, which is called a *center*, is unique. The optimal value of the objective function is called a *radius*. As a notational convenience, the center will be denoted by P^*, and the radius will be denoted by F^*. Moreover, this model has a strongly marked combinatorial feature. The center is the circumcircle of some three points of the set, or defined by two of them as a diameter. It should be noted that although the contour map depends on the transportation cost

$C(\cdot)$, the center is independent of $C(\cdot)$. Many solution methods to solve this model have been proposed. Elzinga and Hearn (1973) suggested a solution method, which is made up of simple geometric procedures, in $O(N^2)$ time. Shamos and Hoey (1975) exhibited an $O(N \log N)$ time resolution method by use of farthest-point Voronoi diagram.

2.2. Construction procedure of the contour map

For $i = 1, \cdots, N$, the *farthest-point Voronoi polygon*, denoted by V_i, for the demand point P_i is defined by

$$V_i = \bigcap_{j \in I-\{i\}} \{P \in R^2 \mid \|P - P_i\| \geq \|P - P_j\|\}. \tag{2.2}$$

That is, every point in farthest-point Voronoi polygon V_i is farther to P_i than to any other $P_j, (j \neq i)$. These N regions partition the plane into a convex net which we shall call the *farthest-point Voronoi diagram*. We call each edge of this diagram a *farthest-point Voronoi edge*. We call each vertex of this diagram a *farthest-point Voronoi vertex*. An extensive survey of Voronoi diagram can be found in Okabe, Boots and Sugihara (1992). The convex hull of $P_1, \cdots, P_N$ is defined as the smallest convex set containing $P_1, \cdots, P_N$. We shall denote its boundary by $CH\{P_1, \cdots, P_N\}$. As is evident from definition, $CH\{P_1, \cdots, P_N\}$ is located within $SEC\{P_1, \cdots, P_N\}$. We shall refer to $NSEC$ and NCH as the number of the demand points on $SEC\{P_1, \cdots, P_N\}$ and the number of the ones on $CH\{P_1, \cdots, P_N\}$, respectively. It should be noted that this diagram is determined only by demand points on $CH\{P_1, \cdots, P_N\}$: see Shamos and Hoey(1975). Examples of the farthest-point Voronoi diagram are shown in Figures 1 and 2. The data in Figure 1 is the location of 87 municipalities in the Ibaraki prefecture in Japan. The data in Figure 2 show the location of 59 municipalities in the Iwate prefecture in Japan. In each figure, the smallest enclosing circle is also delineated. Each figure also shows the demand points on the boundary of the convex hull as bullets. In Figure 1, the center, indicated by an asterisk, lies on a farthest-point

Voronoi vertex. In contrast to this, in Figure 2, the center lies on a farthest-point Voronoi edge.

By the definition of farthest-point Voronoi polygon denoted by (2.2), the farthest demand point for any points in V_i is the i-th demand point. For this reason, the value of the objective function at P in the polygon V_i is $C(\|P-P_i\|)$. Hence, a contour line in V_i is a circular arc emerging from P_i. Thus, a contour line in the plane consists of circular arcs. Figures 3 and 4 illustrate contour maps for the demand sets in Figures 1 and 2 in the case where $C(\|\cdot\|)=\|\cdot\|$. The contour lines shown correspond to the x-values ranging from $0.1F^*$ to F^* at $0.1F^*$ intervals. These figures are computer generated.

Let us now state the procedure to construct the contour map.

(a1) Delineate the farthest-point Voronoi diagram for N demand points.

(a2) Find the center P^* and calculate the radius F^*.

(a3) For constant value of a contour line x, find the intersection points between a circle with its center at P_i and with a radius $C^{-1}(x)$ and the farthest-point Voronoi edge in V_i for $i \in I$.

(a4) Draw these two intersection points by a circular arc.

Shamos and Hoey (1975) showed that the farthest-point diagram can be delineated in $O(N\log N)$ time by use of divide and conquer technique. They also showed that the center can be found in $O(N)$ time, provided that the farthest-point diagram is given. That is, the procedure from Step 1 to Step 2 can be done in $O(N\log N)$ time. As the number of farthest-point Voronoi edge is $O(N)$, Step 3 can be done in $O(N)$ time. Accordingly, for the number of contour lines K, the procedure to construct the contour map can be carried out in total time $O(N\log N+KN)$.

2.3. Calculation procedure of degree of locational freedom

Mathematically the degree of locational freedom, denoted by $S(x)$, can be expressed as follows:

$$S(x) = \mid \{P \in R^2 \mid F(P) \leq x\} \mid, \qquad \forall x > F^*.$$

Provided that the contour map and the farthest-point Voronoi diagram are given, the procedure to compute $S(x)$ is as follows:

(b1) For constant value x, calculate $S(x)$ within V_i by subtracting the area of the polygon determined by P_i and farthest-point Voronoi edges from the area of the sector determined by the circular arc emerging from P_i with a radius $C^{-1}(x)$. This is illustrated in Figure 5.

(b2) Sum up $S(x)$ in each farthest-point Voronoi polygon.

3. Theoretical results

3.1. Bounds on the degree of locational freedom

We shall call the demand set 2-*regular* if all demand points are located at two distinct points and at least one demand point is located at these two points. For $3 \leq m \leq N$, we shall call the demand set *m-regular* if all demand points are located at these vertices of an m-regular polygon and at least one demand point is located at each vertex of the polygon. Therefore, the smallest enclosing circle for an m-regular set is circumscribed around the polygon. It should be noted that the demand points located at an identical point can be considered as one demand point without changing the shape of the contour map. In Figures 6, 7 and 8, the contour maps are depicted for 2-regular, 4-regular and 8-regular sets, respectively. As each farthest-point Voronoi polygon is a convex cone with its vertex at the center, contour lines are circular arcs over each cone. Contour lines for the m-regular set will always converge to become circles as $m \rightarrow \infty$. As m decreases the contour lines become more elongated: see Figures 6, 7 and 8.

Property 1. *When $P_1, \cdots, P_N$ is $m(\geq 2)$-regular, for $\forall x (> F^*)$*

$$S_m(x) = m\{\frac{\pi}{m} - \arcsin(\frac{R^*}{r}\sin(\frac{\pi}{m}))\}r^2 - mR^*\sin\{\frac{\pi}{m} - \arcsin(\frac{R^*}{r}\sin(\frac{\pi}{m}))\}r. \quad (3.1)$$

where $S_m(x)$ is the degree of locational freedom for the m-regular set, $r = C^{-1}(x)$ and $R^* = C^{-1}(F^*)$.

Proof. See Appendix A.1. □

The following characteristics of $S_m(x)$ can be easily seen:

(c1) As special cases, we have

$$S_2(x) = \pi r^2 - 2r^2\arcsin(\frac{R^*}{r}) - 2R^*r\cos(\arcsin(\frac{R^*}{r})); \quad (3.2)$$

$$S_3(x) = \pi r^2 - 3r^2\arcsin(\frac{\sqrt{3}R^*}{2r}) - 3R^*r\sin(\frac{\pi}{3} - \arcsin(\frac{\sqrt{3}R^*}{2r})); \quad (3.3)$$

$$S_4(x) = \pi r^2 - 4r^2\arcsin(\frac{\sqrt{2}R^*}{2r}) - 4R^*r\sin(\frac{\pi}{4} - \arcsin(\frac{\sqrt{2}R^*}{2r})); \quad (3.4)$$

$$S_\infty(x) = \pi(r - R^*)^2.$$

(c2) $S_m(x)$ is a decreasing function of m.

Applications of Property 1 will be shown in the following properties.

To compute $S(x)$ exactly is complicated. This is because, we must delineate the contour map. However, we can evaluate $S(x)$ roughly without using a computer by using the following property:

Property 2. *Lower and upper bounds on $S(x)$ are given as follows:*

$$S_{NCH}(x) \leq S(x) \leq S_2(x), \qquad \forall x (> F^*). \quad (3.5)$$

Proof. See Appendix A.2. □

From a practical viewpoint, to compute these bounds of Property 2 is easy. This is because the upper bound is given by (3.2), and to compute the lower bound it is only

necessary to identify NCH and to compute (3.1). The decision-makers do not often have access to the location of the demand set from which the model (2.1) was obtained. In this case, although we cannot identify NCH, we have the following property:

Property 3. *Lower and upper bounds on $S(x)$ are given as follows:*

$$S_\infty(x) < S(x) \leq S_2(x), \qquad \forall x (> F^*). \tag{3.6}$$

Proof. We obtain the inequality (3.6) directly from the characteristic of (c2) and Property 2. □

The most useful characteristic of Property 3 is that only if we know F^*, we can evaluate $S(x)$. The behaviour of the objective function in a neighbourhood of P^* depends on $NSEC$. However, when we use the actual demand points, they are in general positions, so that no degeneracy occurs. That is, P^* is defined by only either two or three demand points and the set is not 3-regular. In this case, we have the following property:

Property 4. *When no degeneracy occurs and $x - F^*$ is significantly small, we have*

$$S_3(x) < S(x) \leq S_2(x), \qquad \forall x (> F^*). \tag{3.7}$$

Proof. We can consider only the case where $N = 2$ and the case where $N = 3$. Hence, we obtain the inequality (3.7) directly from Property 2. □

As $S(x)$ represents the size of alternative sites when $x - F^*$ is small, it is important for decision-makers to evaluate this size. Property 4 is useful to evaluate roughly the size.

3.2. Approximation to the degree of locational freedom

In the case where P^* is determined by three demand points and their set is not 3-regular, how much does $S(x)$ become? To answer this question, we approximate $S(x)$ by the use of the Taylor-series expansion, provided that $x - F^*$ is significantly small. The

Taylor-series expansion of $S(x)$ about F^* allows us to construct a simple approximation to $S(x)$ in a neighbourhood of F^*. As $S(F^*) = 0$, ignoring all but the linear and quadratic terms of the Taylor series gives:

$$\begin{aligned} S(F^* + \Delta) &\approx S(F^*) + S'(F^*)\Delta + \frac{S''(F^*)}{2}\Delta^2 \\ &= S'(F^*)\Delta + \frac{S''(F^*)}{2}\Delta^2. \end{aligned} \tag{3.8}$$

Let ψ_1, ψ_2 and ψ_3 be these vertices of the angles of the triangle which is determined by connecting these three demand points, as shown in Figure 9. In this case, we have

$$S'(F^*) = 0; \tag{3.9}$$

$$S''(R^*) = \frac{2R^*}{C'(F^*)} \sum_{i=1}^{3} \cot \frac{\psi_i}{2}. \tag{3.10}$$

The derivation is given in Appendix A.3. Substituting (3.9) and (3.10) into (3.8) gives

$$S(F^* + \Delta) \approx \frac{S''(F^*)}{2}\Delta^2 = \frac{R^*}{C'(F^*)}(\sum_{i=1}^{3} \cot \frac{\psi_i}{2})\Delta^2.$$

Dividing both sides by Δ^2 yields

$$\frac{S(F^* + \Delta)}{\Delta^2} \approx \frac{R^*}{C'(F^*)} \sum_{i=1}^{3} \cot \frac{\psi_i}{2}. \tag{3.11}$$

It should be noted that the right-hand side of (3.11) attains its minimum when $\psi_1 = \psi_2 = \psi_3 = \frac{\pi}{3}$. In this case, we have

$$\frac{S(F^* + \Delta)}{\Delta^2} \approx \frac{R^*}{C'(F^*)} 3\sqrt{3}. \tag{3.12}$$

For comparative purposes, we evaluate $S(F^* + \Delta)$ in the case where P^* is determined by two demand points. Differentiating (3.2) gives

$$S'(x) = \frac{1}{C'(x)}\{2\pi r - 4r \arcsin(\frac{R^*}{r}) - 2R^* \cos(\arcsin(\frac{R^*}{r})) + \frac{2R^*\sqrt{r^2 - R^{*2}}}{r}\};$$

$$S''(x) = \frac{1}{C'(x)}\{2\pi - 4 \arcsin(\frac{R^*}{r}) + \frac{4R^*}{\sqrt{r^2 - R^{*2}}}\} - \frac{S'(x)}{C'(x)}.$$

By noting that $0 < C'(F^*) < \infty$, we have

$$S'(F^*) = 0;$$

$$S''(F^*) = \infty.$$

Substituting these into (3.8) yields

$$\frac{S(F^* + \Delta)}{\Delta^2} \approx \infty. \tag{3.13}$$

We shall make a comparison (3.11) with (3.13). In (3.11), we see that the smaller ψ_i, the larger $\frac{S(F^*+\Delta)}{\Delta^2}$. In particular, when $\psi_i = 0$, $\frac{S(F^*+\Delta)}{\Delta^2}$ goes up to infinity. This is identical with the 2-regular case. However, the value of (3.11) is finite, provided that $\psi_i > 0$. Moreover, the function of the cotangent takes an enormous value only for ψ_i sufficiently near 0. Therefore, it can be concluded that $S(x)$ for $NSEC = 2$ is considerably greater than the one for $NSEC = 3$ when $x - F^*$ is significantly small.

4. Empirical results

From properties 2, 3 and 4 obtained in the previous section, we see that the lower and upper bounds on $S(x)$ can be theoretically expressed. First we shall confirm how these bounds are effective using 47 locational data sets from the 47 prefectures in Japan.

In addition, the analyses using Taylor expansion state that $S(x)$ for $NSEC = 2$ is greater than the one for $NSEC = 3$ when $x - F^*$ is significantly small. Second we shall examine whether this property holds or not when the x-value moves farther from F^* using the 47 locational data sets.

Japan consists of 47 prefectures, and each prefecture comprises a number of localities (i.e. municipalities and cities). The 47 prefectures were selected for this study mainly because the location of the principal facilities such as hospitals, police stations and television

stations are determined at the prefectural level. Furthermore, prefectures represent the basic administrative, economic and cultural units of the country. The data only includes these localities situated on areas in the mainland and those connected by bridges to the mainland. We obtained the position of these localities from the Ministry of Construction, Japan (1992). The data illustrated in Figures 1 and 2 were examples of these data sets. The following calculations and geometrical constructions are performed by a personal computer. In addition we consider the situation where $C(\|\cdot\|) = \|\cdot\|$.

The first column of Table 1 gives the names of the 47 prefectures. The second and third columns of this table give the dimensions of each prefecture such as the number of localities(N), the diameter(D), which is defined by the distance between the two municipality points which are farthest apart. In addition, the forth, fifth and sixth columns of this table give the radius(F^*), the number of locality points determining the center($NSEC$), and the number of locality points on the convex hull(NCH). Of course, these results were obtained by solving the model (2.1).

To facilitate comparison with the lower and upper bounds obtained in Section 3, we shall define the normalized degree of locational freedom as $\sigma(x) \stackrel{\text{def}}{=} \frac{S(x/F^*)}{\pi F^{*2}}$ and $\sigma_m(x) \stackrel{\text{def}}{=} \frac{S_m(x/F^*)}{\pi F^{*2}}$. Evidently, the normalized value becomes unity when $S(x)$ is identical with the area of the smallest enclosing circle. The 47 plots of $\sigma(x)$'s against x for the x-values ranging from F^* to $1.1F^*$ at $0.01F^*$ intervals are shown in Figure 10. The contour map of all prefectures can be found in Ohsawa, Koshizuka and Imai(1995). In order to compare $\sigma(x)$'s for $NSEC = 2$ and $\sigma(x)$'s for $NSEC = 3$, $\sigma(x)$'s for $NSEC = 2$ and $\sigma(x)$'s for $NSEC = 3$ are given in Figure 10(a) and (b), respectively. The prefectures in Table 1 are arranged first on $NSEC$ and secondly on $\sigma(1.1F^*)$. According to the third column of Table 1, 21 prefectures in 47 becomes $NSEC = 2$, that is, the percentage for $NSEC = 2$ is

about 45. In order to examine $\sigma(x)$ when x is large, the 47 plots of $\sigma(x)$'s for the x-values ranging from F^* to $2F^*$ at $0.1F^*$ intervals are also given in Figure 11. Similarly as for Figure 10, $\sigma(x)$'s for $NSEC = 2$ and $\sigma(x)$'s for $NSEC = 3$ are given in Figure 11(a) and (b), respectively. In these four figures, the highest, second highest and lowest dotted lines represent $\sigma_2(x)$, $\sigma_3(x)$ and $\sigma_\infty(x)$, respectively. The second lowest lines in Figure 11 represent $\sigma_4(x)$. In these four figures, the medians, which is a convinient measure of central location of the distribution, are also connected by lines. The median is defined to be the middle order statistic if the number of the data is odd, and the average of the middle two order statistics if the number of the data is even. Therefore, in our data, the 11-th largest value is used as the median for $NSEC = 2$, and the average of the 13-th and 14-th largest values are used as the median for $NSEC = 3$. On the other hand, in order to evaluate $S(x)$ in the case where $x - F^*$ is significantly small, we define

$$\rho \stackrel{\text{def}}{=} \begin{cases} \frac{1}{3\sqrt{3}} \sum_{i=1}^{3} \cot \frac{\psi_i}{2}, & \text{if } NSEC = 3; \\ \infty, & \text{if } NSEC = 2. \end{cases}$$

From (3.11), (3.12) and (3.13), it follows that ρ expresses how $S(x)$ times $S_3(x)$ when $x - F^*$ is significantly small. The criterion ρ is also given in the last column of Table 1.

Generally speaking, Figure 10(a) and 11(a) indicate that for $NSEC = 2$ although the difference between $\sigma(x)$ and $\sigma_2(x)$ is small when x is small, as x increases, the smaller the rate of growth of $\sigma(x)$ as compared with the one of $\sigma_2(x)$. We also see from Figure 10(b) and 11(b) that for $NSEC = 3$ although $\sigma(x)$ is greater than $\sigma_2(x)$ when x is small, as x increases, the smaller the rate of growth of $\sigma(x)$ as compared with the one of $\sigma_3(x)$. This is because as x increases, so does the number of the demand points which affects the shape of the contour map.

There are two important observations that can be made upon careful consideration of Figures 10 and 11, and Table 1. First, although the spatial configuration of demand points

significantly influences $S(x)$, an observation of these figures tells us that these bounds presented in Section 3.1 make a reasonable approximation. In addition, inspection of Figure 10 leads to the conclusion that when x is below $1.1F^*$, $\sigma(x)$'s of all prefectures, except that of the Saga prefecture, exceeds $\sigma_3(x)$. The contour map for the Saga prefecture is shown in Figure 12. Moreover, it is interesting from Figure 11 to note that although when x is below $2F^*$, $\sigma(x)$'s of all prefectures are greater than $\sigma_4(x)$. Thus, the empirical results state that when x is small, $S_3(x)$ can be used as the lower bound on $S(x)$, and when x is large, $S_4(x)$ can be used as the lower bound on $S(x)$.

Secondly, comparison of Figure 10(a) with (b) and Figure 11(a) with (b) clearly indicates that $\sigma(x)$'s for $NSEC = 2$ are distributed close to $\sigma_2(x)$, and $\sigma(x)$'s for $NSEC = 3$ are distributed close to $\sigma_3(x)$. This result becomes clearer when x is below $1.1F^*$. In addition, comparing the medians, we see that the median for $NSEC = 2$ is considerably greater than the one for $NSEC = 3$. Also, the results in the last column of Table 1 tells us that ρ's take at most 5.21 and ρ's of 22 prefectures out of 26 prefectures are below 2.0. The contour map for the Mie prefecture, where a maximum of ρ is attained, is shown in Figure 13. This means that when $x - F^*$ is significantly small $\sigma(x)$ for $NSEC = 3$ are considerably smaller than $\sigma(x)$ for $NSEC = 2$ although their sets are not 3-regular. We can conclude that $\sigma(x)$'s for $NSEC = 2$ are frequently greater than $\sigma(x)$'s for $NSEC = 3$.

5. Conclusions

Contour lines provide a useful means of evaluating alternative locations for the new facility. In this article, the size of the alternative sites in a single facility minimax model were examined. On the basis of what we have examined, we are in a position to state our main contributions.

The first main asset of this study is that three types of the lower and upper bounds on the degree of locational freedom are theoretically presented. The first type can be calculated by the diameter and the number of the demand points on the boundary of the convex hull. The second type can be calculated only by the diameter. The third type is useful to evaluate the degree of locational freedom in a neighbourhood of the center. The application to Japanese prefectural data revealed that these bounds make a reasonably good approximation. In particular, we see empirically that with few exceptions the degree of locational freedom for a 3-regular set can be used as the lower bound when x is small, and that the one for a 4-regular set can be used as the lower bound when x is large.

The second main contribution of this work is that in general the normalized degree of locational freedoms in the case where the center is determined by two demand points is greater that the ones in the case where the center is determined by three demand points. This conclusion is more apparent when r nears to F^*.

A. Mathematical Appendix

A.1. Proof of Property 1.

Let $\theta_i(r)$ denote the angle which defines $S_m(x)$ within V_i, as shown in Figure A1, where V_i is shown hatched. Taking advantage of symmetry of V_i with respect to $\overline{P^*P_i}$ gives

$$S_m(x) = \sum_{i=1}^{m} \frac{r^2}{2}\theta_i(r) - R^* r \sin(\frac{\theta_i(r)}{2}) \tag{A.1}$$

Let λ_i be the angle of the vertex of V_i. Making use of the sine formula yields

$$\begin{aligned}
&\frac{r}{\sin(\pi - \frac{\lambda_i}{2})} = \frac{R^*}{\sin(\pi - \frac{\theta_i(r)}{2} - (\pi - \frac{\lambda_i}{2}))} \\
\Leftrightarrow &\frac{r}{\sin(\frac{\lambda_i}{2})} = \frac{R^*}{\sin(\frac{\lambda_i}{2} - \frac{\theta_i(r)}{2})} \\
\Leftrightarrow &\sin(\frac{\lambda_i}{2} - \frac{\theta_i(r)}{2}) = \frac{R^*}{r}\sin(\frac{\lambda_i}{2}) \\
\Leftrightarrow &\theta_i(r) = \lambda_i - 2\arcsin(\frac{R^*}{r}\sin(\frac{\lambda_i}{2})).
\end{aligned} \tag{A.2}$$

The insertion of $\lambda_i = \frac{2\pi}{m}$ in (A.2) yields

$$\theta_i(r) = \frac{2\pi}{m} - 2\arcsin(\frac{R^*}{r}\sin(\frac{\pi}{m})).$$

The substitution of this into (A.1) yields

$$\begin{aligned}
S_m(x) &= \pi r^2 - mr^2 \arcsin(\frac{R^*}{r}\sin(\frac{\pi}{m})) - mR^* r \sin\{\frac{\pi}{m} - \arcsin\{\frac{R^*}{r}\sin(\frac{\pi}{m}))\} \\
&= m\{\frac{\pi}{m} - \arcsin(\frac{R^*}{r}\sin(\frac{\pi}{m}))\}r^2 - mR^* \sin\{\frac{\pi}{m} - \arcsin(\frac{R^*}{r}\sin(\frac{\pi}{m}))\}r. \square
\end{aligned}$$

A.2. Proof of Property 2.

A few notations that are used in the proof need to be defined. For $i = 1, \cdots, N$, define

$$P_i^I \stackrel{\text{def}}{=} \begin{cases} P_i, & \text{if } P_i \text{ is on } SEC\{P_1, \cdots, P_N\}; \\ P^*, & \text{otherwise;} \end{cases}$$

$$P_i^O \stackrel{\text{def}}{=} \begin{cases} \frac{R^*}{\|P_i - P^*\|}P_i, & \text{if } P_i \text{ is on } CH\{P_1, \cdots, P_N\}; \\ P^*, & \text{otherwise.} \end{cases}$$

as shown in Figure A2. The definition of P_i^O states that for P_i on $CH\{P_1, \cdots, P_N\}$, P_i^O is the intersection of the extension of $\overline{OP_i}$ and $SEC\{P_1, \cdots, P_N\}$. The definitions indicate that $NSEC$ demand points of $P_1^I, \cdots, P_N^I$ align on a common circle, and NCH demand points of $P_1^O, \cdots, P_N^O$ align on a common circle. It should be noted that both the center of $P_1^I, \cdots, P_N^I$ and that of $P_1^O, \cdots, P_N^O$ are identical with the one of $P_1, \cdots, P_N$. The following Lemmas A1 and A2 prove that Property 2 is true.

Lemma A1.

$$S^O(r) \leq S(r) \leq S^I(r), \qquad \forall r(> R^*), \tag{A.3}$$

where $S^I(r)$ represents the degree of locational freedom for $P_1^I, \cdots, P_N^I$ and $S^O(r)$ represents the degree of locational freedom for $P_1^O, \cdots, P_N^O$.

Proof. We shall show that

$$\max_{k \in I} \|P - P_k^I\| \leq \max_{k \in I} \|P - P_k\| \leq \max_{k \in I} \|P - P_k^O\|, \qquad \forall P(\in R^2). \tag{A.4}$$

This means that

$$R^I(r) \supseteq R(r) \supseteq R^O(r), \qquad r(> R^*),$$

where, $R^I(r) \stackrel{\text{def}}{=} \{P \mid \max_{k \in I} \|P - P_k^I\| \leq r\}$, $R(r) \stackrel{\text{def}}{=} \{P \mid \max_{k \in I} \|P - P_k\| \leq r\}$, and $R^O(r) \stackrel{\text{def}}{=} \{P \mid \max_{k \in I} \|P - P_k^O\| \leq r\}$. Obviously, this relation of inclusion means that (A.3) is true.

First, we shall show that the first inequality of (A.4) is true. Let I^{SEC} be $\{k \mid P_k$ on $SEC\{P_1, \cdots, P_N\}\}$. For $i \notin I^{SEC}$, P_i^I is not on $CH\{P_1^I, \cdots, P_N^I\}$. This means that when the farthest-point Voronoi diagram of $P_1^I, \cdots, P_N^I$ is delineated, the farthest-point Voronoi polygon associated with P_i^I is empty. This is equivalent to $\max_{k \in I} \|P - P_k^I\| = \max_{k \in I^{SEC}} \|P - P_k^I\|$. On the other hand, from the definition of P_k^I, we have

$\max_{k\in I^{SEC}} \|P - P_k^I\| = \max_{k\in I^{SEC}} \|P - P_k\|$. As $\max_{k\in I^{SEC}} \|P - P_k\| \leq \max_{k\in I} \|P - P_k\|$, combining these equations gives the first inequality of (A.4).

Second, we shall show that the second inequality of (A.4) is true. Define $I^{CH-SEC} = \{k \mid P_k \text{ on } CH\{P_1, \cdots, P_N\}\} - I^{SEC}$. For the farthest-point Voronoi diagram of $P_1, \cdots, P_N$, define $V^{SEC} = \cup_{i\in I^{SEC}} V_i$ and $V^{CH-SEC} = \cup_{i\in I^{CH-SEC}} V_i$. Of course $V^{SEC} \cup V^{CH-SEC} = R^2$ and $V^{SEC} \cap V^{CH-SEC} = \phi$. There are two cases, corresponding as to $P \in V^{SEC}$ or $P \in V^{CH-SEC}$. In the case where $P \in V^{SEC}$, $\max_{k\in I} \|P - P_k\| = \max_{k\in I^{SEC}} \|P - P_k\| = \max_{k\in I^{SEC}} \|P - P_k^O\|$. Combining these equations with $\max_{k\in I^{SEC}} \|P - P_k^O\| \leq \max_{k\in I} \|P - P_k^O\|$ gives

$$\max_{k\in I} \|P - P_k\| \leq \max_{k\in I} \|P - P_k^O\|, \qquad \forall P(\in V^{SEC}). \tag{A.5}$$

We turn to the case where $P \in V^{CH-SEC}$. We assume that $P \in V_i, i \in I^{CH-SEC}$. Since P_i does not determine the center, there exist P_A and P_B such that both P_A and P_B determine the center and $\angle P_i P_A P_B$ is a non-acute angled ($\geq \frac{\pi}{2}$). Define $V_0 = \{P \mid \|P - P_i\| \geq \|P - P_A\|, \|P - P_i\| \geq \|P - P_B\|\}$. The situation is shown pictorially in Figure A3, where V_0 is shown hatched. Hence the circumcenter of this triangle, that is the vertex of V_0, denoted by P_0, lies on the opposite side of the line connecting P_A and P_B from P_i. Let l_0 be a line perpendicular to the line $\overline{P^* P_i}$ and passing through P_0.

We shall show that $\forall P \in V_0$, $\|P - P_i\| < \|P - P_i^O\|$. Let Ω be the convex cone which is generated by $\overline{P_i P_A}$ and $\overline{P_i P_B}$ and whose vertex is P_i. Let l_0' be the perpendicular to $\overline{P^* P_i}$ at P_i. Let V_0' be the set which consists of the points such that the line connecting the point and P_i makes a non-obtuse angle ($\leq \frac{\pi}{2}$) with the line connecting any point within Ω and P_i. This is illustrated in Figure A4, where Ω is shown horizontally hatched and V_0' is shown vertically hatched. As the half-line from P_i to P^* lies in Ω, making use fo Farkas' theorem of alternative: see Panik (1993), $\forall P(\in V_0')$ lies on the opposite side of l_0' from

P_i^O. By noting that V_0' is formed by making a parallel translation of V_0, and l_0' is formed by making a parallel translation of l_0, we see that $\forall P(\in V_0)$ lies on the opposite side of l_0 from P_i. As a result, $\forall P(\in V_0)$ lies on the opposite side of the line through the midpoint of $\overline{P_iP_i'}$ and parallel to l_0, denoted by l_0'', from P_i^O: see Figure A5. This means that for $\forall P \in V_0$, $\|P - P_i\| < \|P - P_i^O\|$.

As $V_i \subseteq V_0$, it follows that for $\forall P \in V_i$, $\|P - P_i\| < \|P - P_i^O\|$. Therefore, we have

$$\max_{k\in I}\|P - P_k\| = \|P - P_i\| < \|P - P_i^O\| \leq \max_{k\in I}\|P - P_k^O\|, \qquad \forall P(\in V_i).$$

This states that

$$\max_{k\in I}\|P - P_k\| < \max_{k\in I}\|P - P_k^O\|, \qquad \forall P(\in V^{CH-SEC}). \tag{A.6}$$

The inequalities (A.5) and (A.6) yields the second inequality of (A.4). □

Lemma A2. *When $P_1, \cdots, P_m$ lie on $CH\{P_1, \cdots, P_m\}$, for any $r > R^*$, the maximum of $S(r)$ is attained if and only if the demand set is 2-regular, its minimum is attained if and only if the demand set is m-regular.*

Proof. Without loss of generality we can assume that $P_1, \cdots, P_m$ are arranged in clockwise order. Define $\mu_i = \frac{1}{2}\angle P_{i-1}P^*P_i$. This is illustrated in Figure A6. Let Q_A and Q_B be the intersection points of the circular arc with a radius $r(> R^*)$ which is emerging from P_i, and the boundary of V_i. Define $\beta_i = \angle P^*P_iQ_A$ and $\alpha_i = \angle P^*P_iQ_B$. This definition is illustrated in Figure A7, where V_i is shown hatched.

As $\angle P_iP^*Q_A = \pi - \mu_{i+1}$, making use of the sine rule gives

$$\begin{aligned}\frac{r}{\sin(\angle P_iP^*Q_A)} = \frac{R^*}{\sin(\angle P_iQ_AP^*)} &\Leftrightarrow \frac{r}{\sin(\pi - \mu_{i+1})} = \frac{R^*}{\sin(\mu_{i+1} - \beta_i)} \\ &\Leftrightarrow \sin(\mu_{i+1} - \beta_i) = \frac{R^*}{r}\sin\mu_{i+1} \\ &\Leftrightarrow \beta_i = \mu_{i+1} - \arcsin(\frac{R^*}{r}\sin\mu_{i+1}).\end{aligned}$$

Likely, as $\angle P_i P^* Q_B = \pi - \mu_i$, we have

$$\frac{r}{\sin(\angle P_i P^* Q_B)} = \frac{R^*}{\sin(\angle P_i Q_B P^*)} \Leftrightarrow \frac{r}{\sin(\pi - \mu_i)} = \frac{R^*}{\sin(\mu_i - \alpha_i)}$$
$$\Leftrightarrow \sin(\mu_i - \alpha_i) = \frac{R^*}{r} \sin \mu_i$$
$$\Leftrightarrow \alpha_i = \mu_i - \arcsin(\frac{R^*}{r} \sin \mu_i).$$

It is evident from Figure A7,

$$S(r) = \sum_{i=1}^{m} \frac{r^2}{2}(\beta_i + \alpha_i) - \frac{rR^*}{2} \sin \beta_i - \frac{rR^*}{2} \sin \alpha_i.$$

As $\alpha_i = \beta_{i-1}$, we have

$$S(r) = \sum_{i=1}^{m} r^2 \alpha_i - rR^* \sin \alpha_i. \tag{A.7}$$

Defining $\varphi(\alpha_i) = r^2 \alpha_i - rR^* \sin \alpha_i$, (A.7) indicates that $S(r)$ is considered to be the sum of the identical functions. Differentiating $\varphi(\alpha_i)$ one and two times with respect to μ_i yields

$$\frac{\partial \varphi(\alpha_i)}{\partial \mu_i} = r(r - R^* \cos \alpha_i) \frac{\partial \alpha_i}{\partial \mu_i} > 0; \tag{A.8}$$
$$\frac{\partial^2 \varphi(\alpha_i)}{\partial \mu_i^2} = r(r - R^* \cos \alpha_i) \frac{\partial^2 \alpha_i}{\partial \mu_i^2} + rR^* \sin \alpha_i (\frac{\partial \alpha_i}{\partial \mu_i})^2 > 0. \tag{A.9}$$

This is because as $0 < \alpha_i < \pi$ and $r > R^*$, we have

$$\frac{\partial \alpha_i}{\partial \mu_i} = 1 - \frac{R^* \cos \mu_i}{\sqrt{r^2 - R^{*2} \sin^2 \mu_i}} > 0;$$
$$\frac{\partial^2 \alpha_i}{\partial \mu_i^2} = \frac{1}{(r^2 - R^{*2} \sin^2 \mu_i)} (R^* \sin \mu_i \sqrt{r^2 - R^{*2} \sin^2 \mu_i} - \frac{R^{*3} \sin \mu_i \cos^2 \mu_i}{\sqrt{r^2 - R^{*2} \sin^2 \mu_i}})$$
$$= \frac{R^* \sin \mu_i (r^2 - R^{*2} \sin^2 \mu_i - R^{*2} \cos^2 \mu_i)}{(r^2 - R^{*2} \sin^2 \mu_i) \sqrt{r^2 - R^{*2} \sin^2 \mu_i}}$$
$$= \frac{R^* (r^2 - R^{*2}) \sin \mu_i}{(r^2 - R^{*2} \sin^2 \mu_i) \sqrt{r^2 - R^{*2} \sin^2 \mu_i}} > 0.$$

The inequalities (A.8) and (A.9) indicates that $\varphi_i(r)$ is increasing and convex. Hence, it follows that on the condition of $\sum_{i=1}^{m} \mu_i = \pi$, $S(r)$ attains its minimum if and only if $\mu_i = \frac{\pi}{m}$, that is, the set is m-regular.

On the other hand, the smallest enclosing circle is determined by at least two points. Therefore, it follows that on the condition of $\sum_{i=1}^{m} \mu_i = \pi$, $S(r)$ attains its maximum if and only if the set is 2-regular.

A.3. Proof of Equations (3.9) and (3.10)

As we consider the case where $x - F^*$ is significantly small, we can consider the case where the demand set consists of three demand points, P_1, P_2 and P_3. Let λ_i be the angle of the vertex of V_i. Let Q_i be the middle point of P_i and P_{i+1}. This is illustrated in Figure 9. We see from this figure that $\angle Q_i P^* Q_{i-1} = \pi - \psi_i$ by using the fact that the sum of the four angles of a quadrangle is 2π. It follows that $\lambda_i = \pi - \psi_i$. Let $\theta_i(r)$ denote the angle which defines the length of the contour line within V_i. Similarly as for the equation (A.2), it follows

$$\begin{aligned}\theta_i(r) &= \pi - \psi_i - 2\arcsin(\frac{R}{r}\sin(\frac{\pi - \psi_i}{2})) \\ &= \pi - \psi_i - 2\arcsin(\frac{R}{r}\cos(\frac{\psi_i}{2})).\end{aligned}$$

Hence, we have

$$S(x) = \frac{r^2}{2}\sum_{i=1}^{3}\theta_i(r) - rR^*\sum_{i=1}^{3}\sin(\frac{\theta_i(r)}{2}).$$

Differentiating $S(x)$ with respect to r gives

$$\frac{\partial S(x)}{\partial r} = r\sum_{i=1}^{3}\theta_i(r) - R^*\sum_{i=1}^{3}\sin(\frac{\theta_i(r)}{2}) + \frac{r}{2}\sum_{i=1}^{3}(r - R^*\cos(\frac{\theta_i(r)}{2}))\theta_i'(r). \qquad (A.10)$$

$$\begin{aligned}\frac{\partial^2 S(x)}{\partial r^2} &= \sum_{i=1}^{3}\theta_i(r) + \sum_{i=1}^{3}(2r - R^*\cos(\frac{\theta_i(r)}{2}))\theta_i'(r) \\ &\quad + \frac{rR^*}{4}\sum_{i=1}^{3}\sin(\frac{\theta_i(r)}{2})(\theta_i'(r))^2 + \frac{r}{2}\sum_{i=1}^{3}(r - R^*\cos(\frac{\theta_i(r)}{2}))\theta_i''(r). \qquad (A.11)\end{aligned}$$

It should be noted that

$$\theta_i'(r) = \frac{2R^*\cos(\frac{\psi_i}{2})}{r\sqrt{r^2 - R^{*2}\cos^2(\frac{\psi_i}{2})}};$$

$$\theta_i''(r) = \frac{2R^*\cos(\frac{\psi_i}{2})}{r^2(r^2 - R^{*2}\cos^2(\frac{\psi_i}{2}))}(-\sqrt{r^2 - R^{*2}\cos^2(\frac{\psi_i}{2})} - \frac{r^2}{\sqrt{r^2 - R^{*2}\cos^2(\frac{\psi_i}{2})}})$$
$$= \frac{2R^*\cos(\frac{\psi_i}{2})(R^{*2}\cos^2(\frac{\psi_i}{2}) - 2r^2)}{r^2(r^2 - R^{*2}\cos^2(\frac{\psi_i}{2}))\sqrt{r^2 - R^{*2}\cos^2(\frac{\psi_i}{2})}}.$$

Therefore,

$$\theta_i'(R^*) = 2\cot(\frac{\psi_i}{2}); \tag{A.12}$$

$$\theta_i''(R^*) < \infty. \tag{A.13}$$

Substituting (A.12) into (A.10) and (A.11), and noting (A.13) and $\theta(R^*) = 0$ gives

$$\left.\frac{\partial S(x)}{\partial r}\right|_{x=F^*} = 0;$$
$$\left.\frac{\partial^2 S(x)}{\partial r^2}\right|_{x=F^*} = 2R^*\sum_{i=1}^{3}\cot\frac{\psi_i}{2}.$$

By noting that $0 < \left.\frac{\partial r}{\partial x}\right|_{x=F^*} = \frac{1}{C'(F^*)} < \infty$, we have

$$S'(F^*) = \left.\frac{\partial S(x)}{\partial r}\right|_{x=F^*}\left.\frac{\partial r}{\partial x}\right|_{x=F^*} = 0;$$
$$S''(F^*) = \left.\frac{\partial^2 S(x)}{\partial r^2}\right|_{x=F^*}\left.\frac{\partial r}{\partial x}\right|_{x=F^*} + \left.\frac{\partial S(x)}{\partial r}\right|_{x=F^*}\left.\frac{\partial^2 r}{\partial x^2}\right|_{x=F^*}$$
$$= \frac{2R^*}{C'(F^*)}\sum_{i=1}^{3}\cot\frac{\psi_i}{2}.\square$$

Reference

[1] Brady, S.D. and R.E. Rosenthal (1980): Iterative Computer Graphical Solutions of Constrained Minimax Location Problems. *AIIE Transactions, 12*, pp.241-247.

[2] Elzinga, J., and D.W. Hearn (1972): Geometrical Solution for Some Minimax Location Problems, *Transportation Science, 6*, pp.379-394.

[3] Francis, R.L., and J.A. White (1974): *Facility Layout and Location.* Prentice-Hall, Englewood Cliffs, New Jersey.

[4] Love, R.F., Morris J.G. and G.O. Wesolowsky (1988): *Facilities Location: Models and Methods.* North-Holland, New York.

[5] Ministry of Construction, Japan (1992): *Coordinates of Localities in Japan.* Nippon Chizu Center, Tokyo. (in Japanese)

[6] Okabe, A., B. Boots and K. Sugihara (1992): *Spatial Tessellations: Concepts and Applications of Voronoi Diagrams.* Wiley, Chichester.

[7] Ohsawa, Y. and T. Koshizuka and A. Imai (1995): Contour Lines in a Single Facility Euclidean Minimax Location Problem, Discussion paper no.623, Institute of Socio-Economic Planning, University of Tsukuba, Tsukuba.

[8] Panik, M.J. (1993): *Fundamentals of Convex Analysis.* Kluwer Academic Publishers, Dordrecht.

[9] Preparata, F.P. and M.I. Shamos (1985): *Computational Geometry: An Introduction.* Springer-Verlag, New York.

[10] Shamos, M.I., and D. Hoey (1975): Closest-Point Problems. Proceedings of the 16th Annual IEEE Symposium on Foundations of Computer Science, pp.151-162.

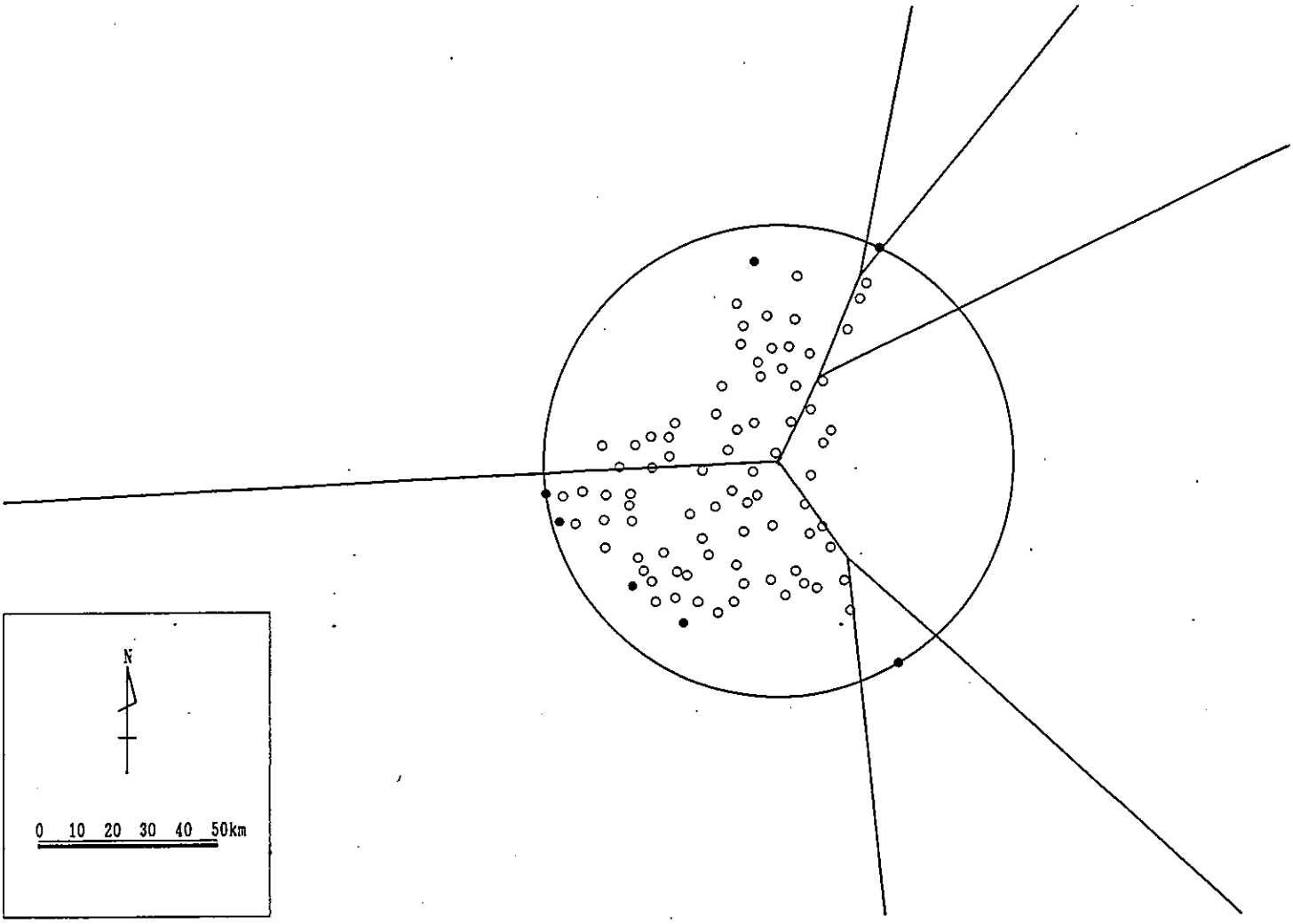

Figure 1. Farthest-point Voronoi diagram in the Ibarki prefecture

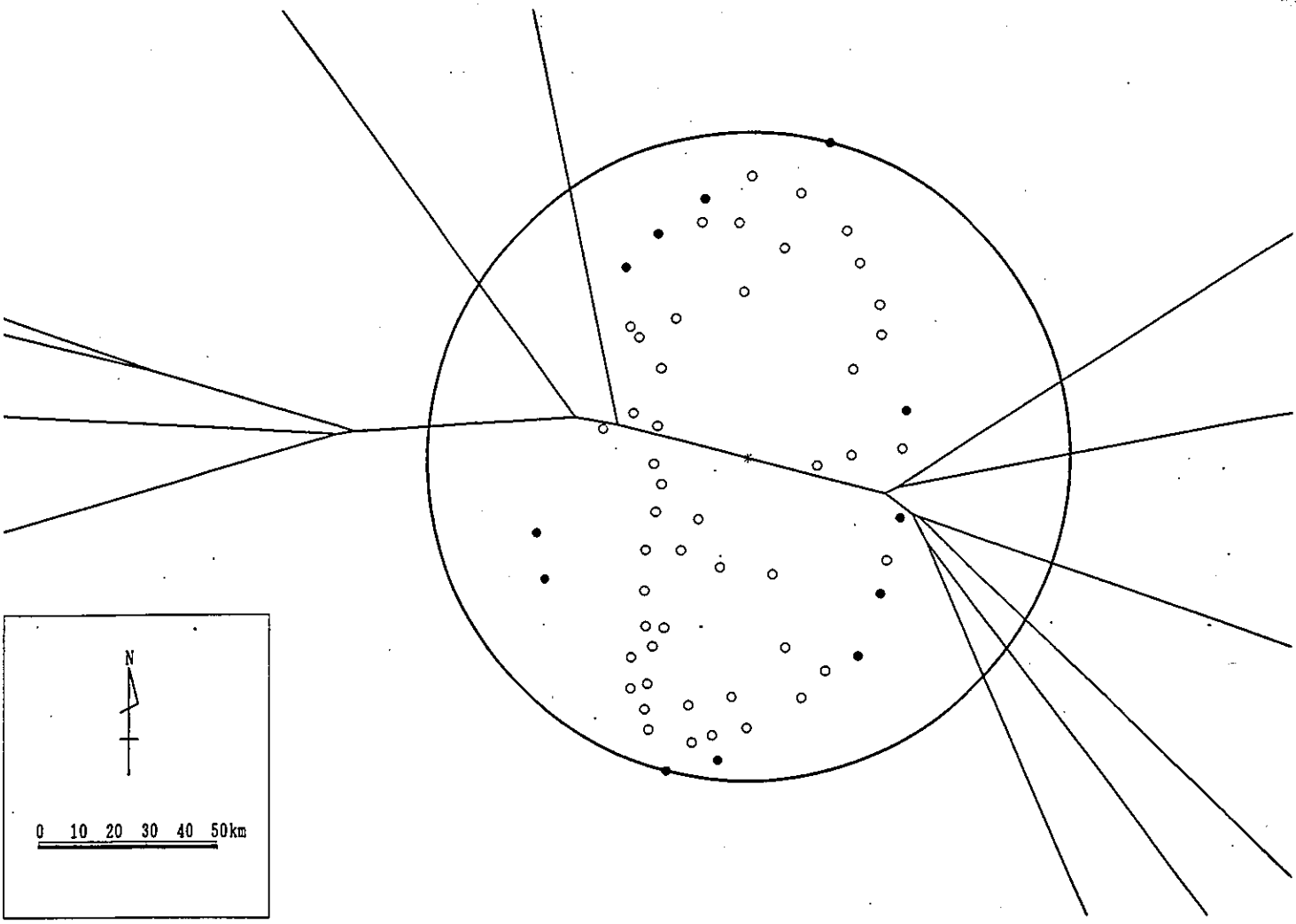

Figure 2. Farthest-point Voronoi diagram in the Iwate prefecture

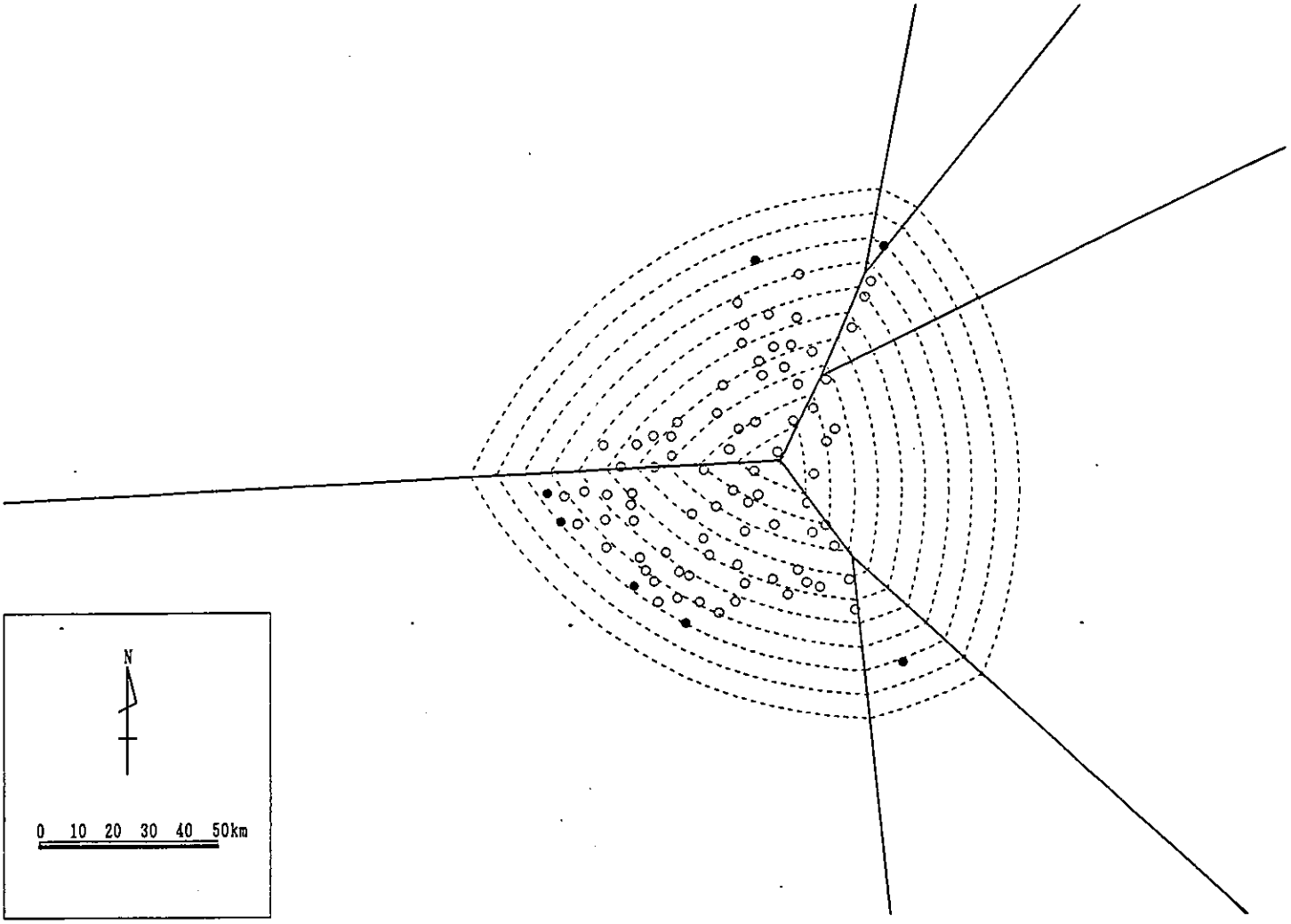

Figure 3. Contour map of the Ibarki prefecture

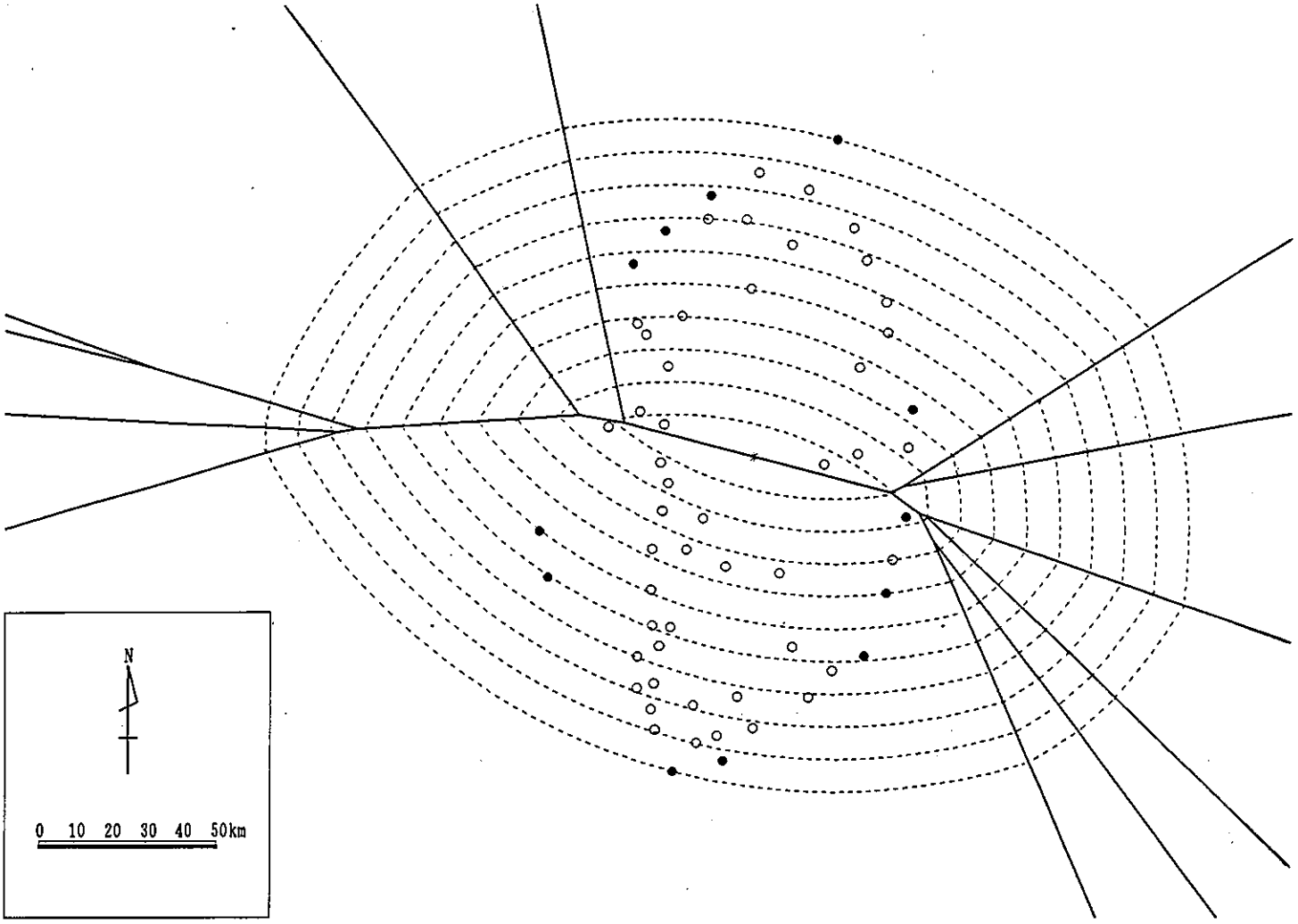

Figure 4. Contour map of the Iwate prefecture

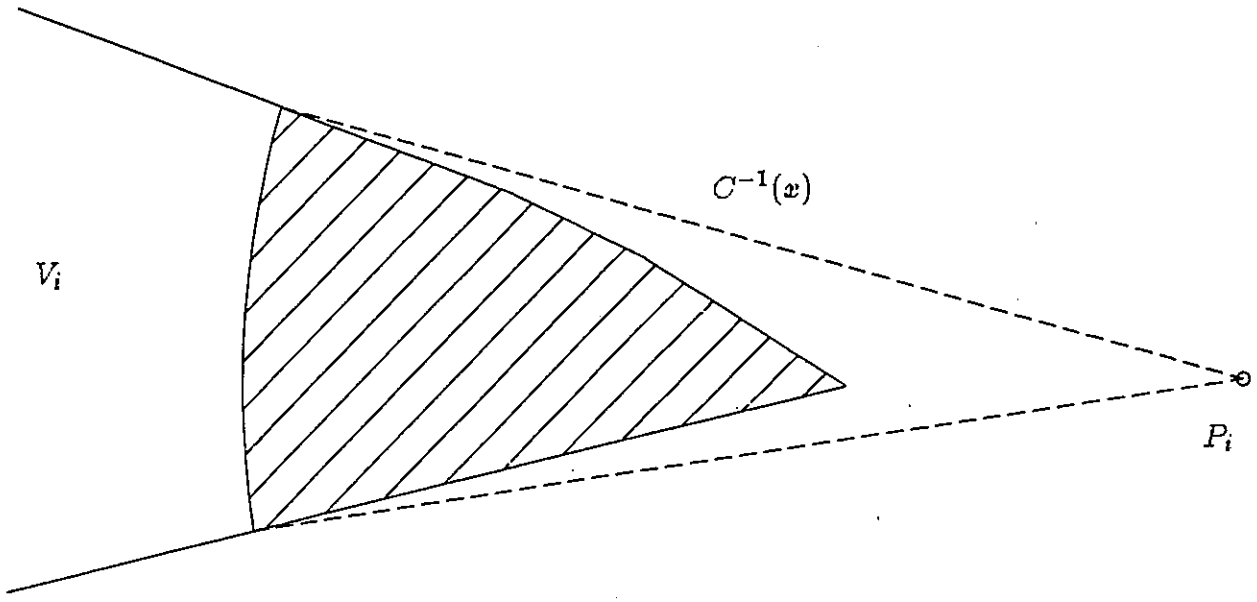

Figure 5. Construction procedure of the preferable locational area

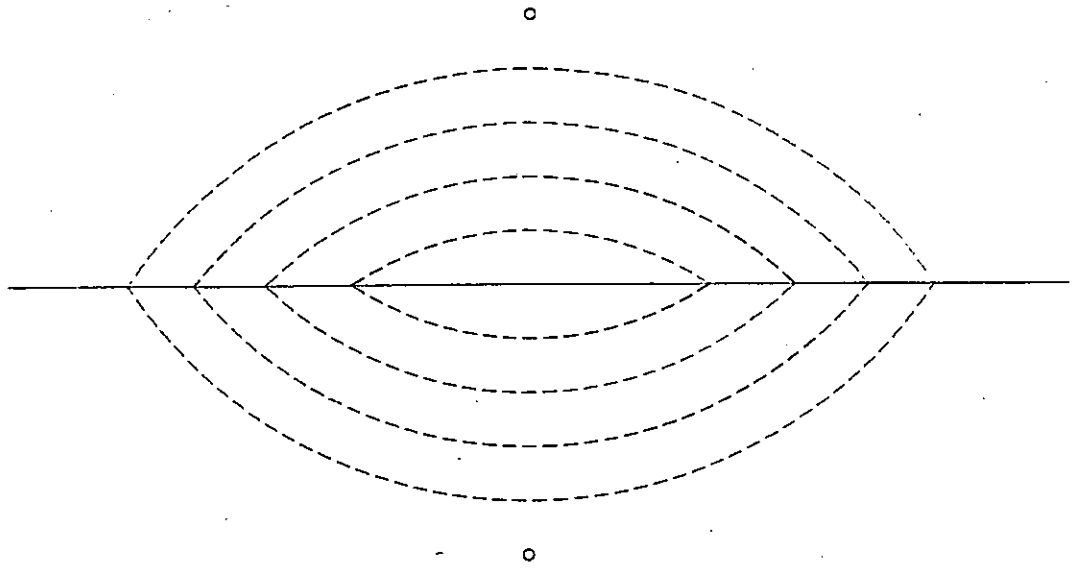

Figure 6. Contour map for a 2-regular set

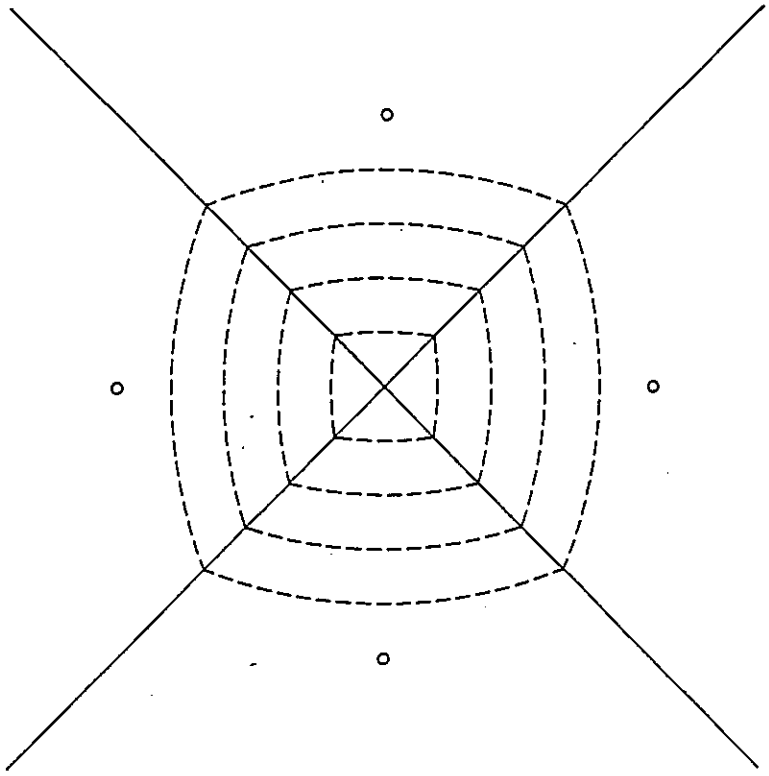

Figure 7. Contour map for a 4-regular set

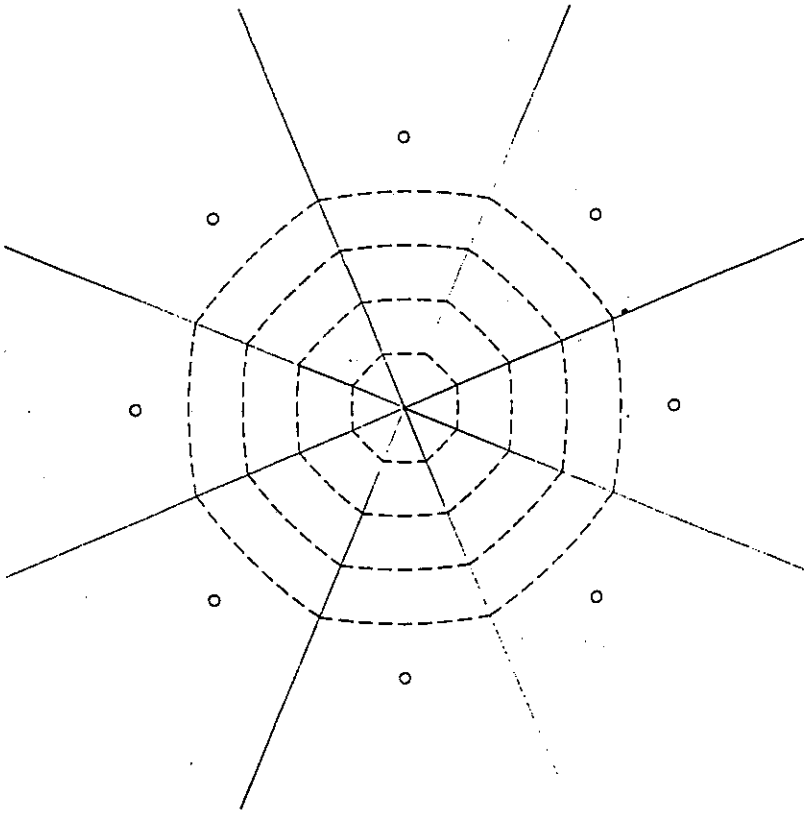

Figure 8. Contour map for an 8-regular set

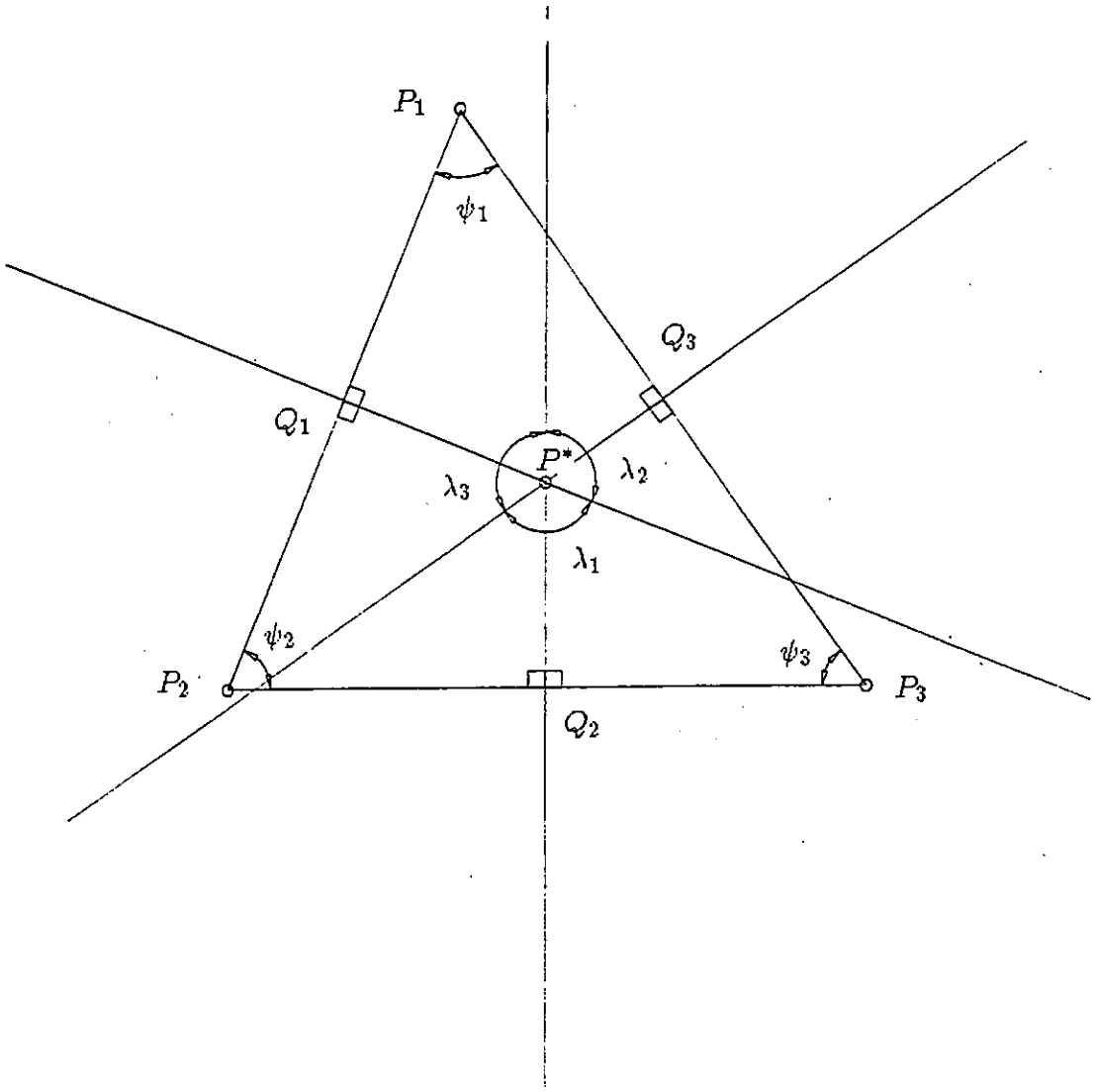

Figure 9. Definition of the angles (ψ_1, ψ_2, ψ_3)

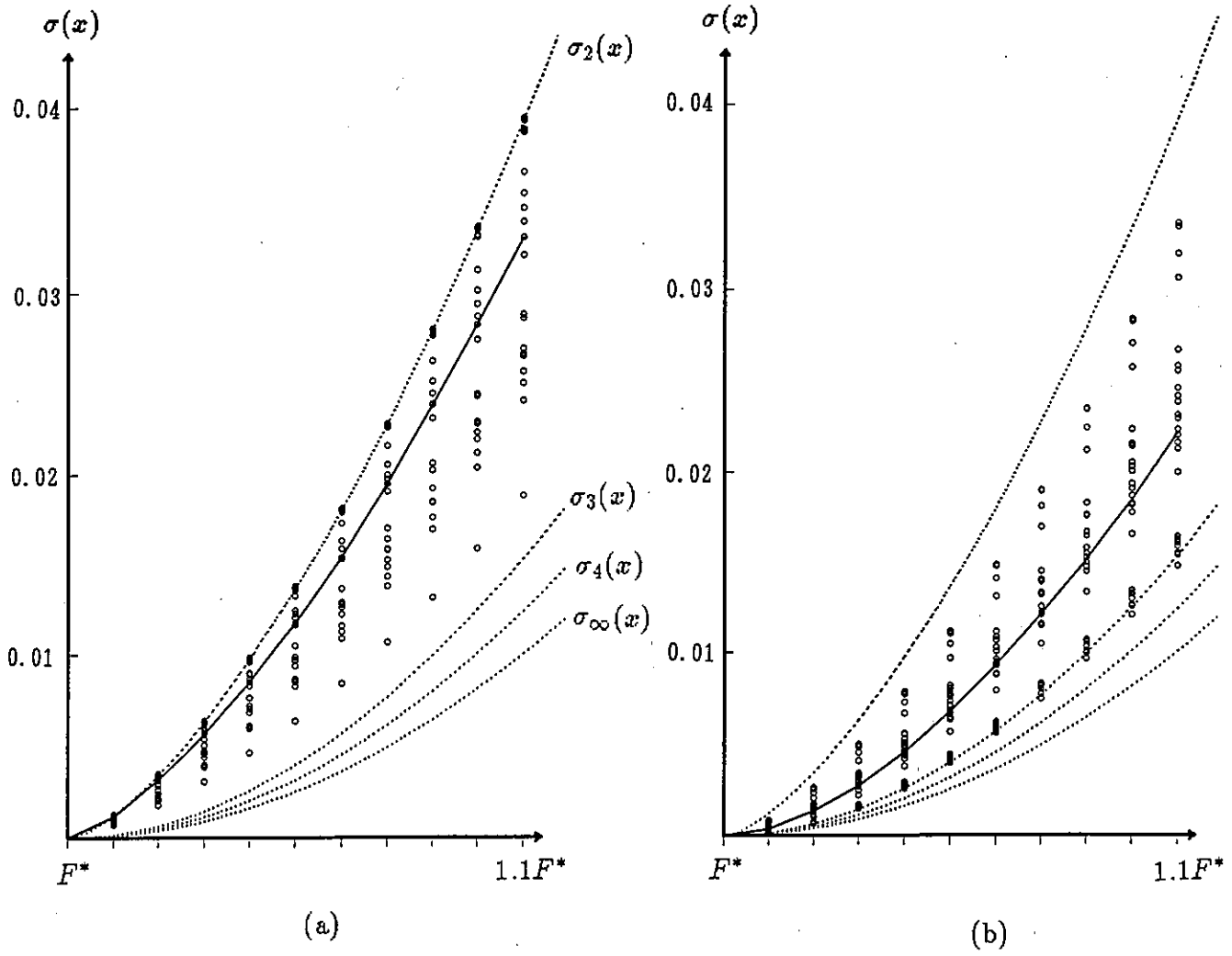

Figure 10. 47 plots of $\sigma(x)$ against r for the x-values ranging from F^* to $1.1F^*$

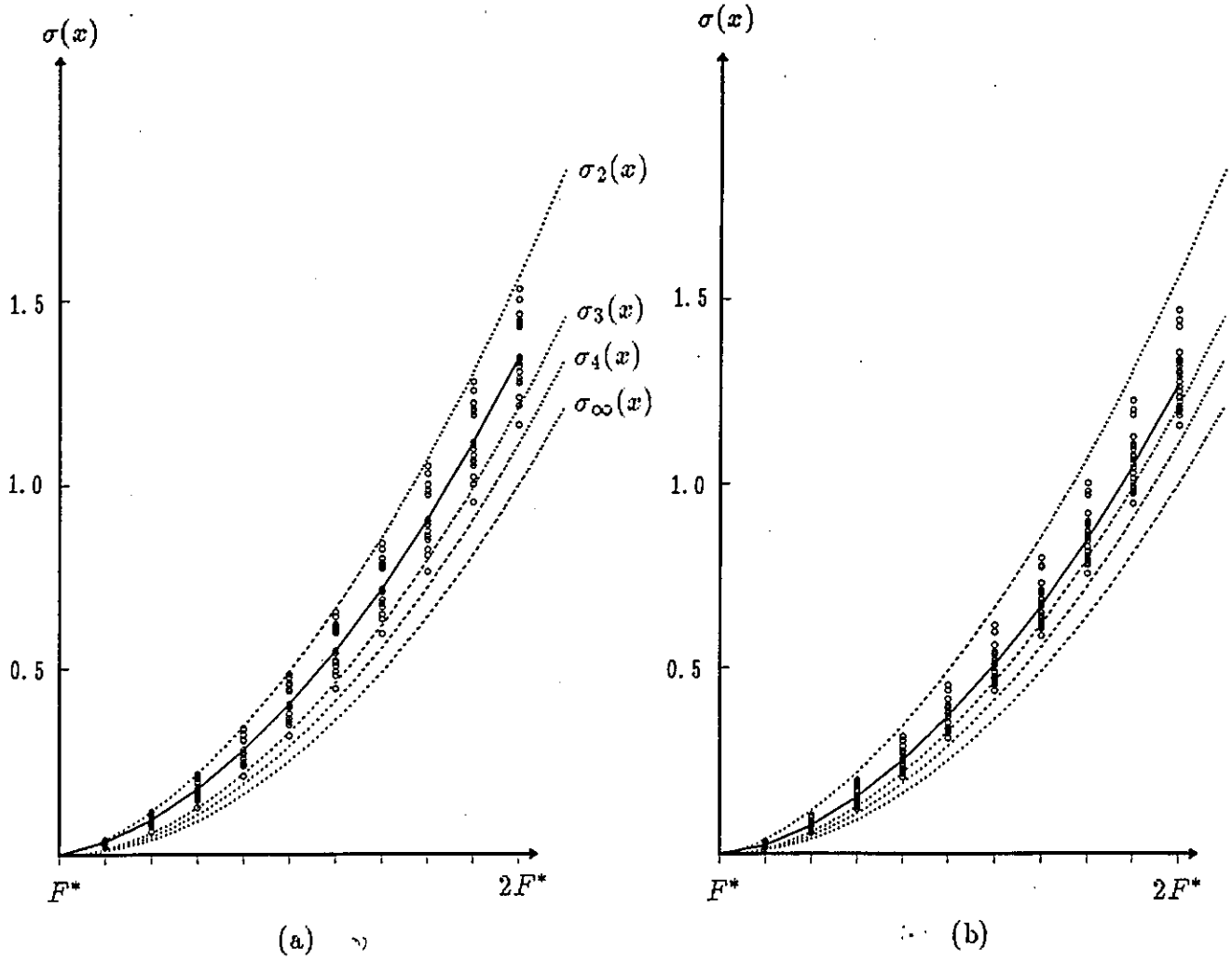

Figure 11. 47 plots of $\sigma(x)$ against r for the x-values ranging from F^* to $2F^*$

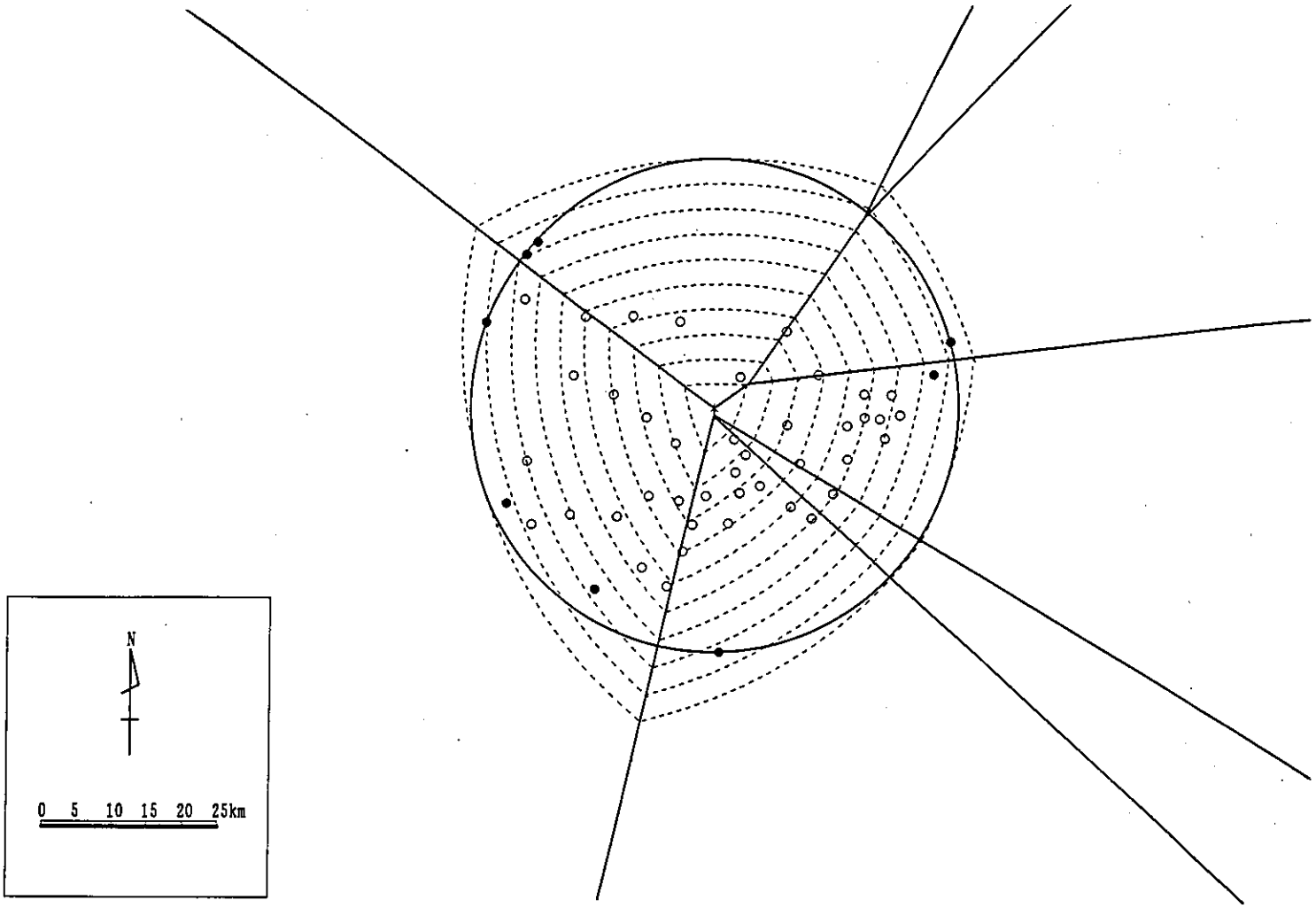

Figure 12. Contour map of the Saga prefecture

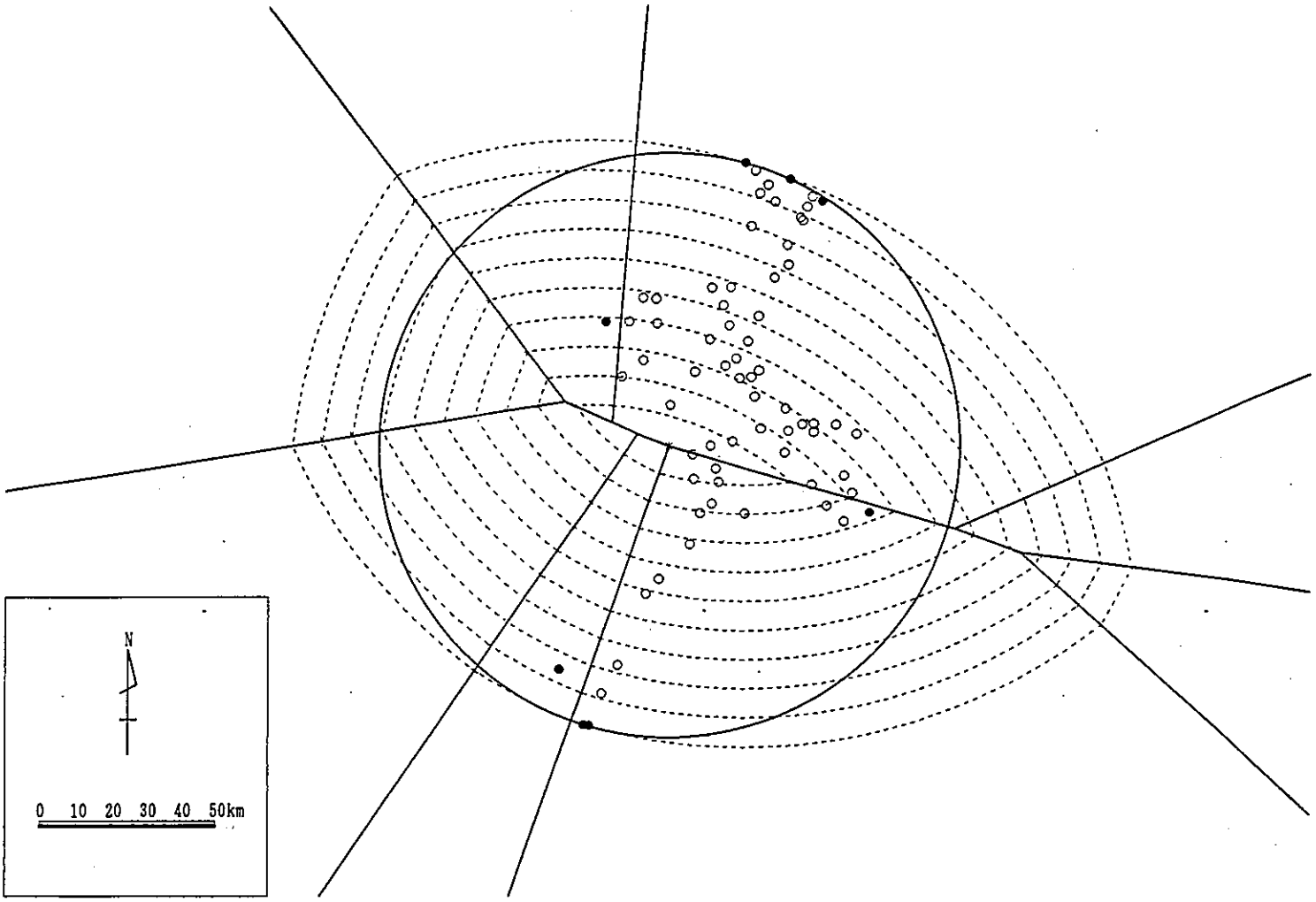

Figure 13. Contour map of the Mie prefecture

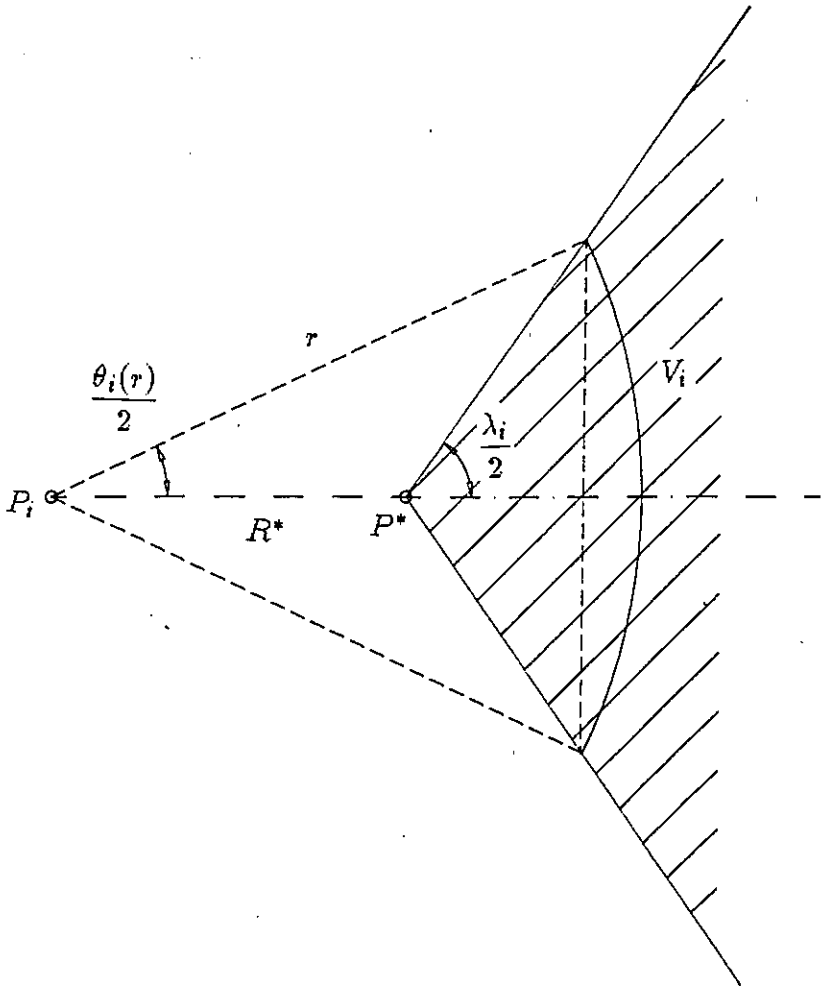

Figure A1. Illustration of the proof of property 1

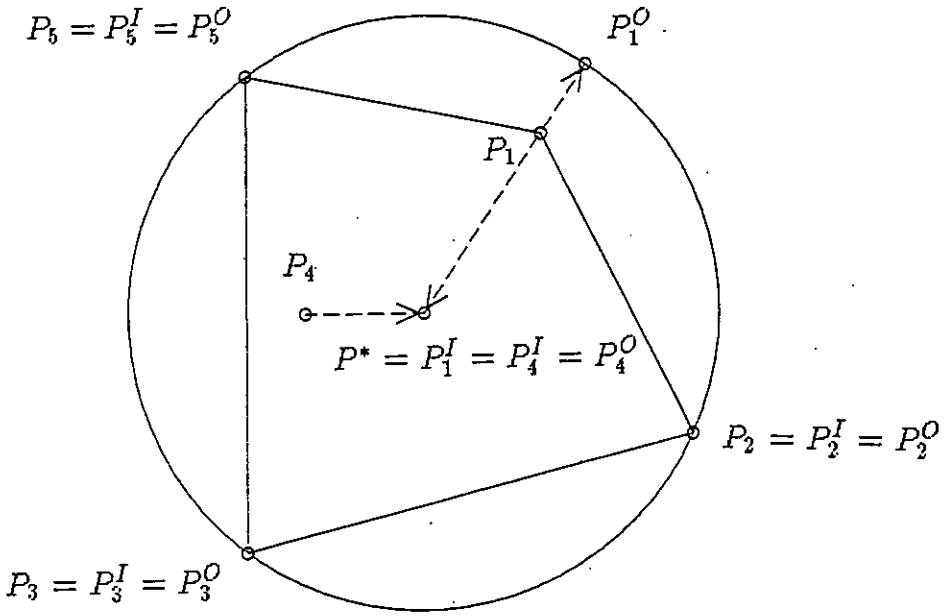

Figure A2. Definitions of P_i^I and P_i^O

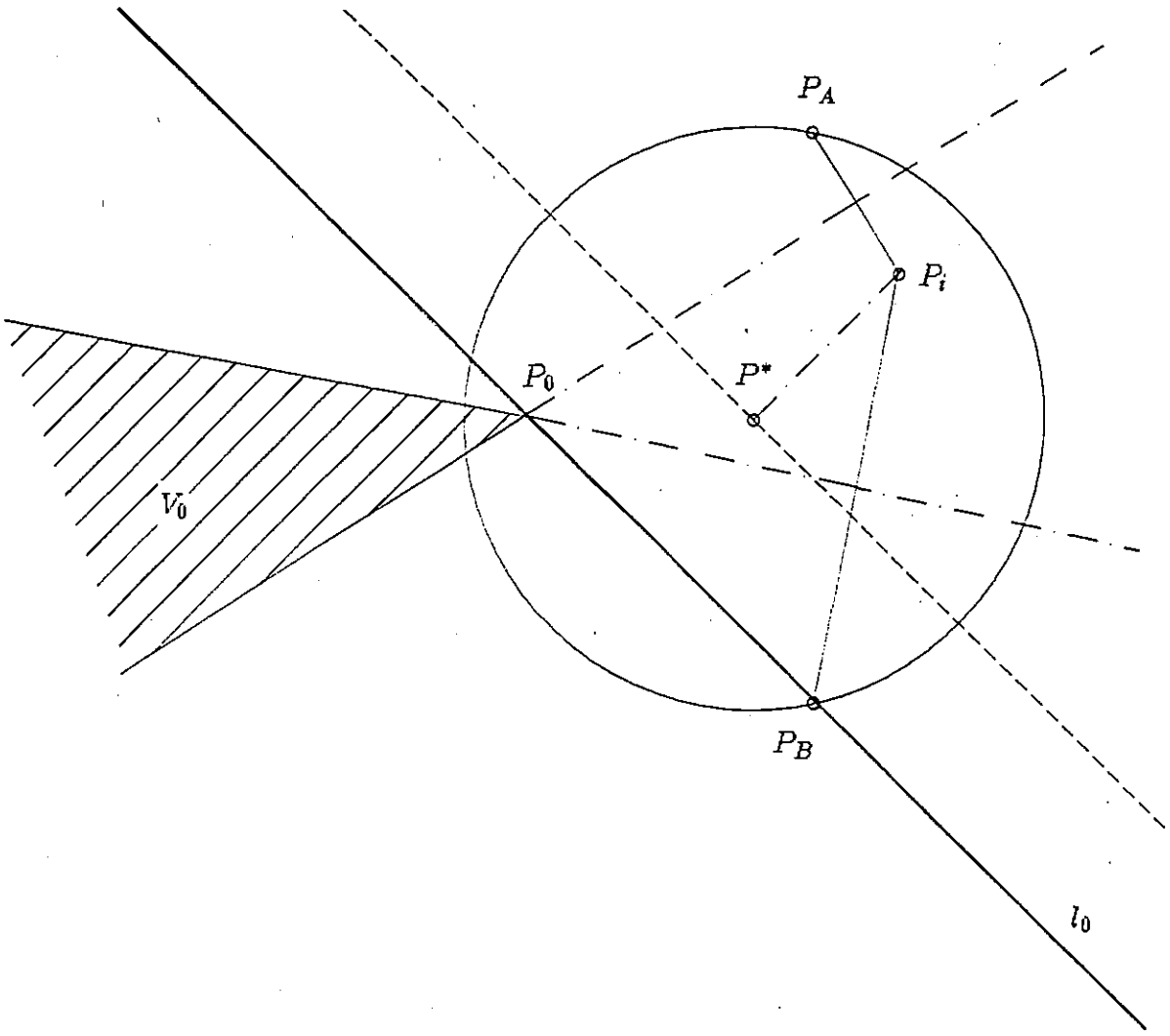

Figure A3. Definitions of l_0 and V_0

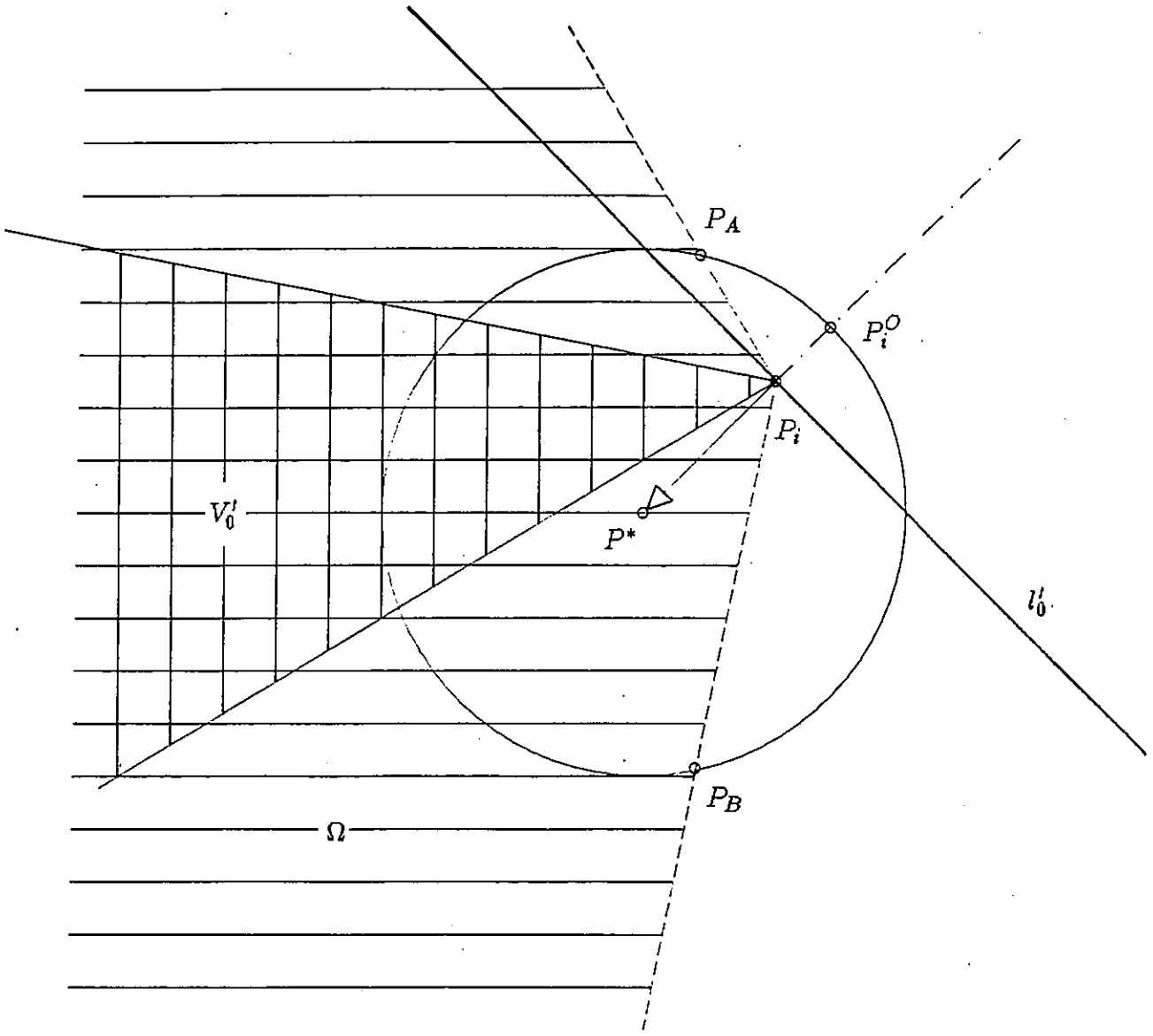

Figure A4. Definitions of Ω, l_0' and V_0'

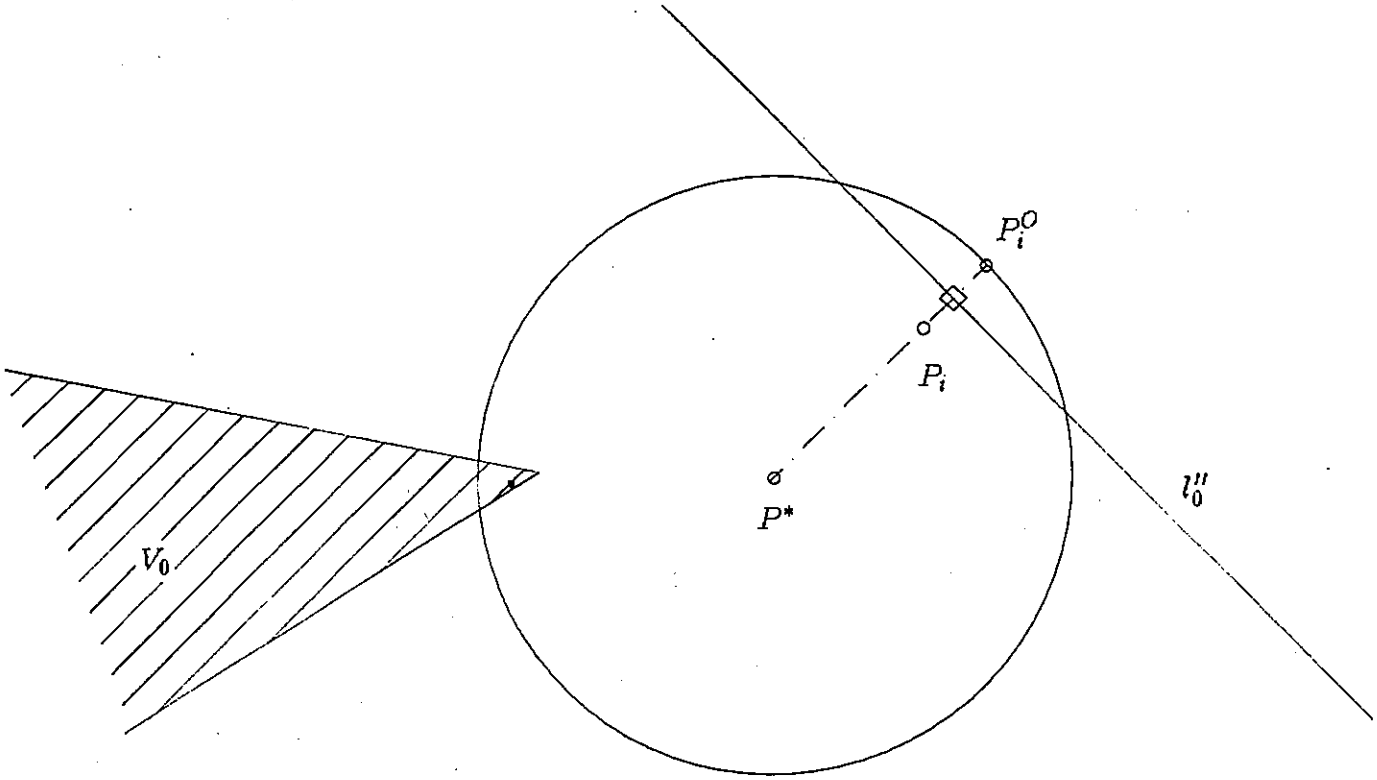

Figure A5. Definitions of l_0''

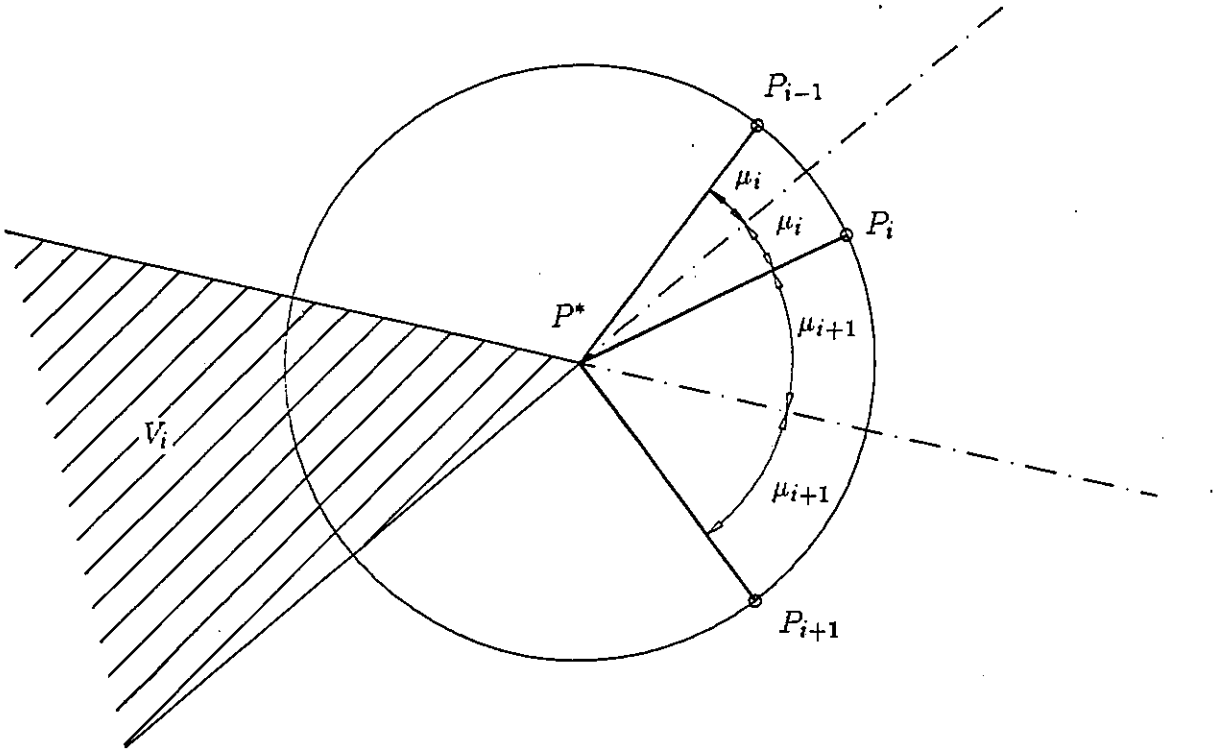

Figure A6. Definitions of μ_i

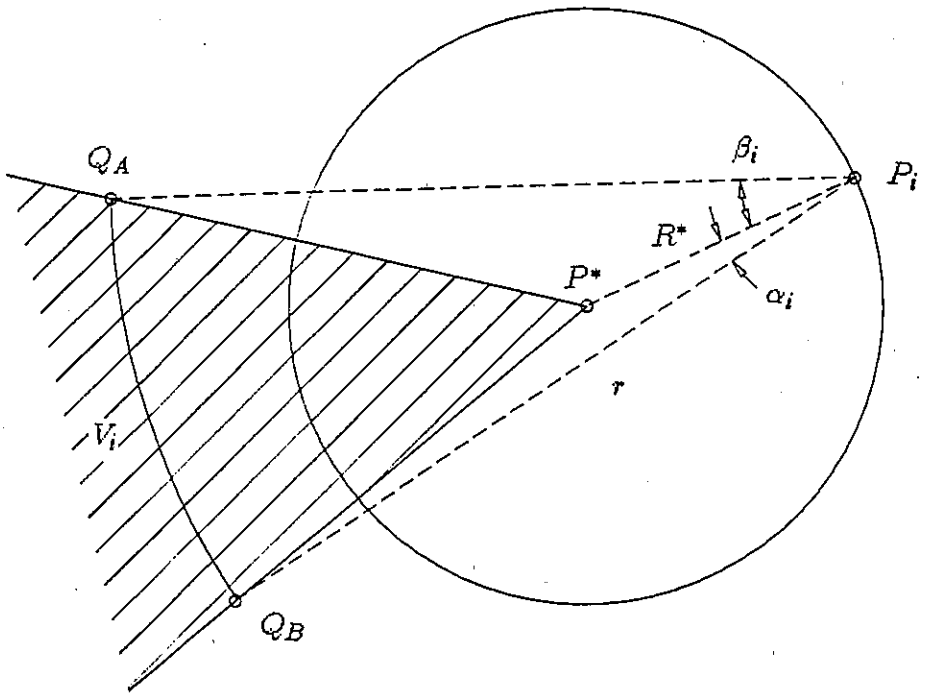

Figure A7. Definitions of Q_A, Q_B, α_i and β_i

Table 1. Data and results of the 47 prefectures in Japan

prefecture	N	D(km)	F^*(km)	$NSEC$	NCH	ρ
Nagano	121	212	106	2	9	∞
Okinawa	53	85	43	2	7	∞
Iwate	59	181	91	2	12	∞
Tokyo	64	71	35	2	6	∞
Miyagi	76	146	73	2	7	∞
Toyama	35	84	42	2	6	∞
Kochi	53	165	82	2	9	∞
Niigata	112	225	112	2	7	∞
Kagawa	43	72	36	2	6	∞
Ishikawa	41	154	77	2	6	∞
Shiga	50	75	38	2	9	∞
Yamagata	44	123	61	2	8	∞
Miyazaki	44	149	75	2	6	∞
Fukuoka	111	112	56	2	9	∞
Fukushima	90	165	82	2	9	∞
Gunma	70	102	51	2	7	∞
Nagasaki	79	106	53	2	8	∞
Hiroshima	93	121	60	2	12	∞
Tottori	39	108	54	2	5	∞
Yamaguchi	56	136	68	2	8	∞
Kanagawa	60	71	35	2	7	∞
Shimane	59	177	89	3	7	3.92
Mie	69	166	83	3	8	5.21
Kumamoto	94	142	71	3	13	3.21
Kyoto	55	136	68	3	6	2.67
Tochigi	49	96	48	3	7	1.72
Osaka	68	79	40	3	6	1.65
Shizuoka	74	151	75	3	9	1.73
Kagoshima	96	133	67	3	9	1.66
Hyogo	100	132	66	3	8	1.11
Nara	47	83	42	3	6	1.46
Wakayama	50	101	51	3	11	1.39
Saitama	92	86	43	3	9	1.31
Fukui	35	110	55	3	6	1.24
Ehime	70	154	78	3	6	1.42
Akita	69	152	76	3	7	1.38
Okayama	78	106	53	3	12	1.26
Gifu	99	139	70	3	10	1.09
Chiba	86	124	67	3	6	1.04
Tokushima	50	84	43	3	8	1.02
Hokkaidou	221	503	262	3	6	1.03
Aichi	104	101	52	3	9	1.04
Oita	58	112	56	3	10	1.08
Aomori	67	144	79	3	8	1.00
Yamanashi	64	76	42	3	8	1.00
Ibaraki	87	120	66	3	7	1.00
Saga	49	68	35	3	8	1.02

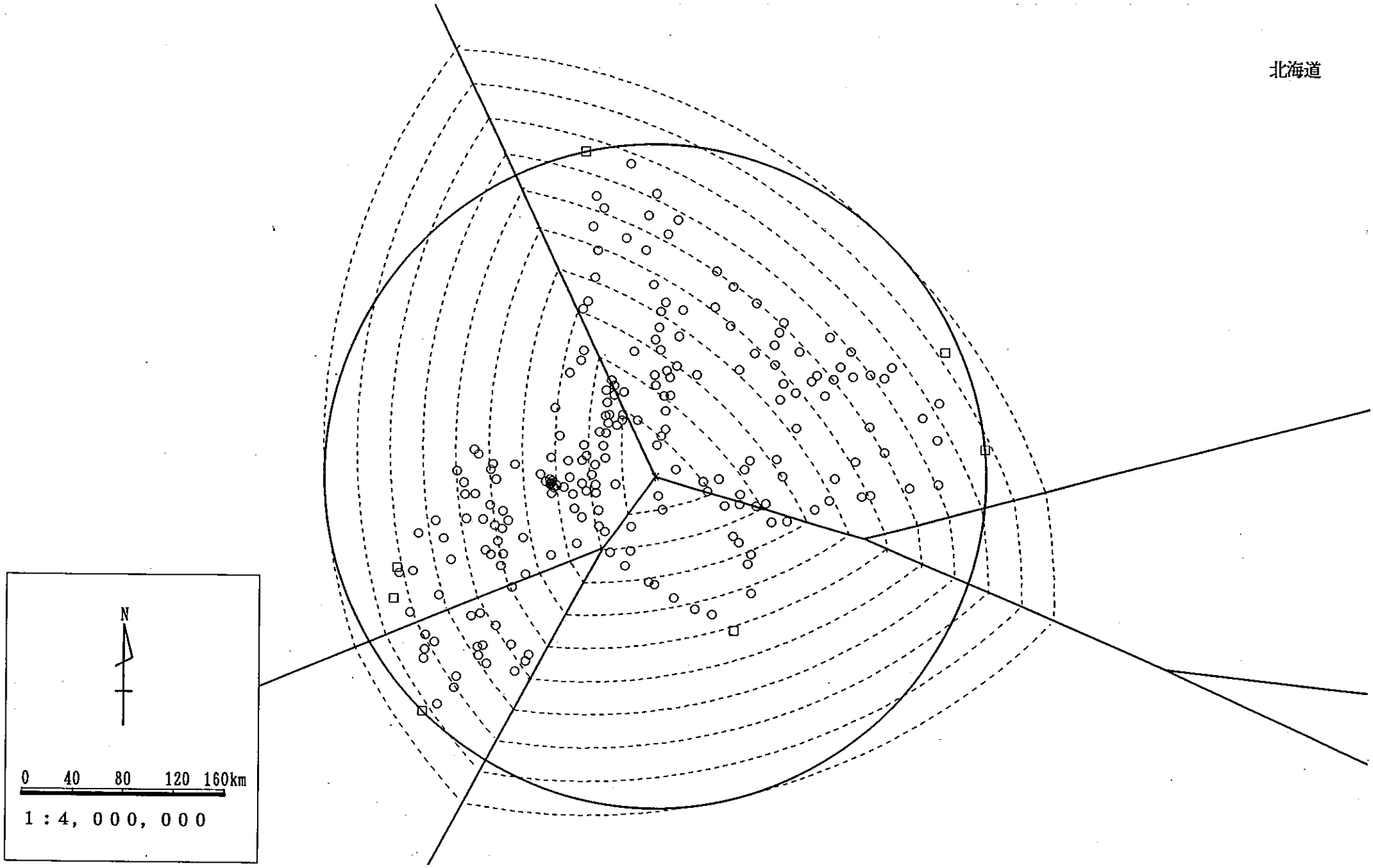

Figure B1. Contour map of the Hokkaidou Prefecture

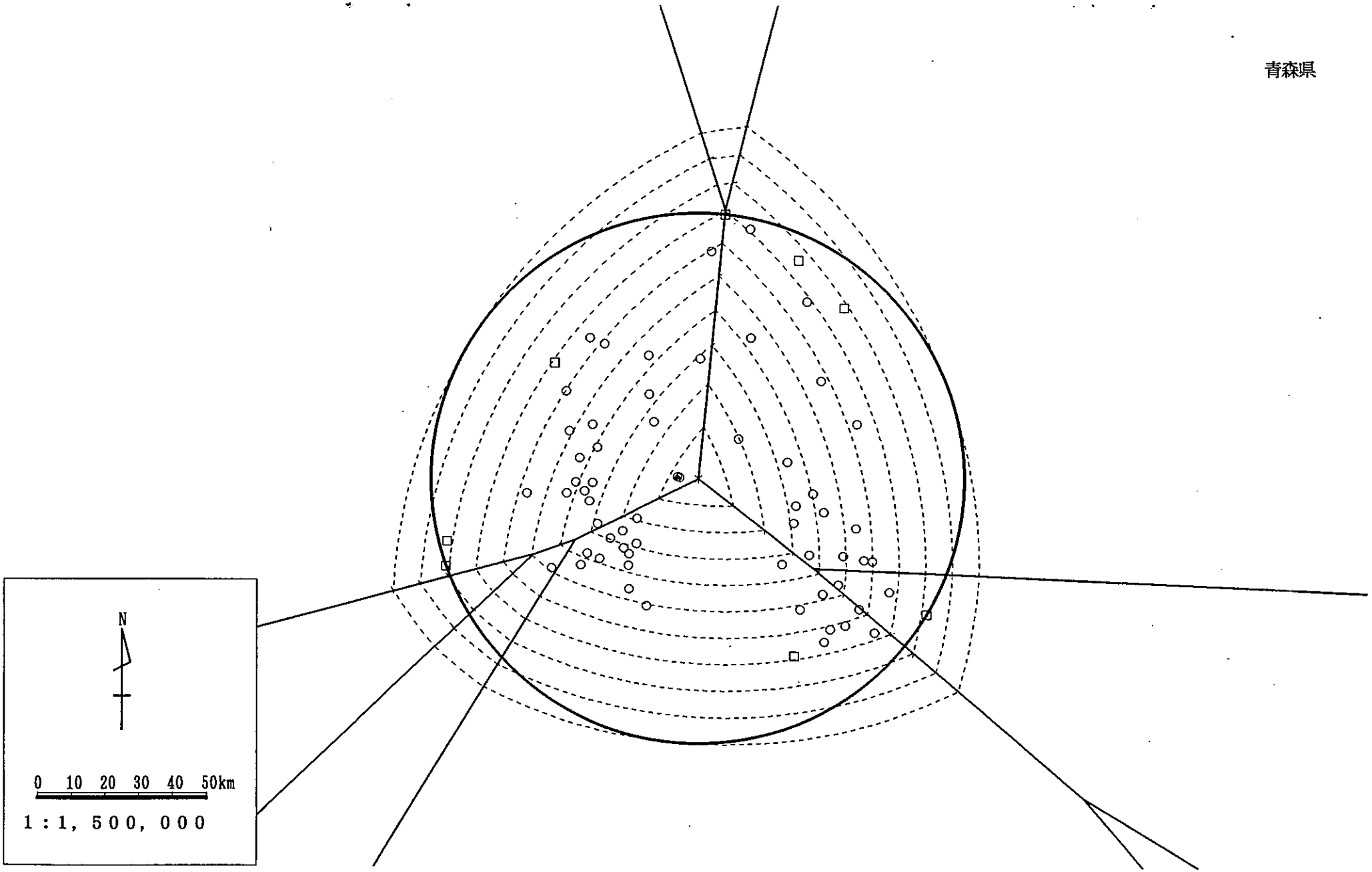

Figure B2. Contour map of the Aomori Prefecture

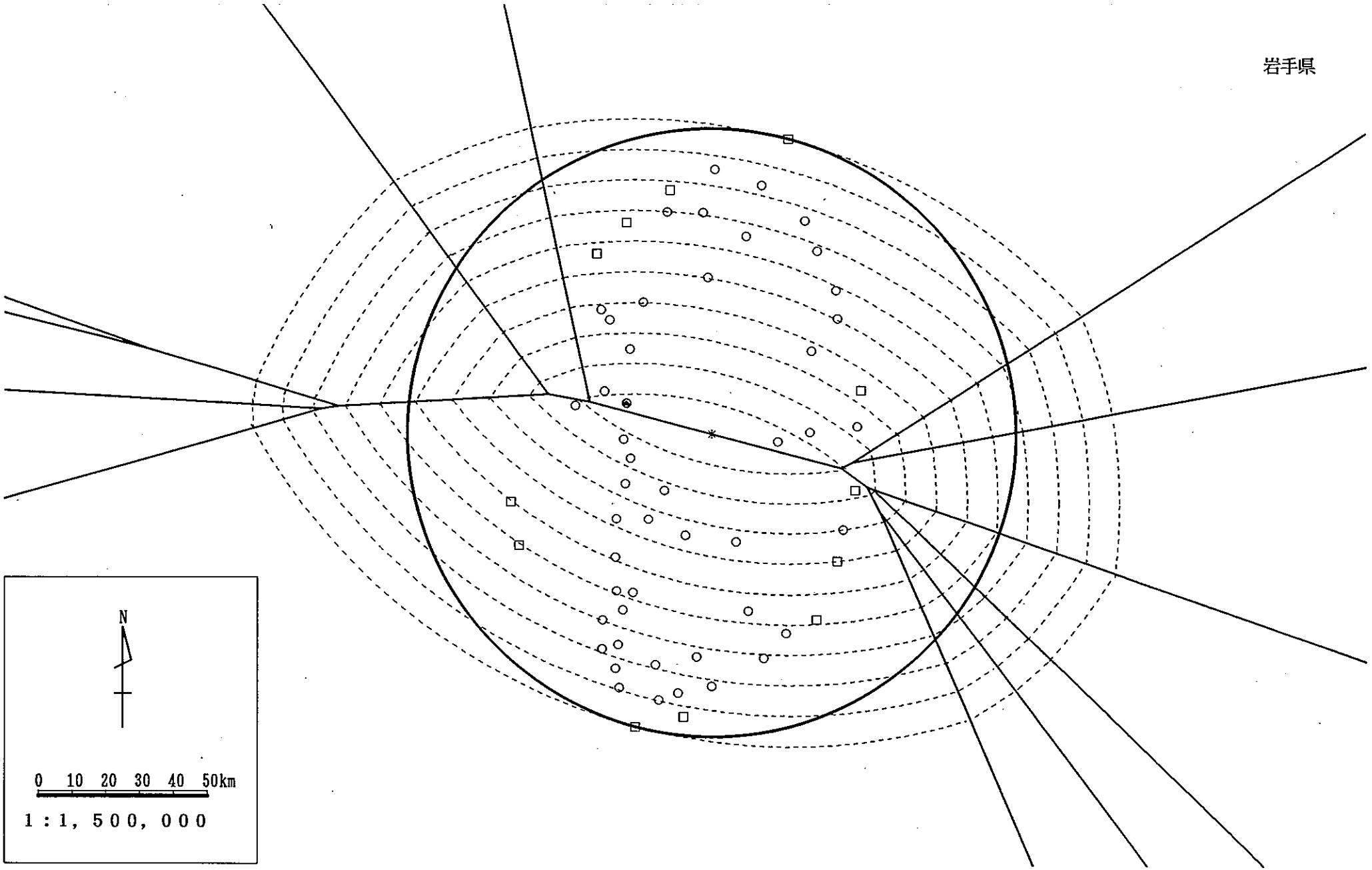

Figure B3. Contour map of the Iwate Prefecture

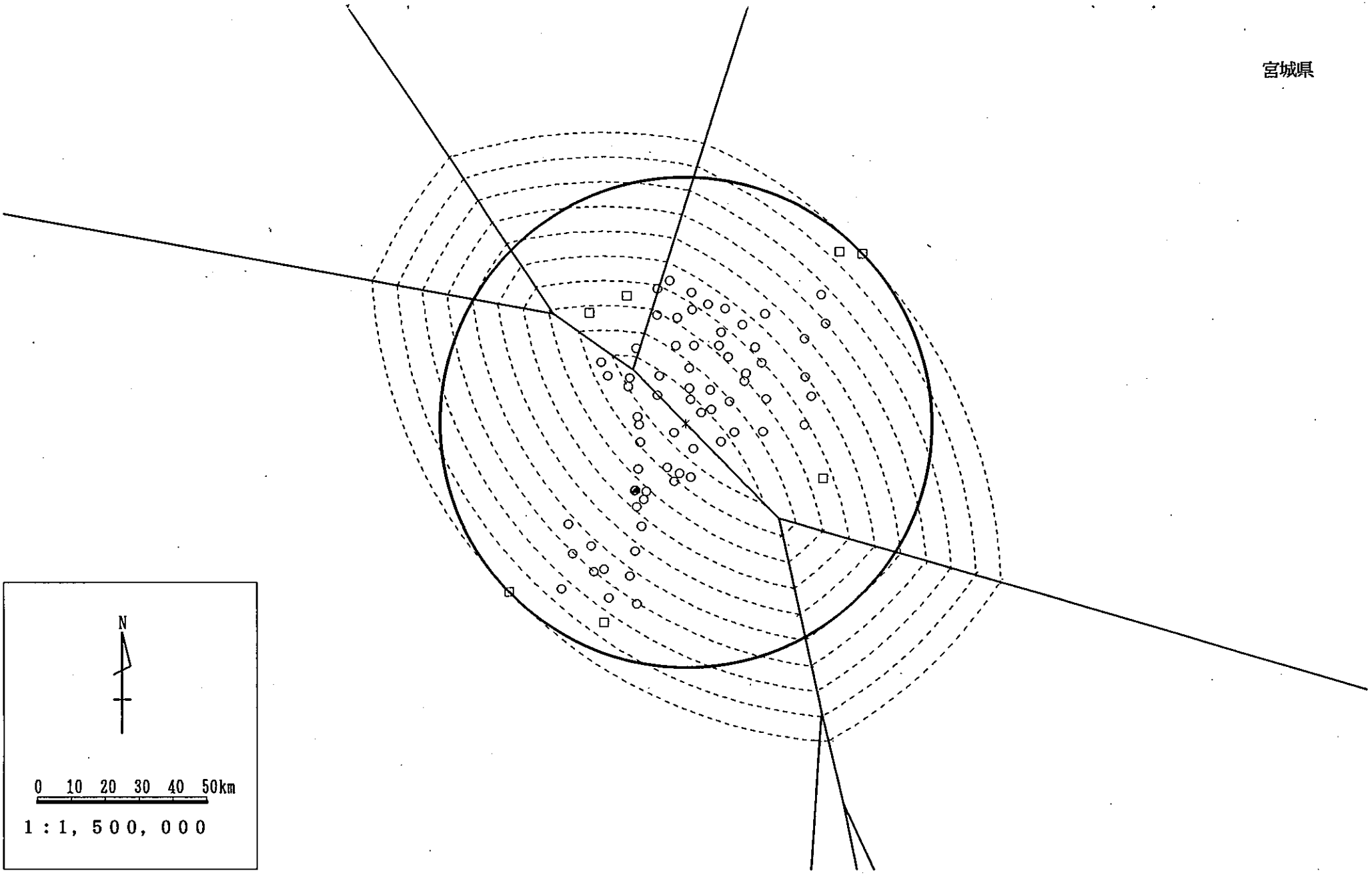

Figure B4. Contour map of the Miyagi Prefecture

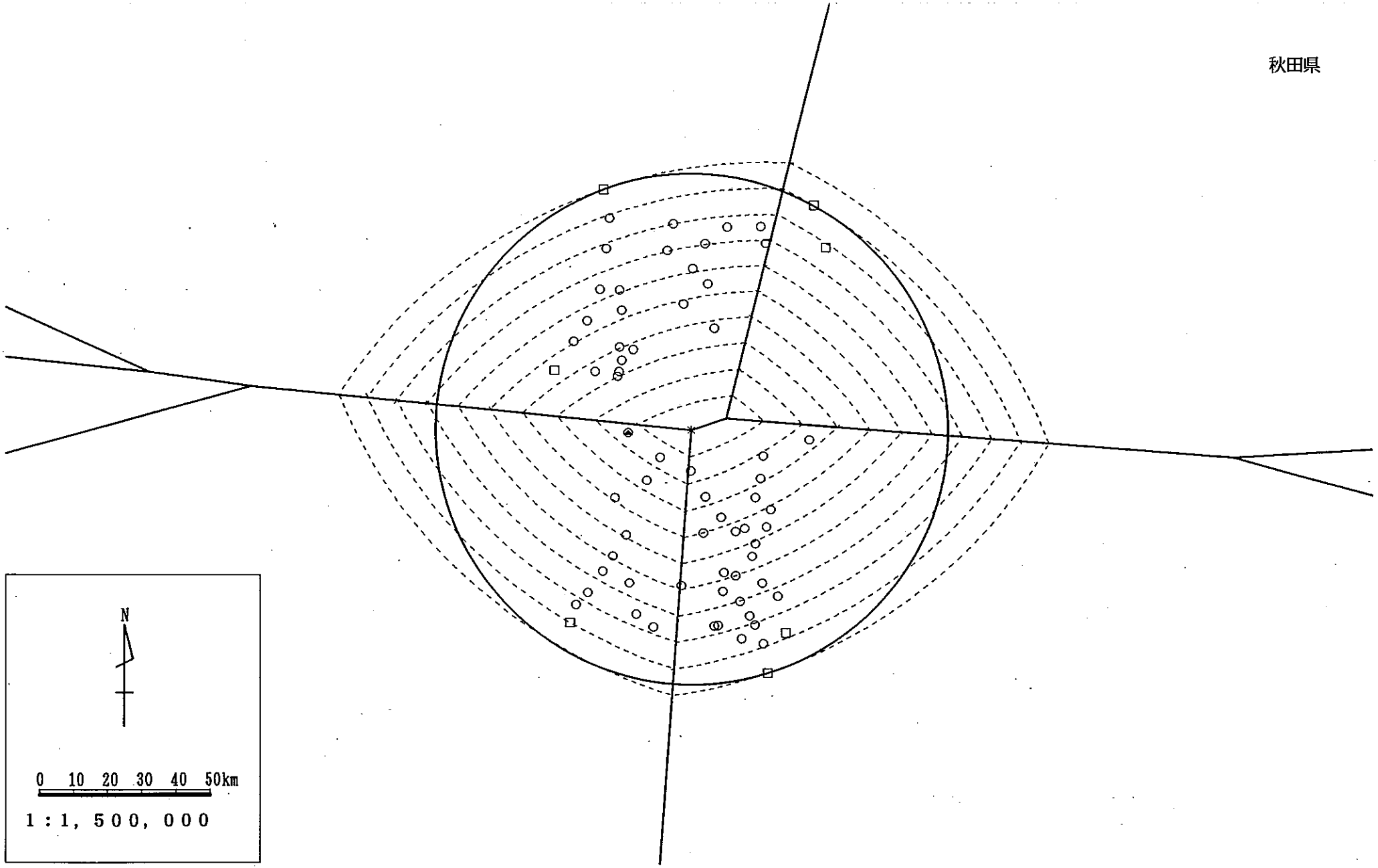

Figure B5. Contour map of the Akita Prefecture

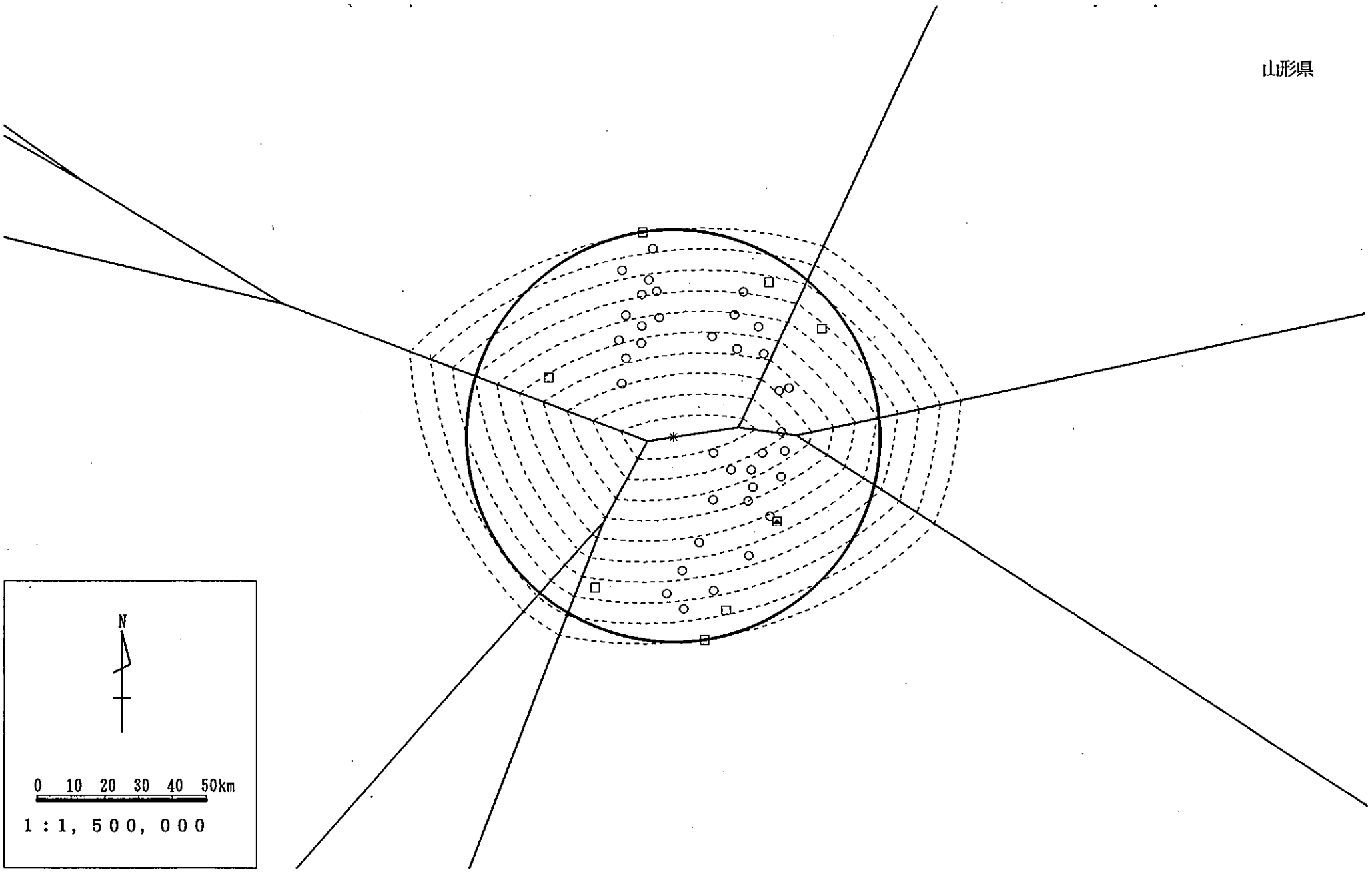

Figure B6. Contour map of the Yamagata Prefecture

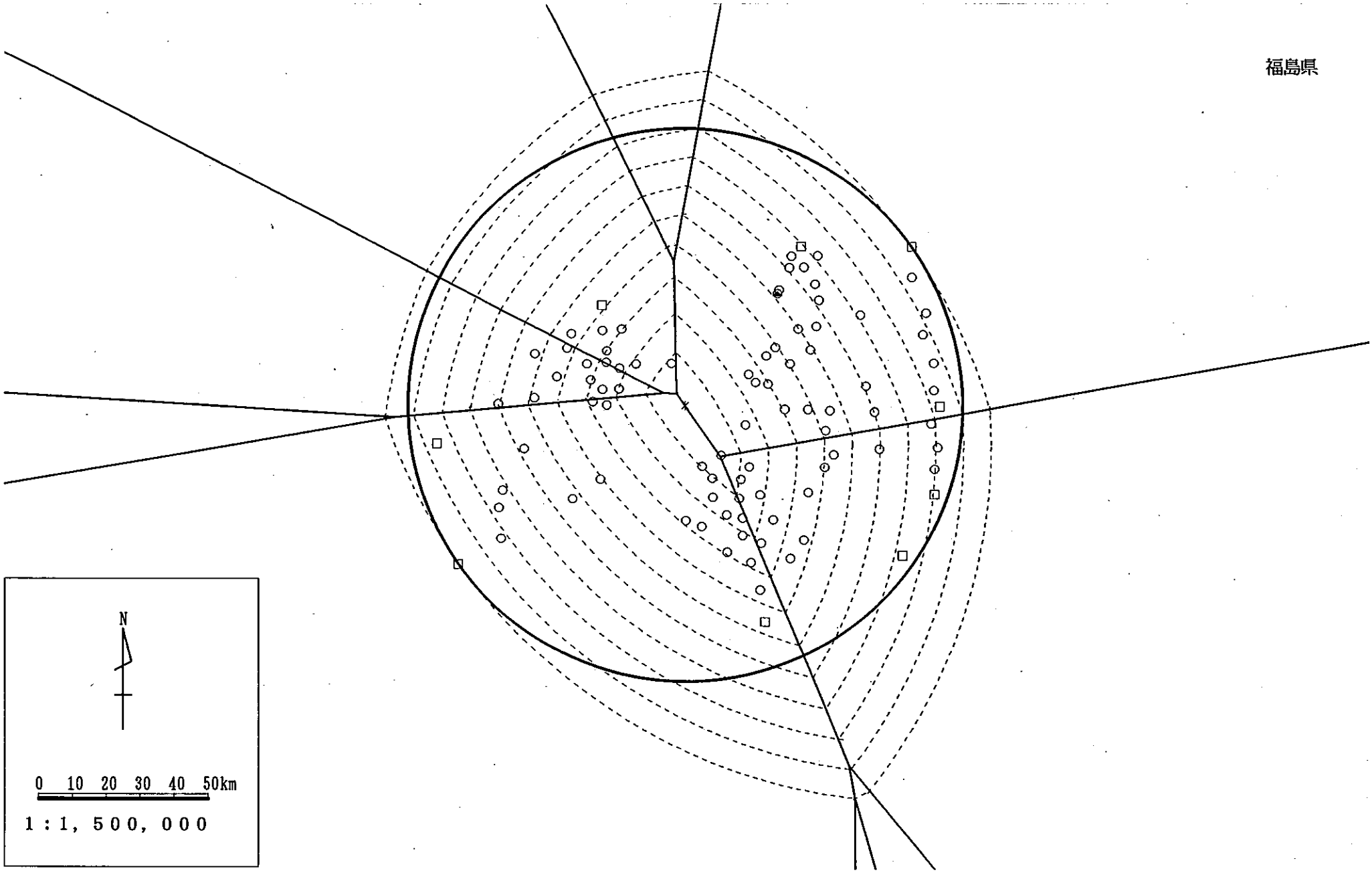

Figure B7. Contour map of the Fukushima Prefecture

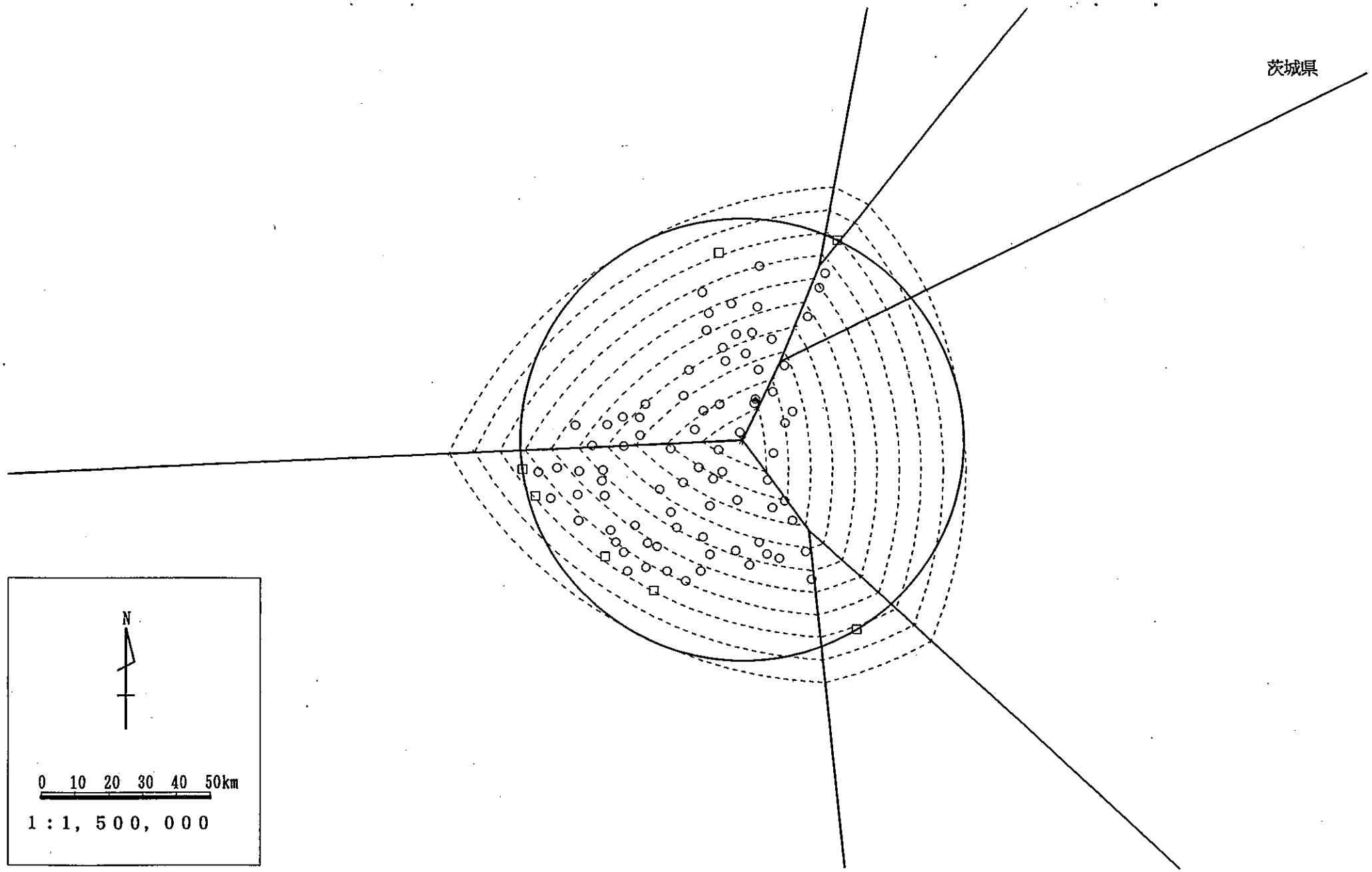

Figure B8. Contour map of the Ibaragi Prefecture

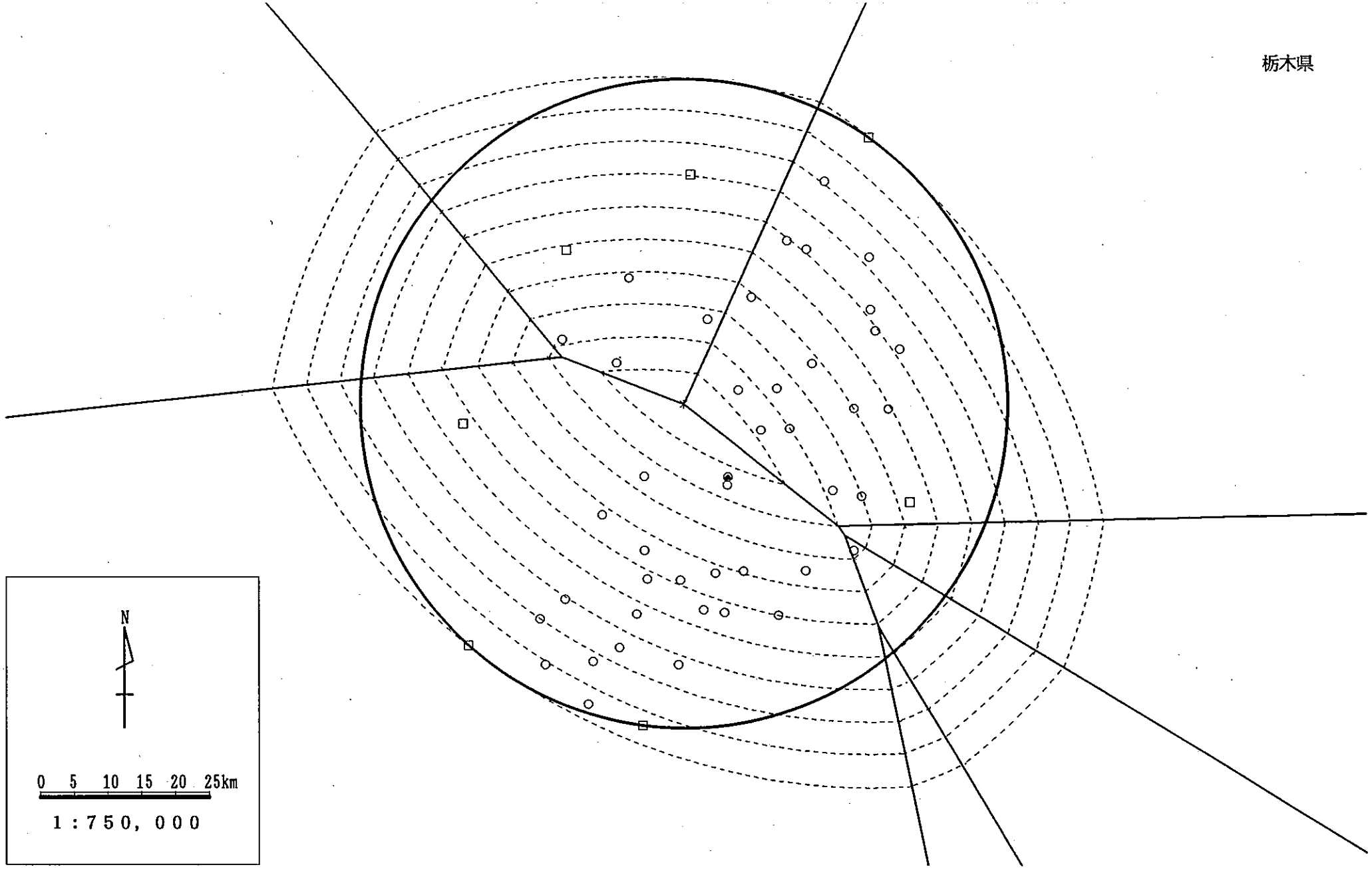

Figure B9. Contour map of the Tochigi Prefecture

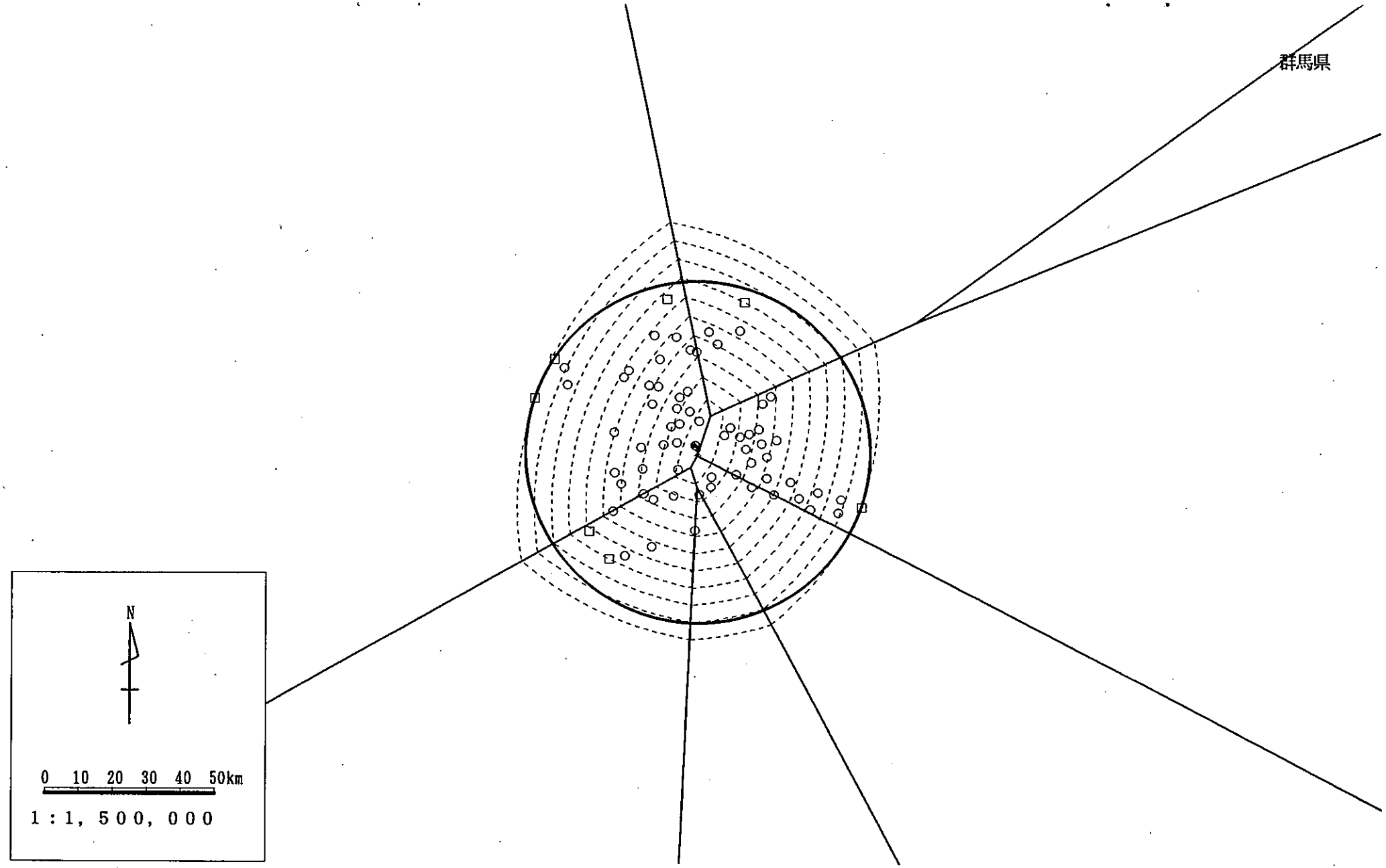

Figure B10. Contour map of the Gunma Prefecture

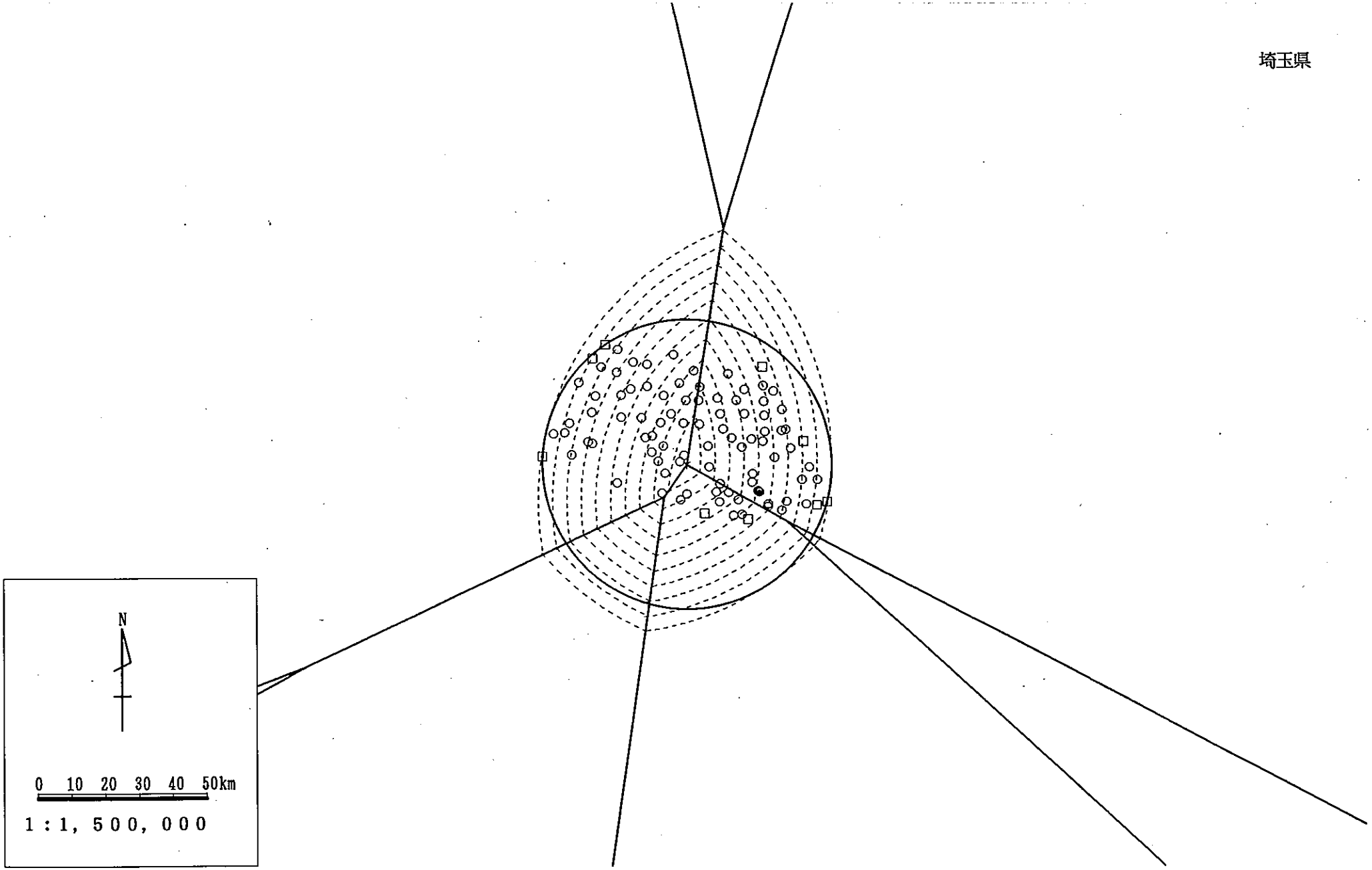

Figure B11. Contour map of the Saitama Prefecture

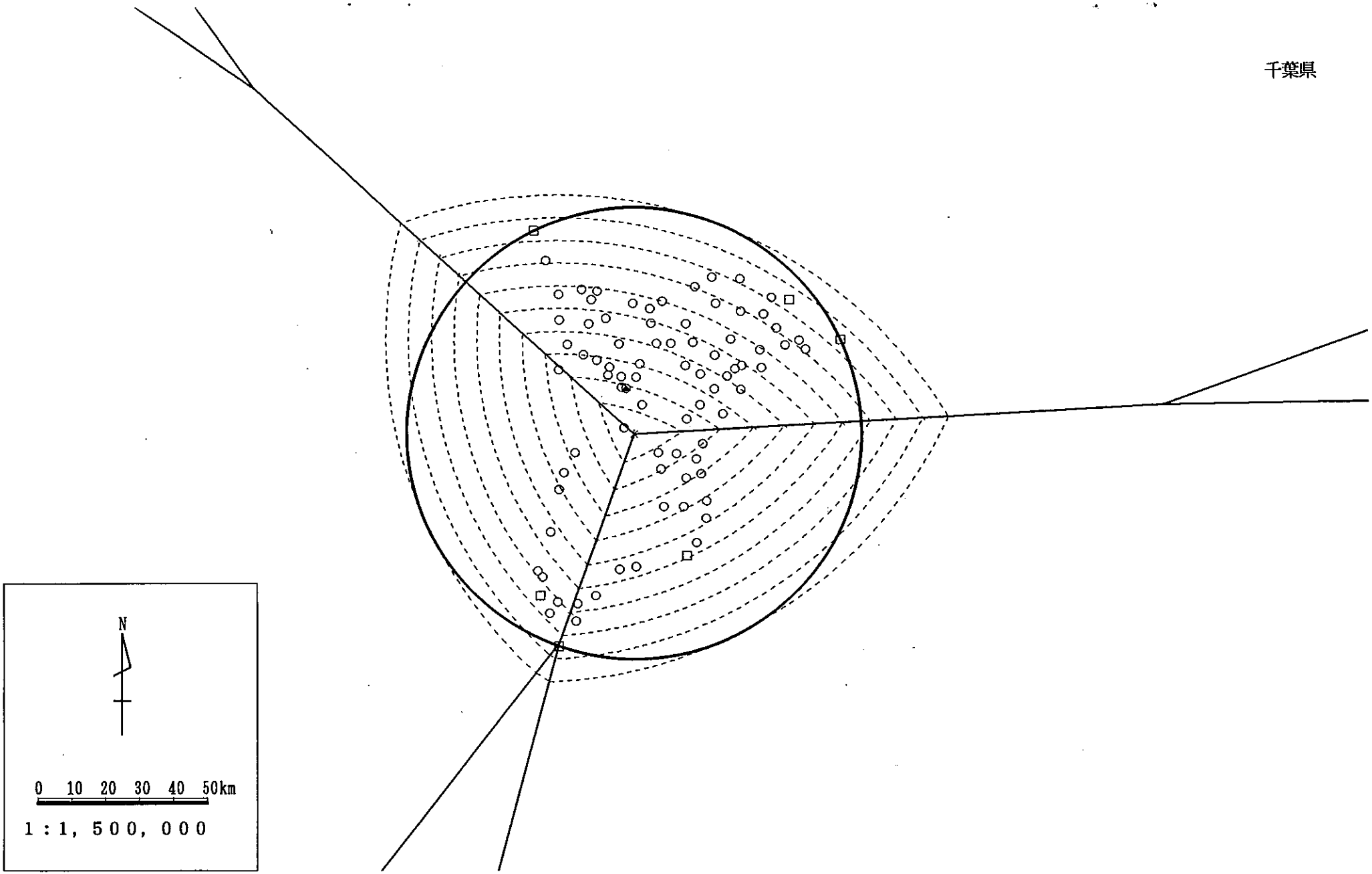

Figure B12. Contour map of the Chiba Prefecture

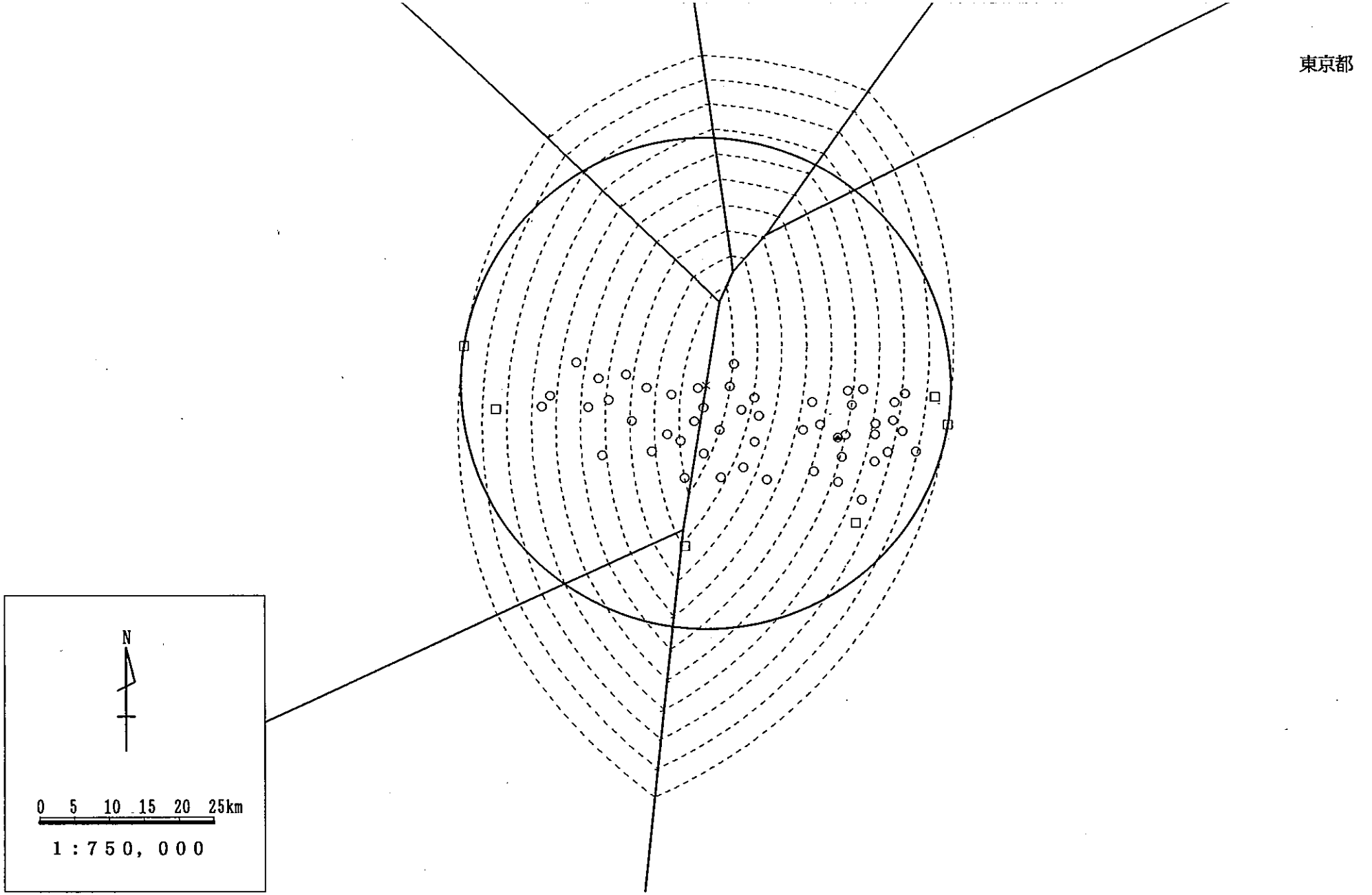

Figure B13. Contour map of the Tokyou Prefecture

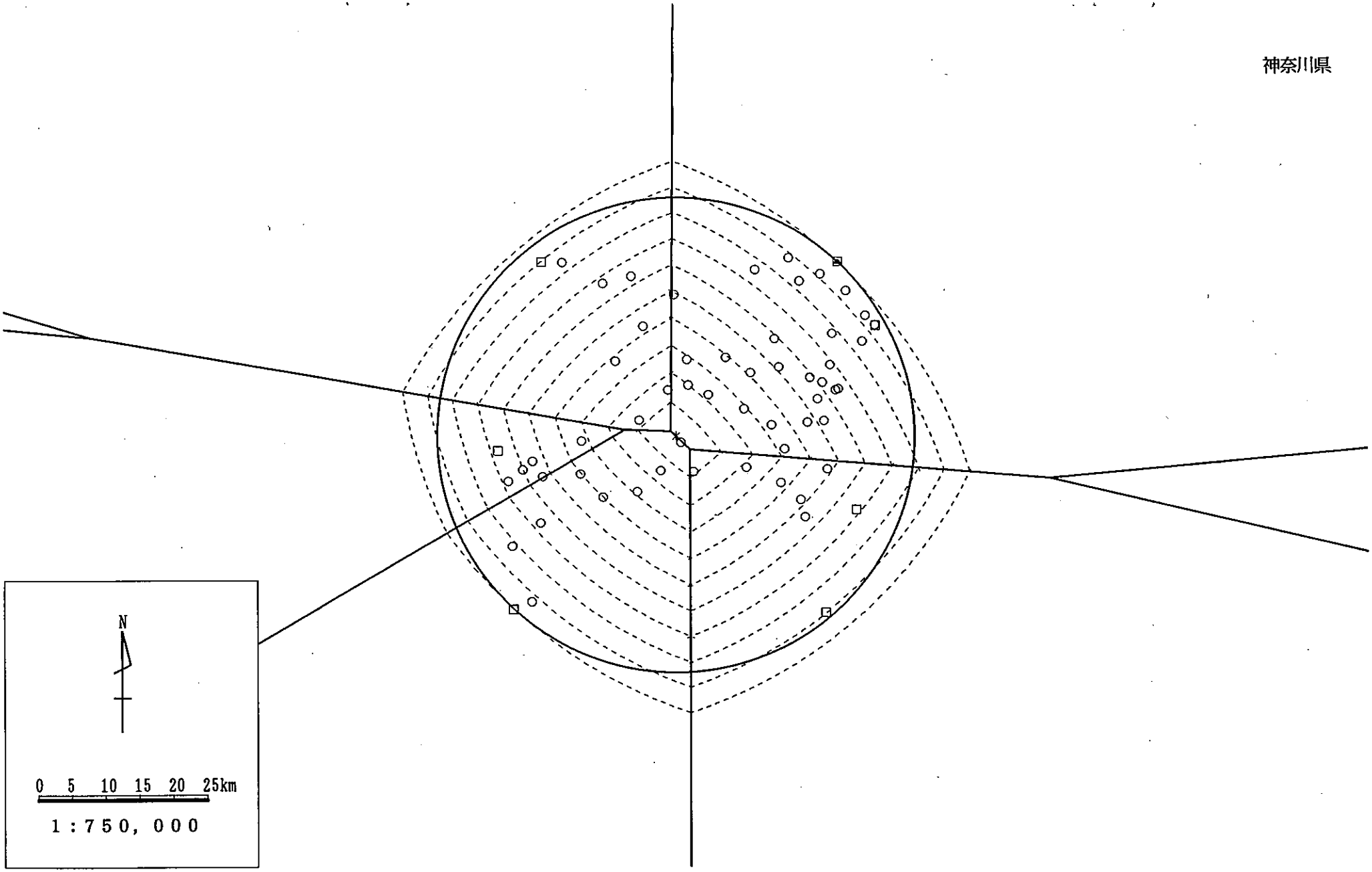

Figure B14. Contour map of the Kanagawa Prefecture

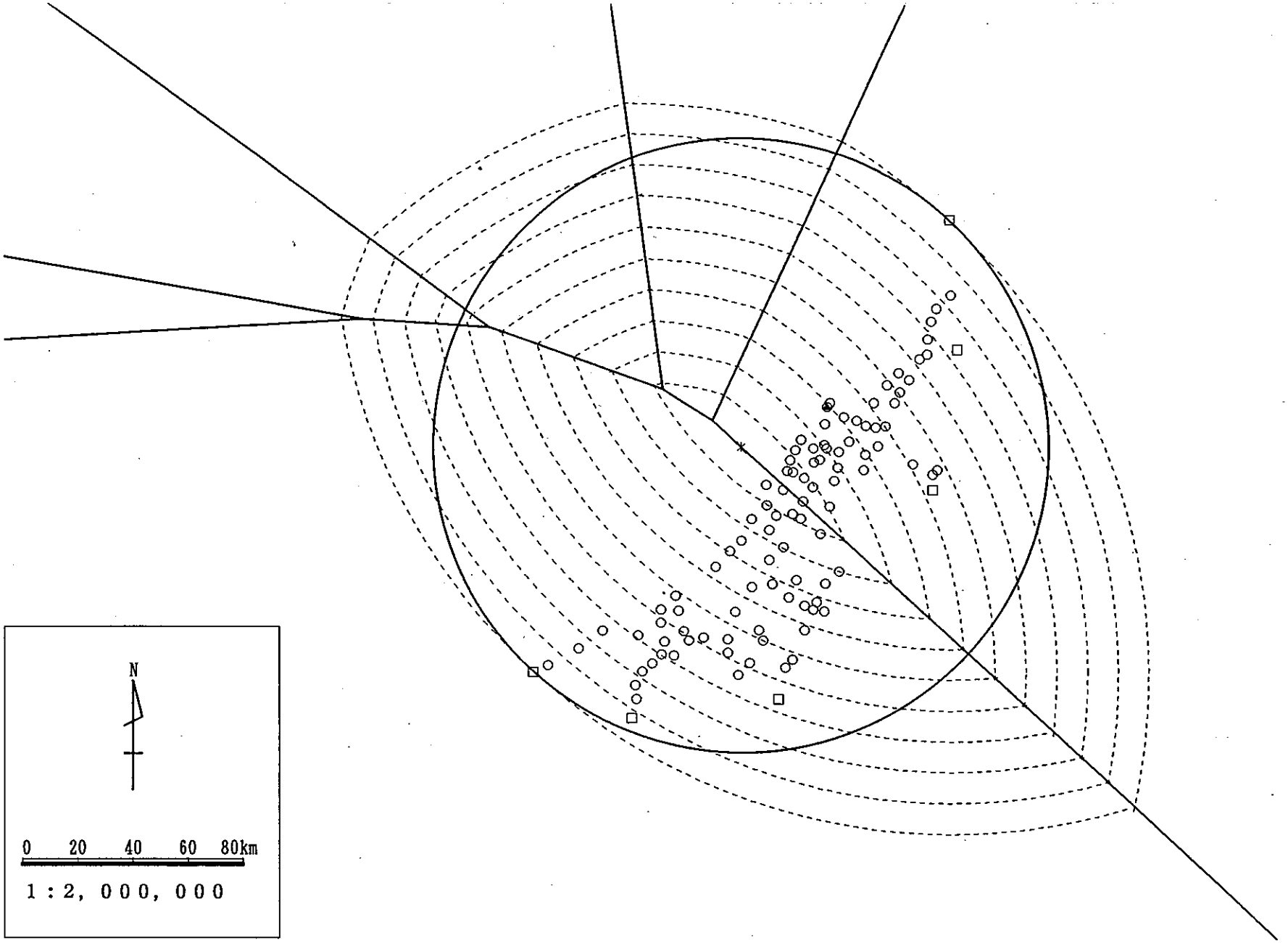

Figure B15. Contour map of the Nigata Prefecture

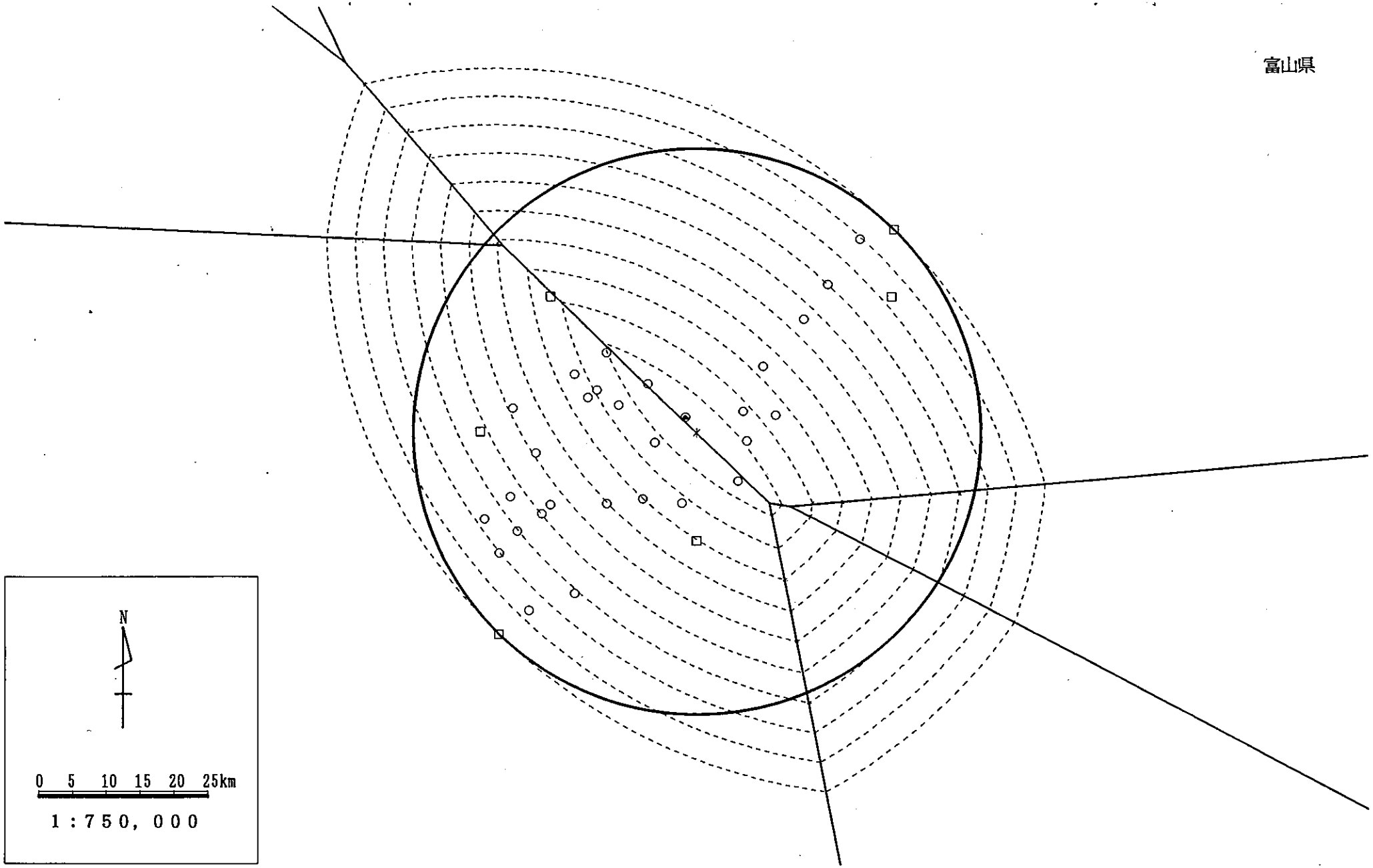

Figure B16. Contour map of the Toyama Prefecture

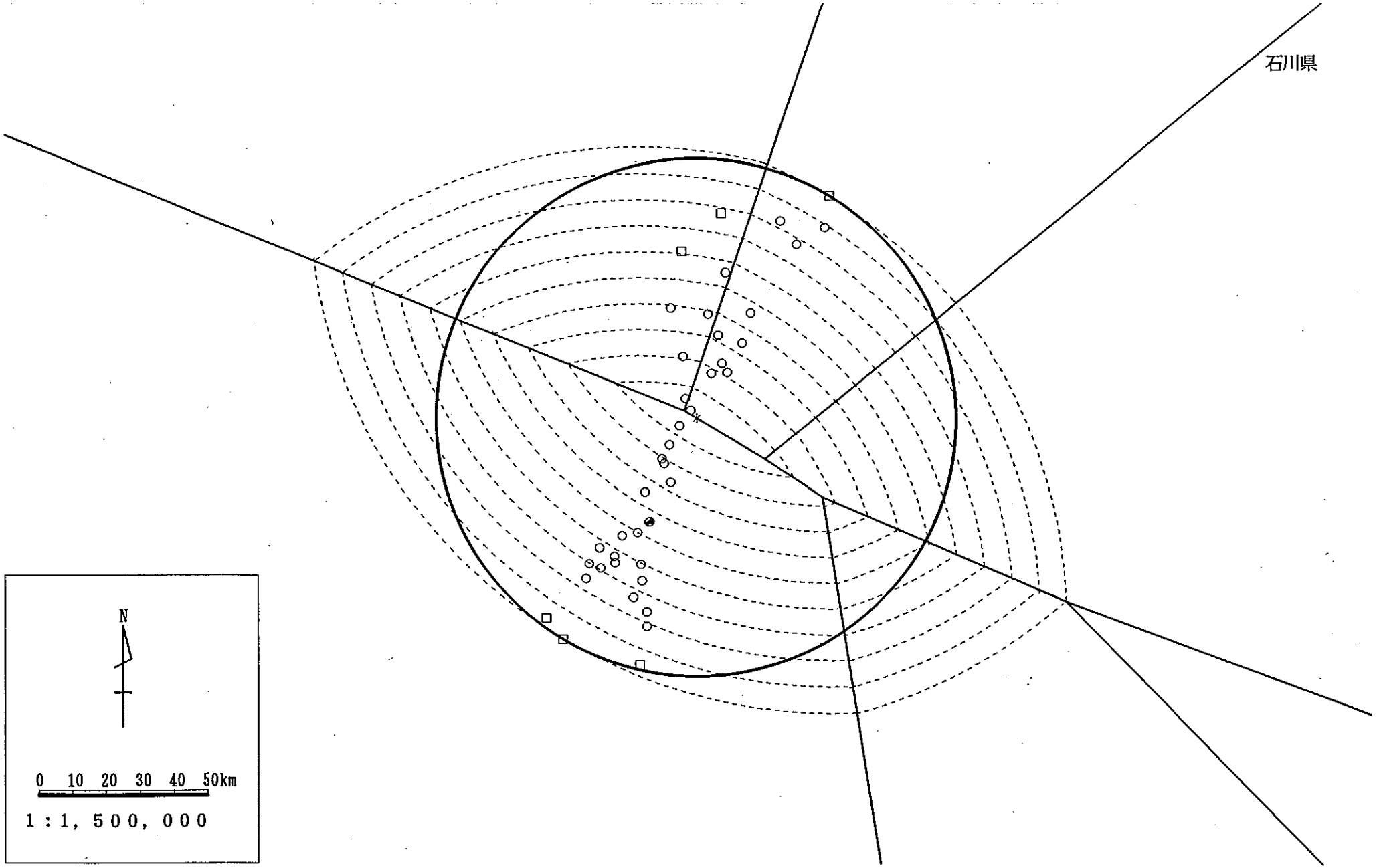

Figure B17. Contour map of the Ishikawa Prefecture

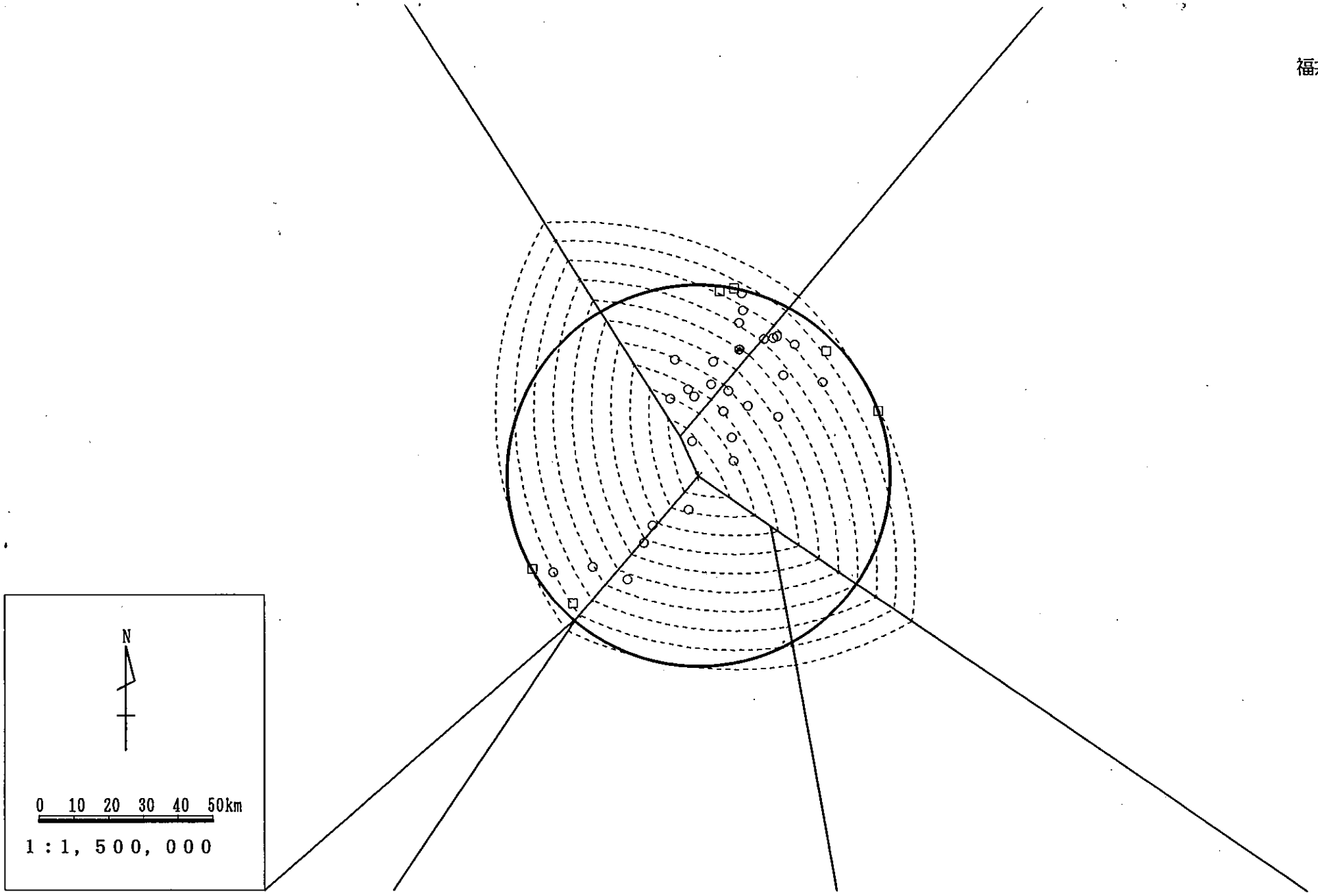

Figure B18. Contour map of the Fukui Prefecture

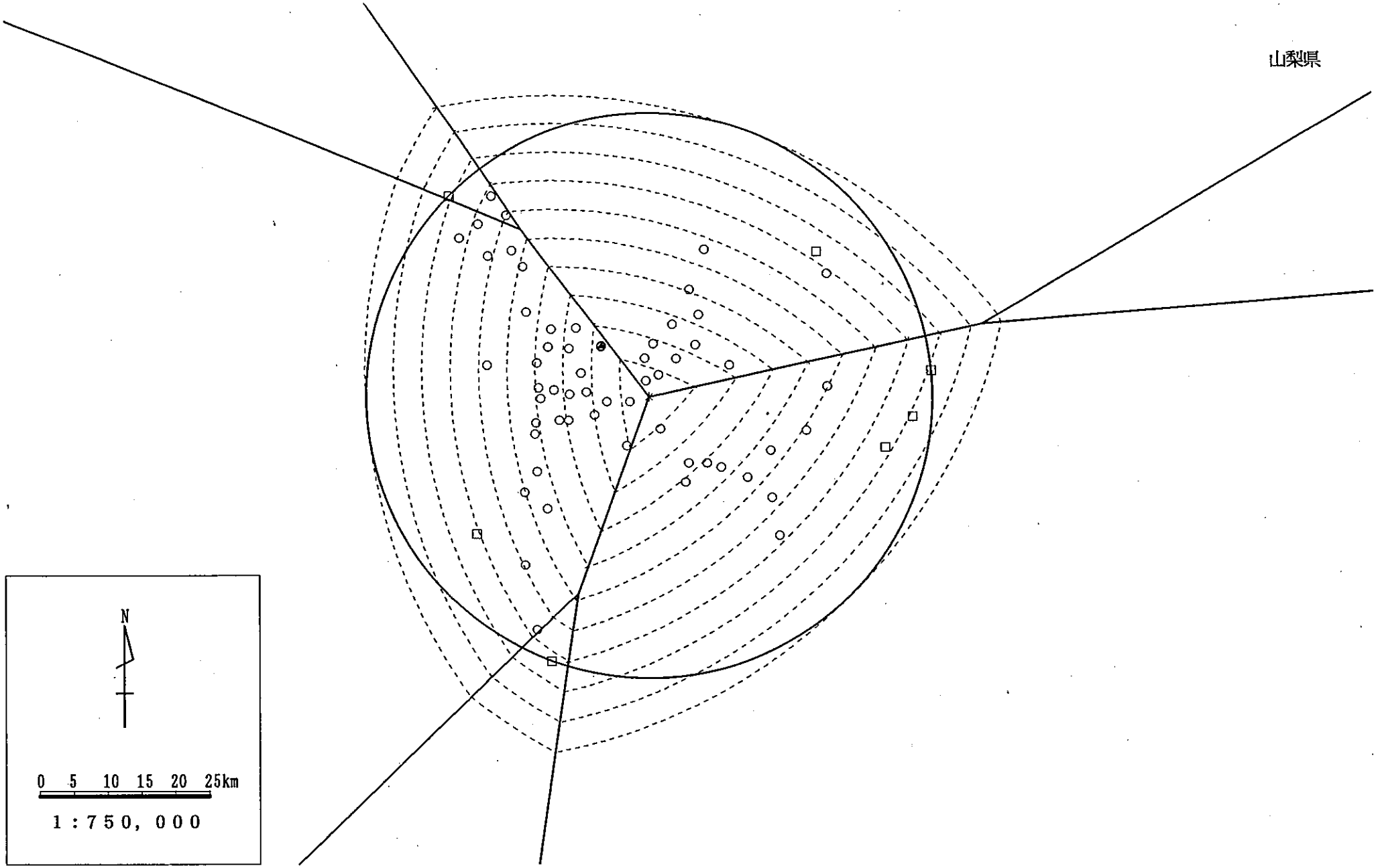

Figure B19. Contour map of the Yamanashi Prefecture

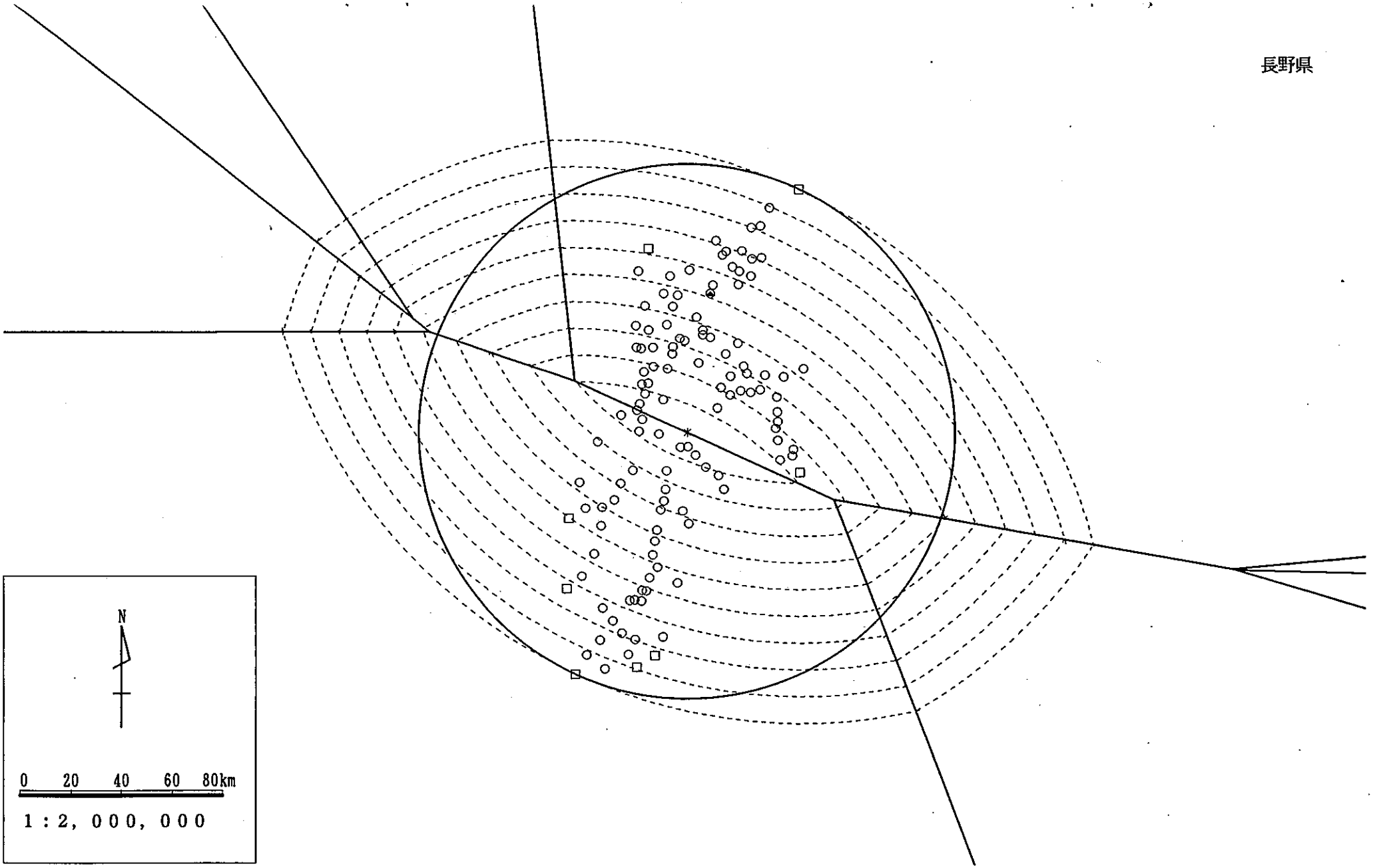

Figure B20. Contour map of the Nagano Prefecture

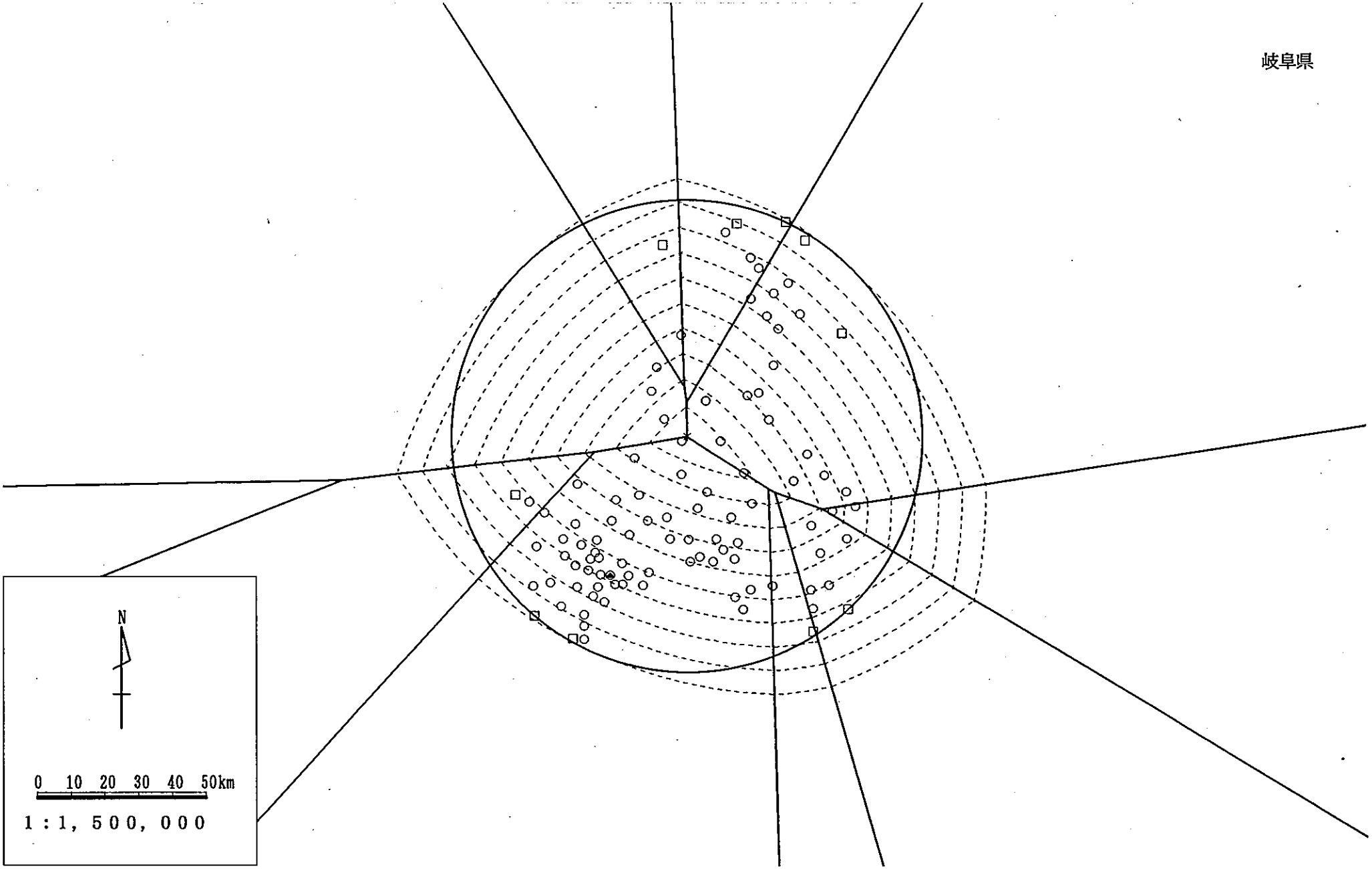

Figure B21. Contour map of the Gifu Prefecture

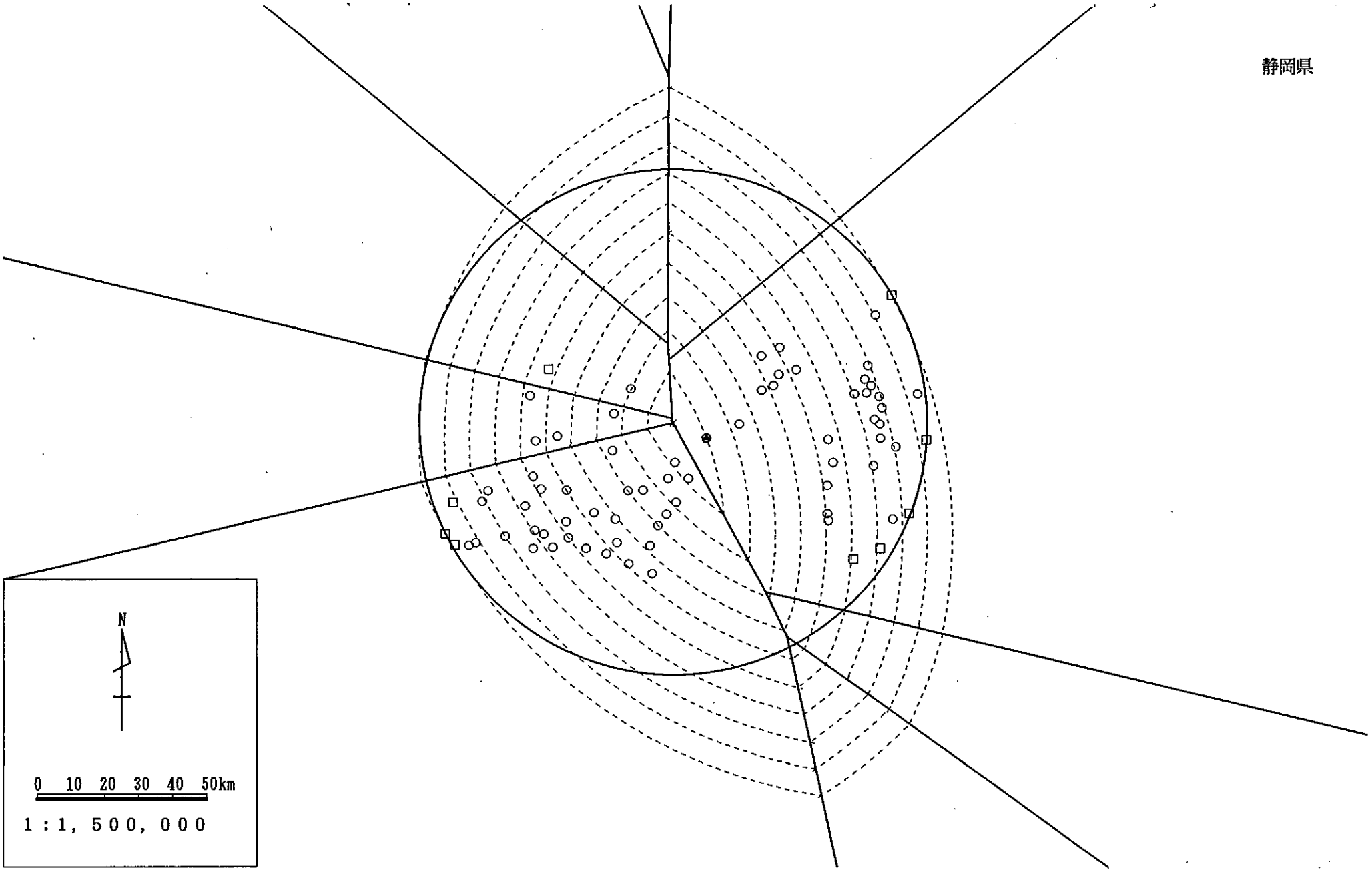

Figure B22. Contour map of the Shizuoka Prefecture

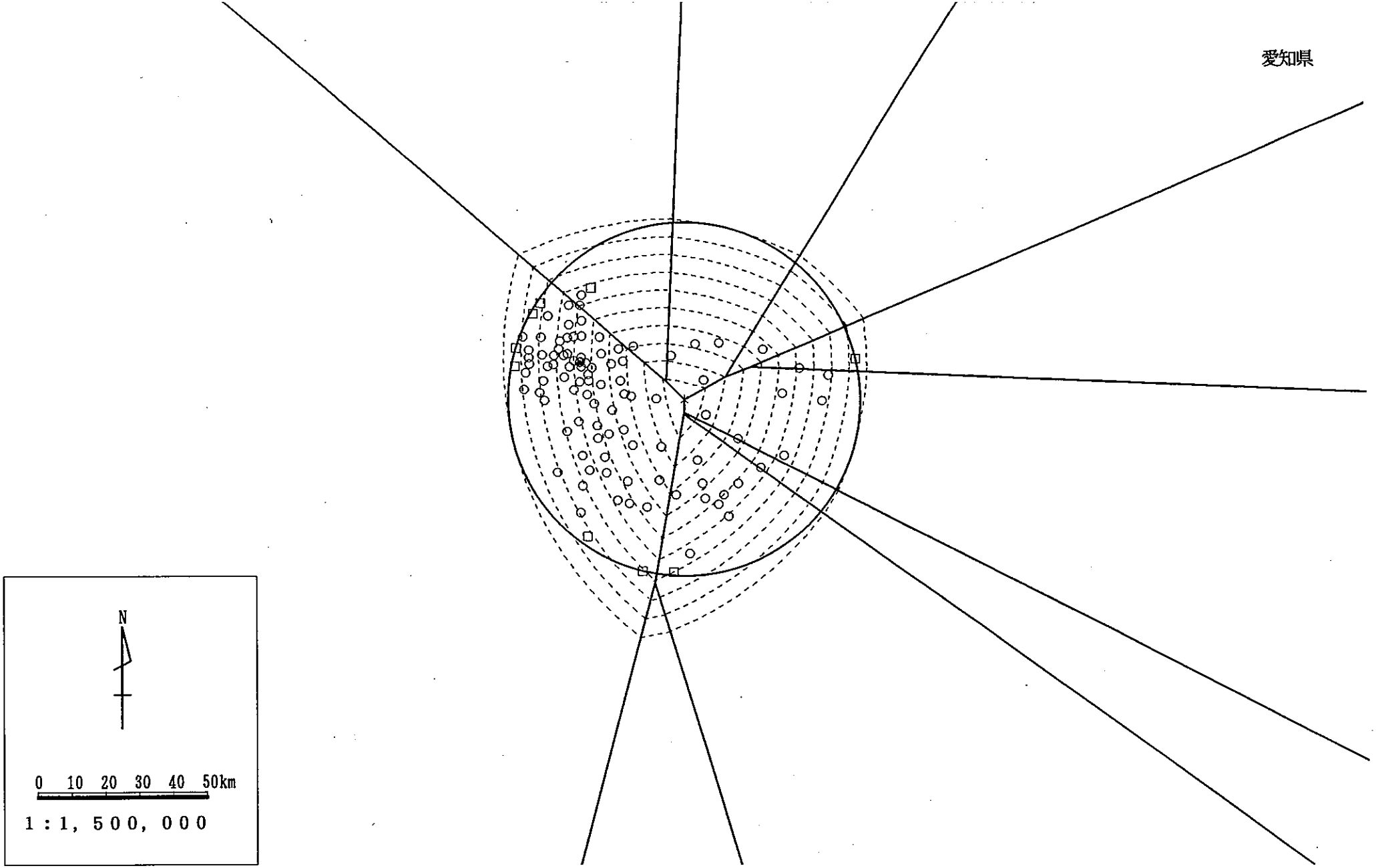

Figure B23. Contour map of the Aichi Prefecture

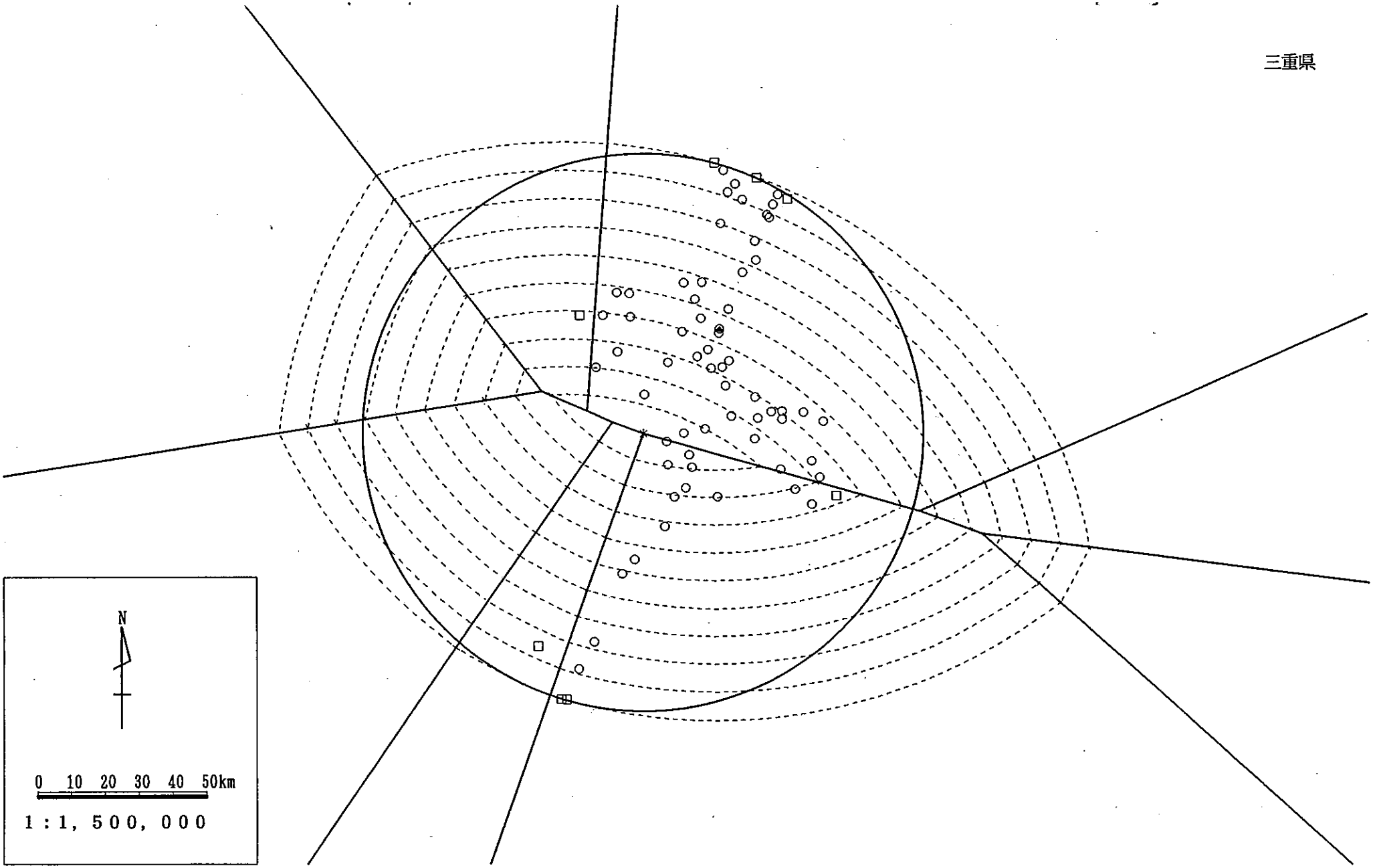

Figure B24. Contour map of the Mie Prefecture

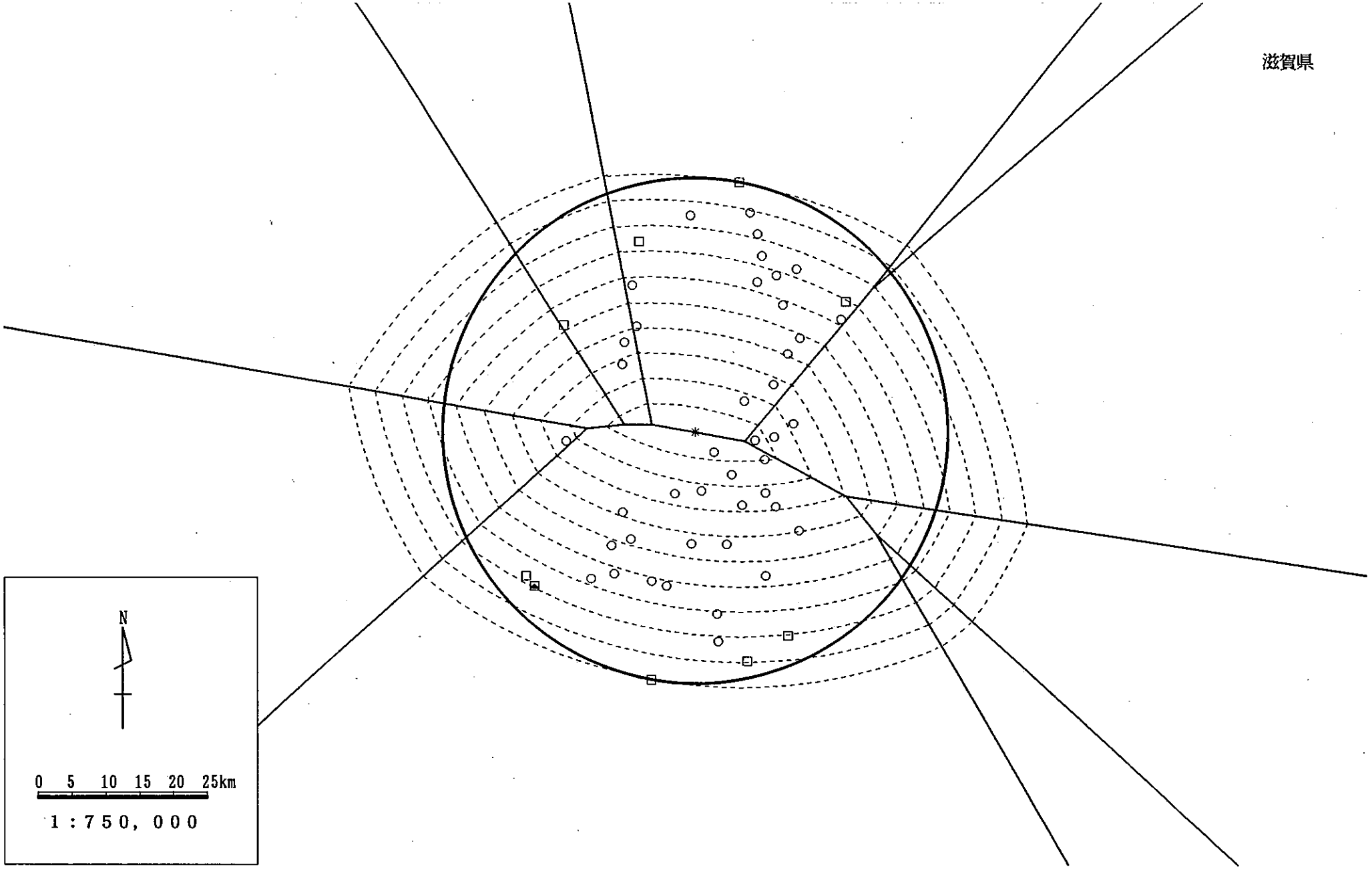

Figure B25. Contour map of the Shiga Prefecture

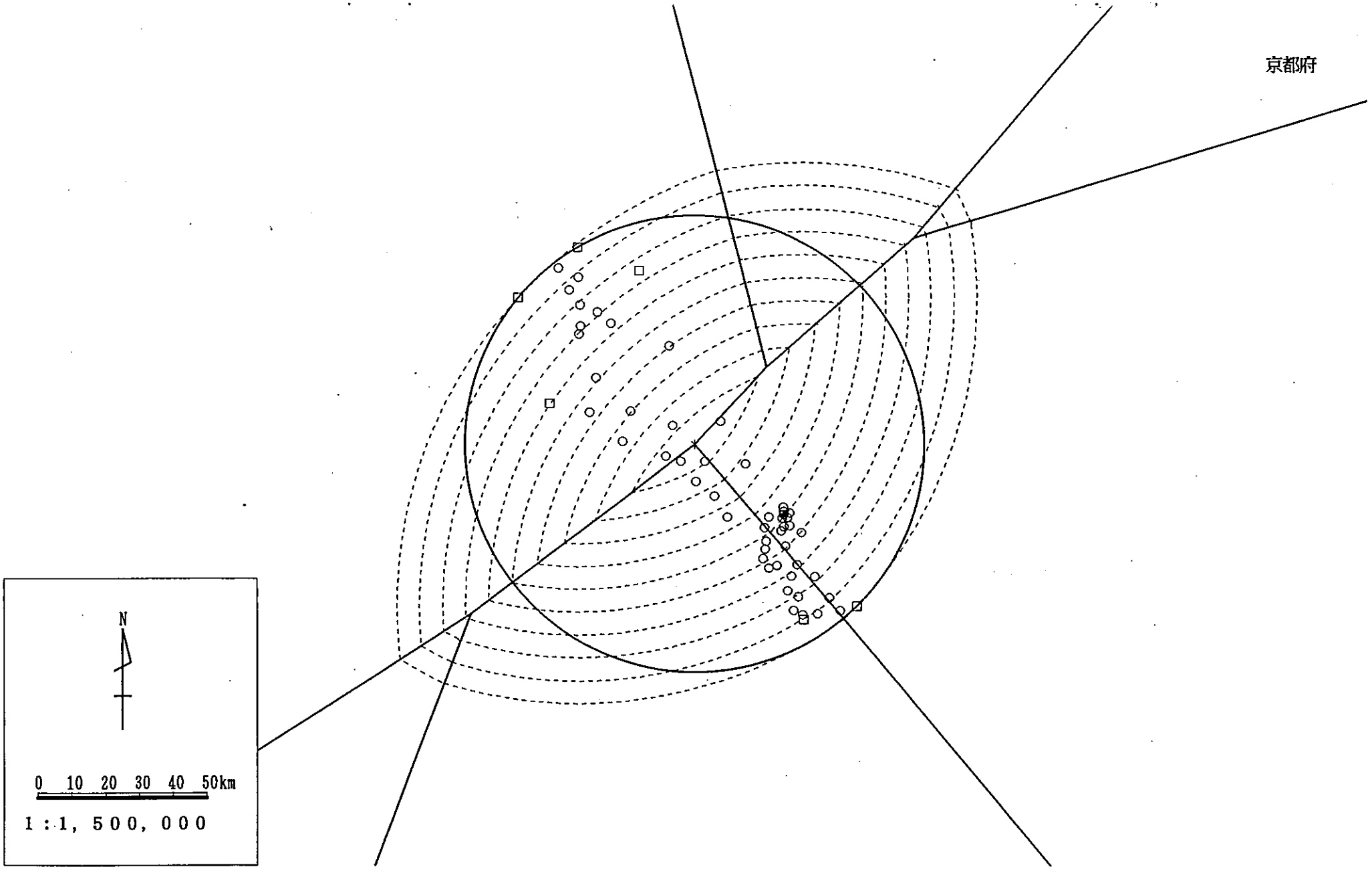

Figure B26. Contour map of the Kyoto Prefecture

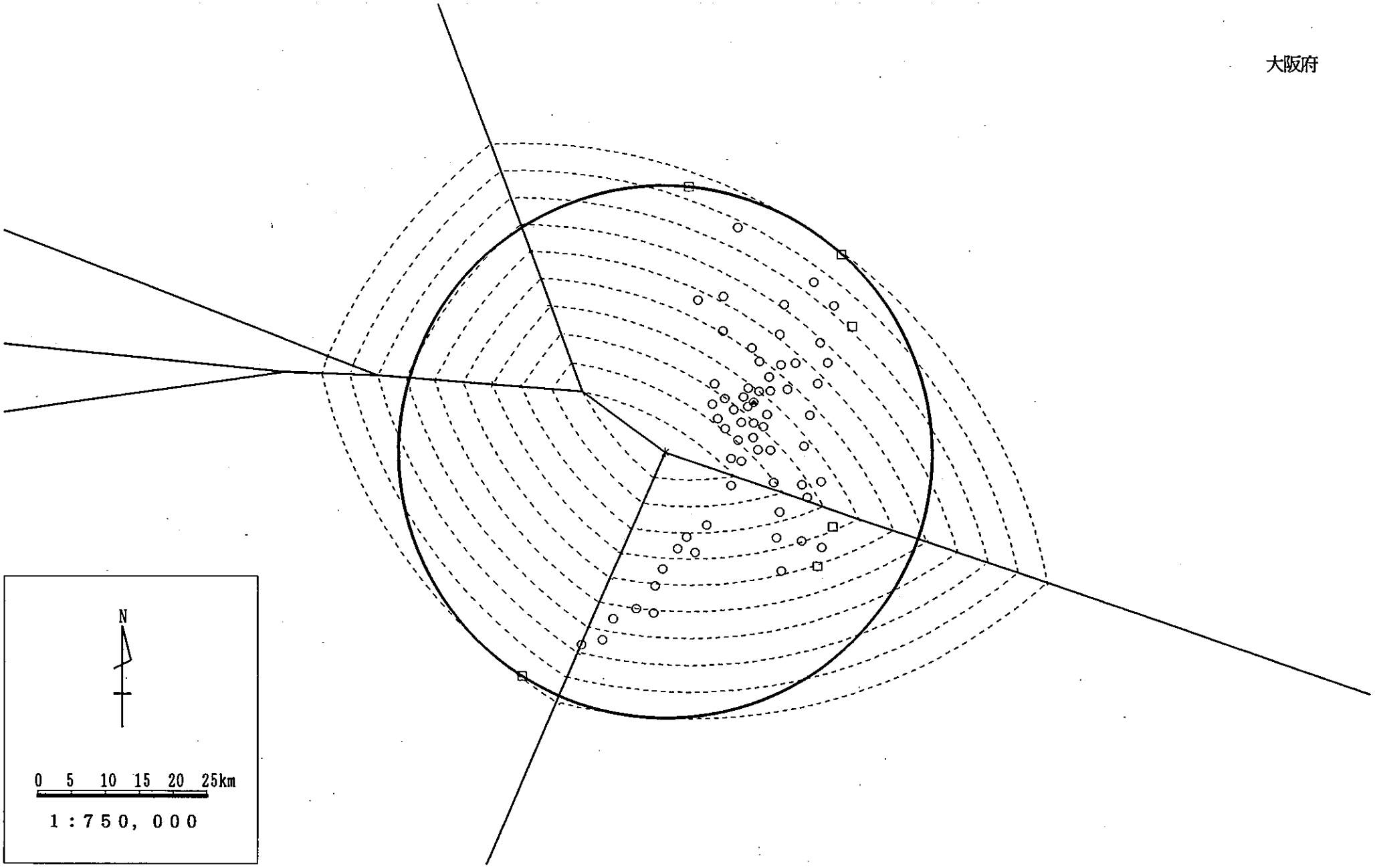

Figure B27. Contour map of the Osaka Prefecture

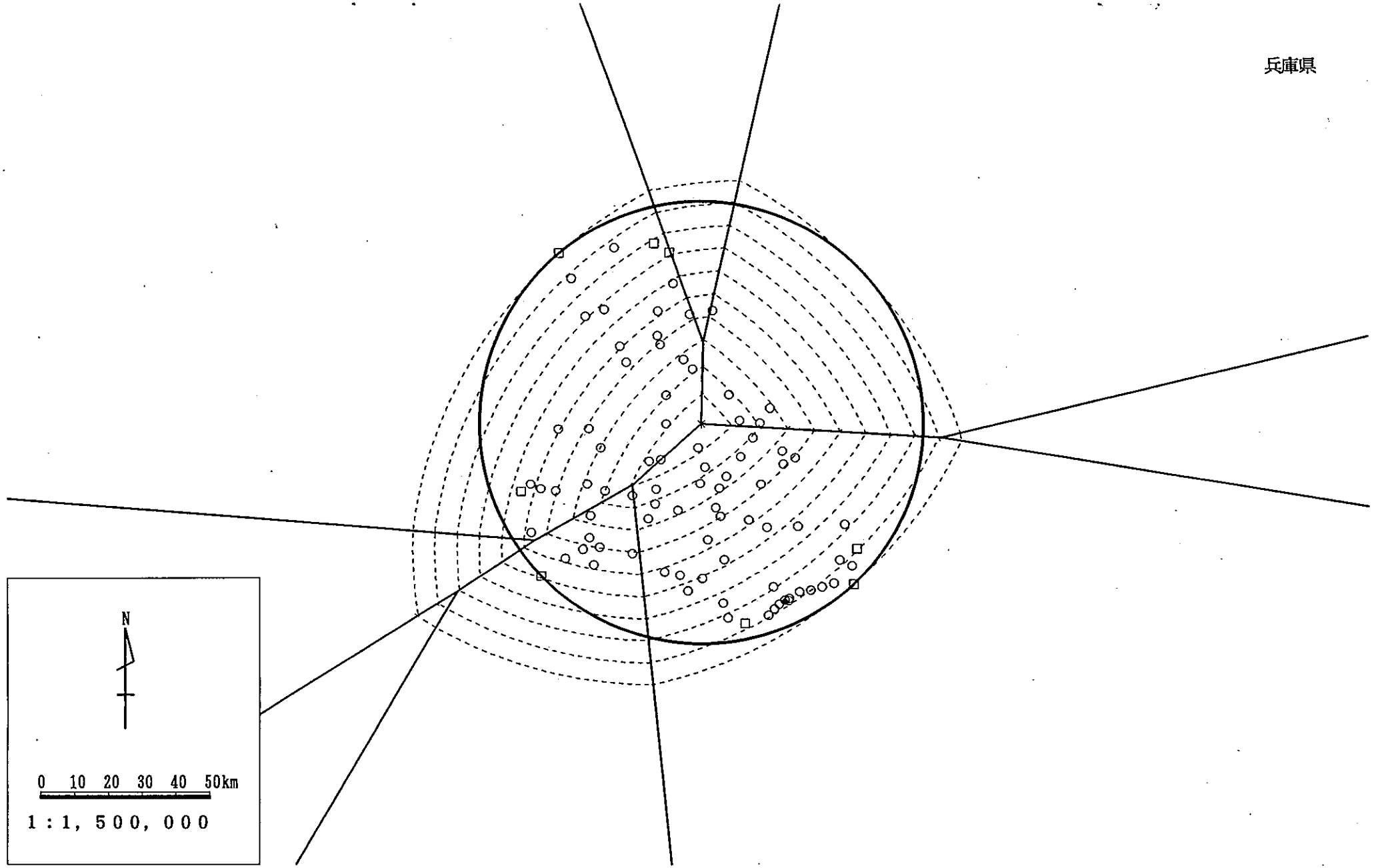

Figure B28. Contour map of the Hyogo Prefecture

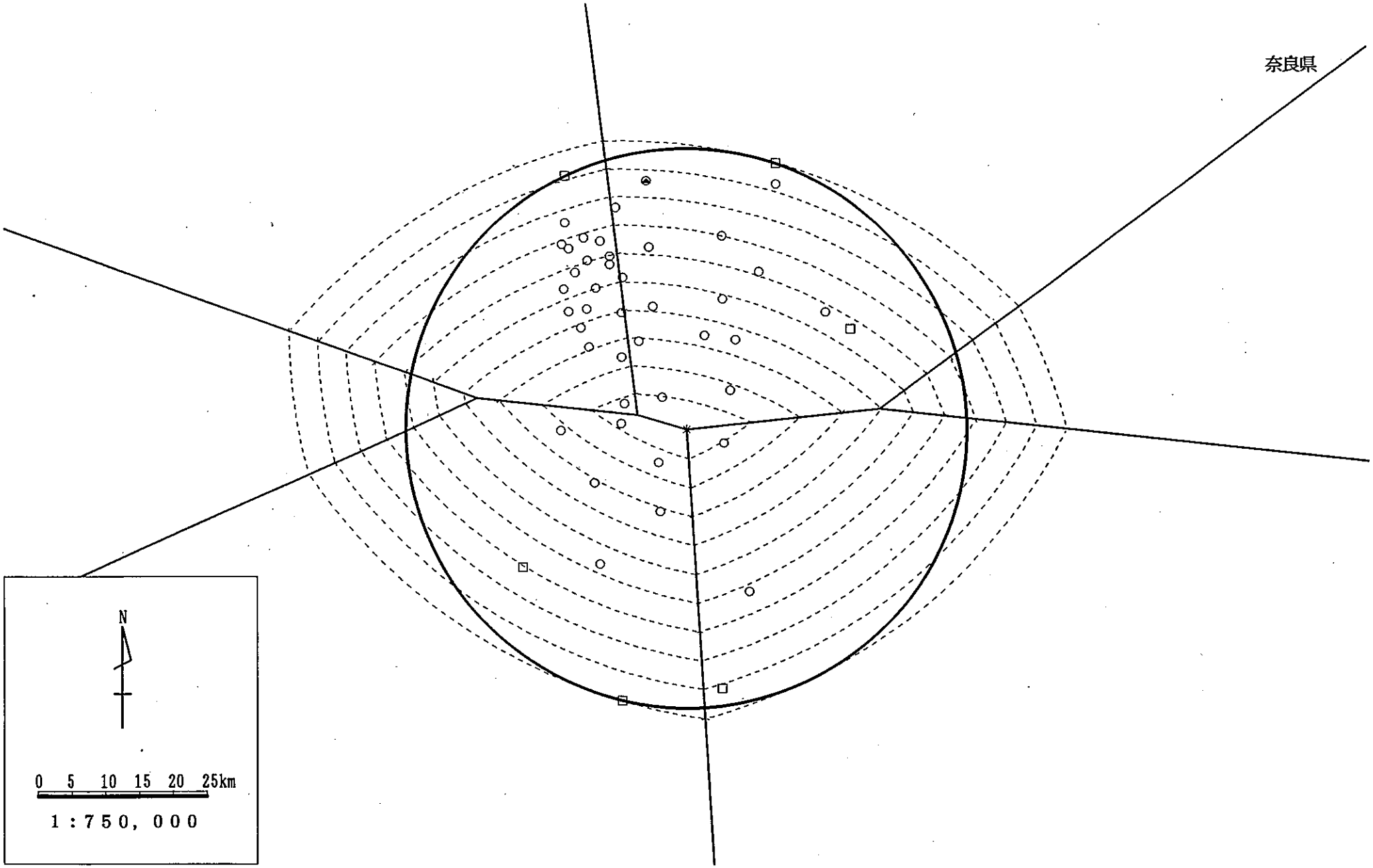

Figure B29. Contour map of the Nara Prefecture

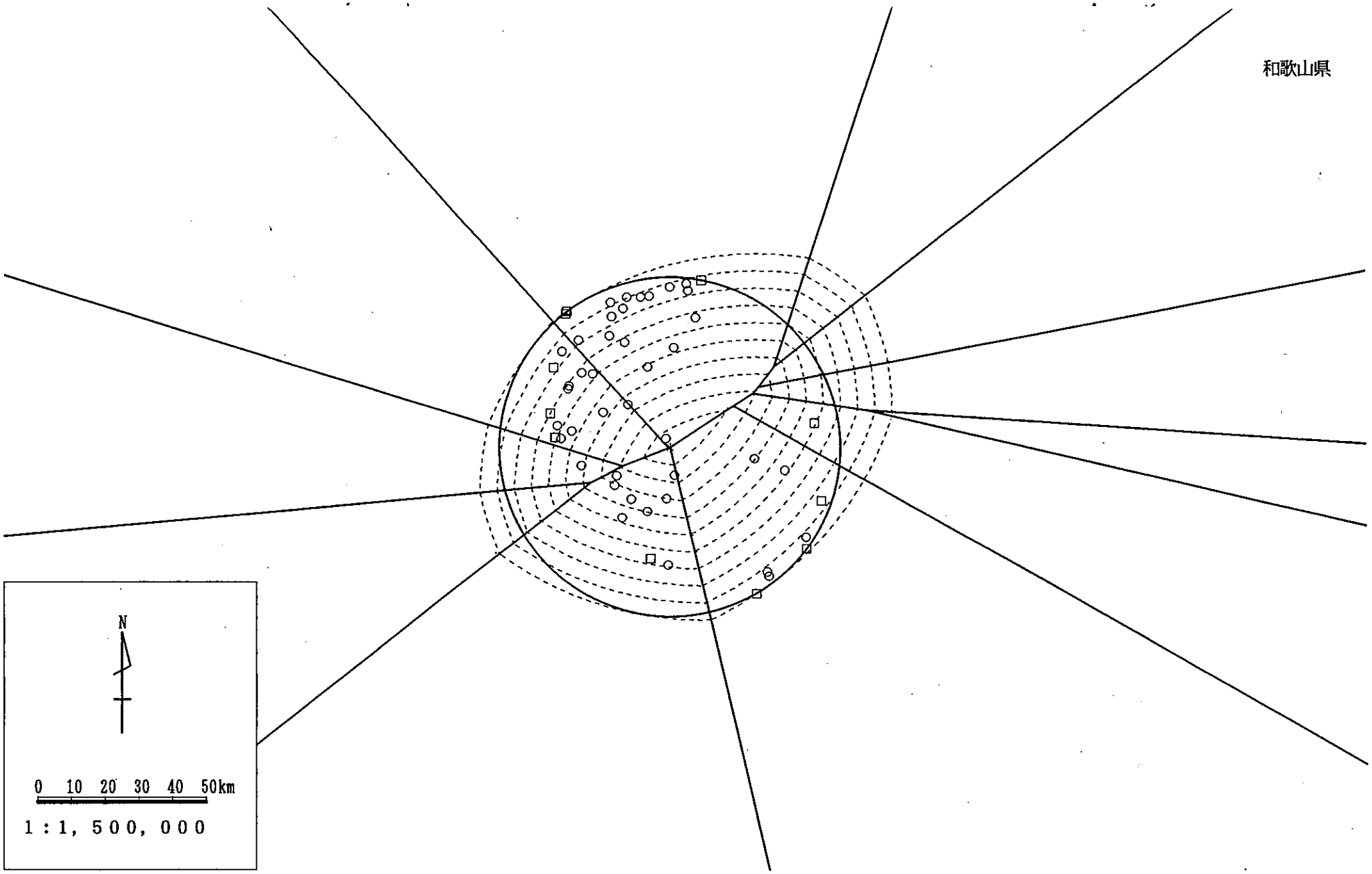

Figure B30. Contour map of the Wakayama Prefecture

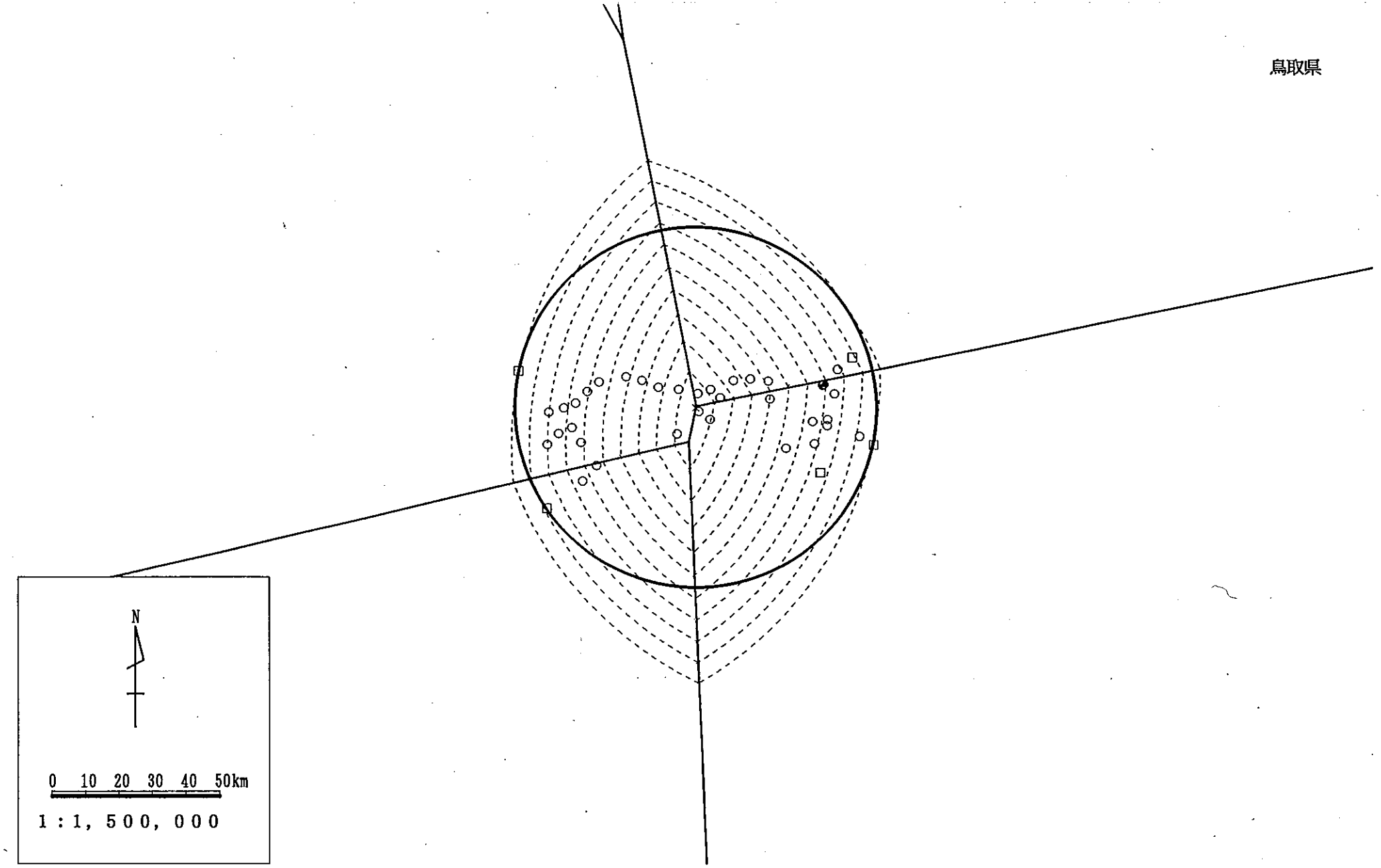

Figure B31. Contour map of the Tottori Prefecture

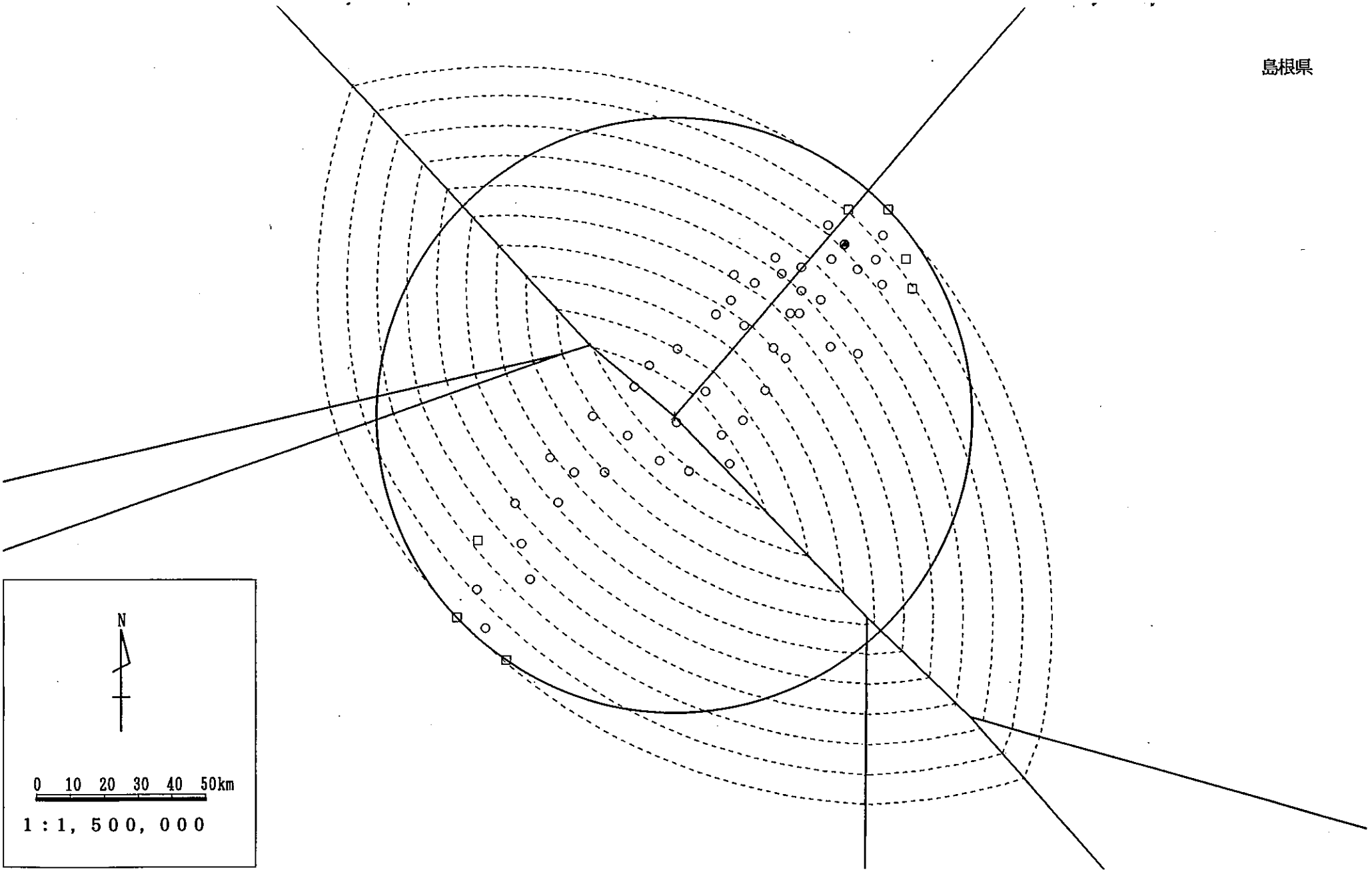

Figure B32. Contour map of the Shimane Prefecture

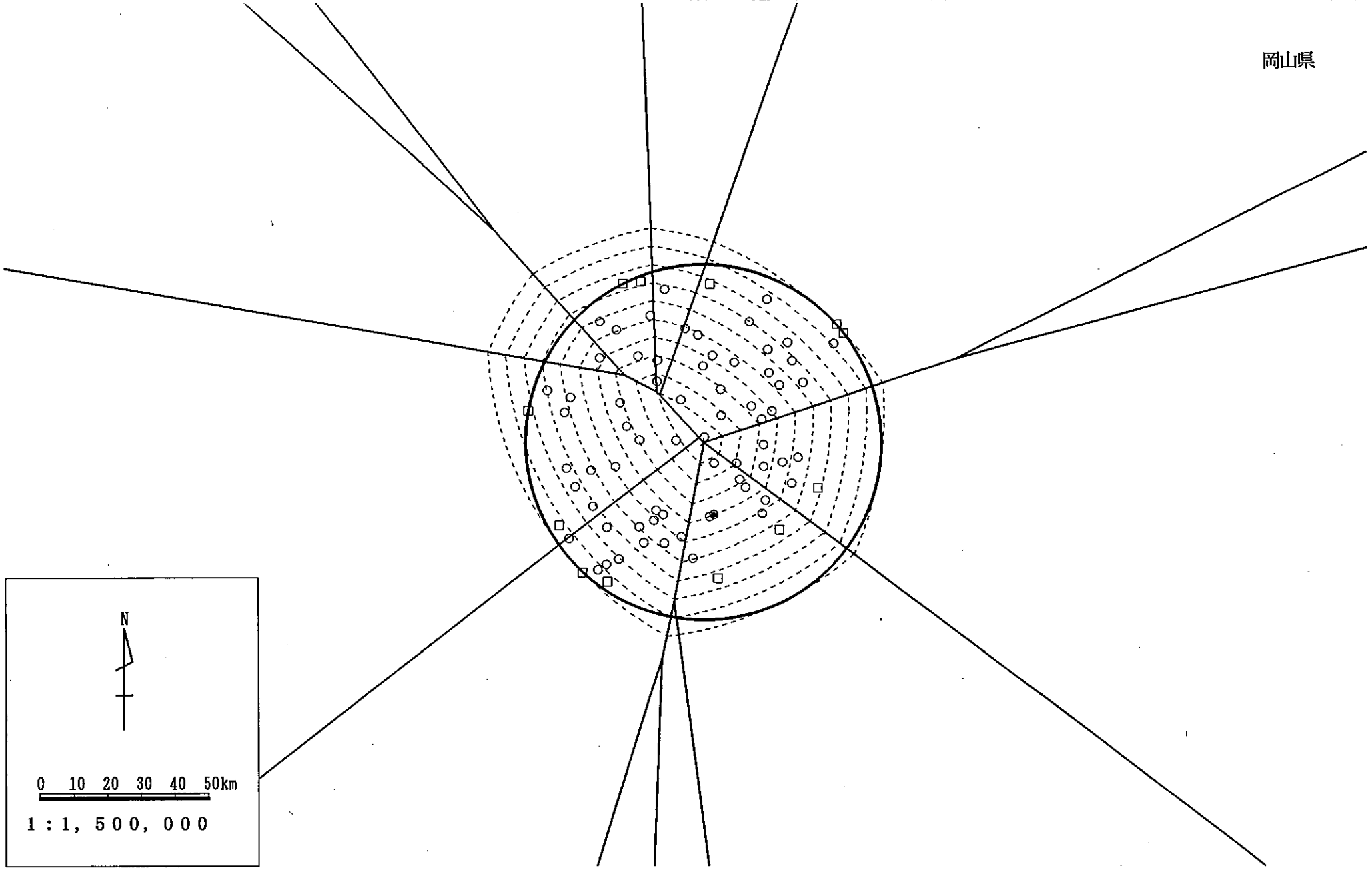

Figure B33. Contour map of the Okayama Prefecture

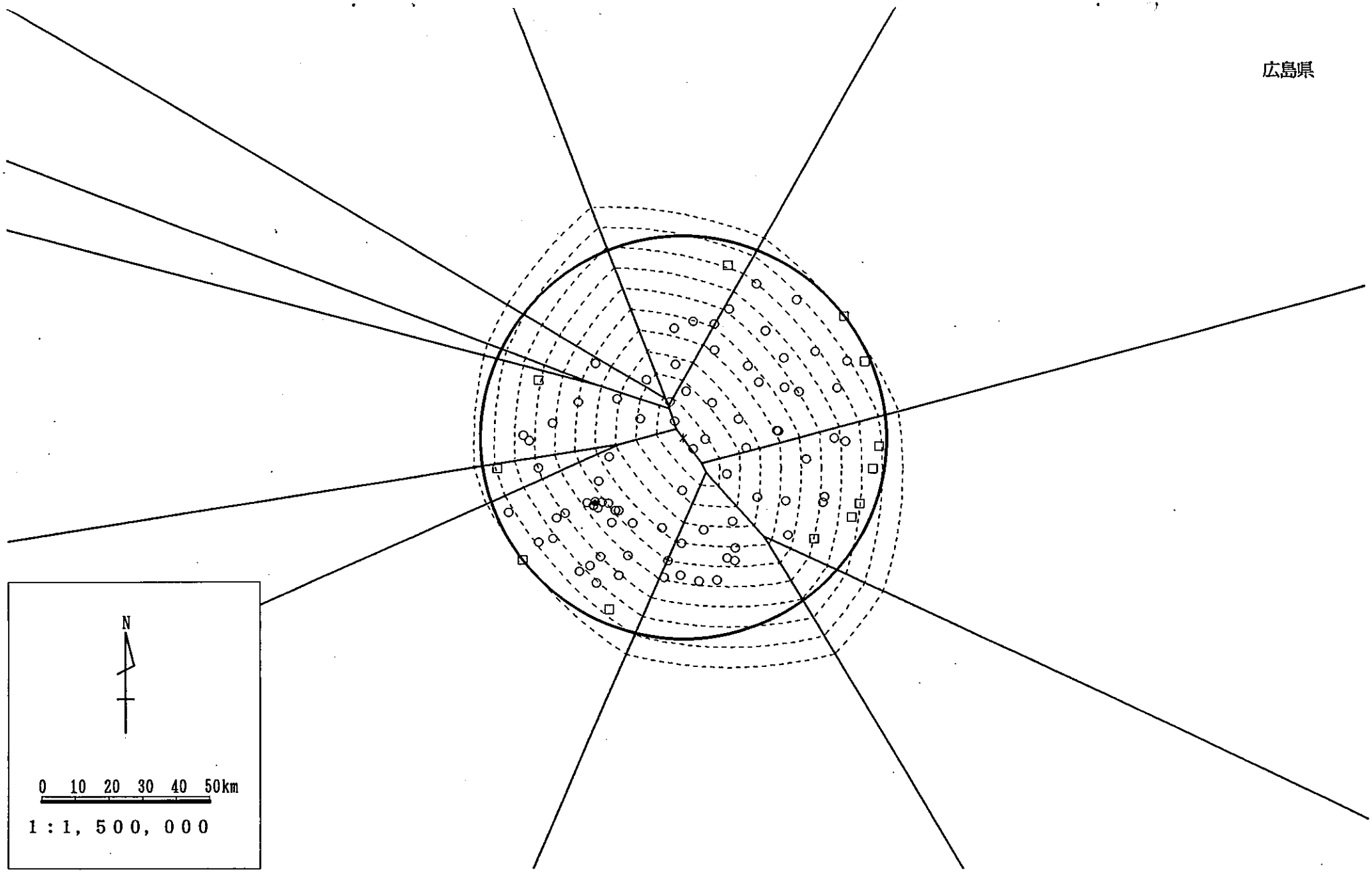

Figure B34. Contour map of the Hiroshima Prefecture

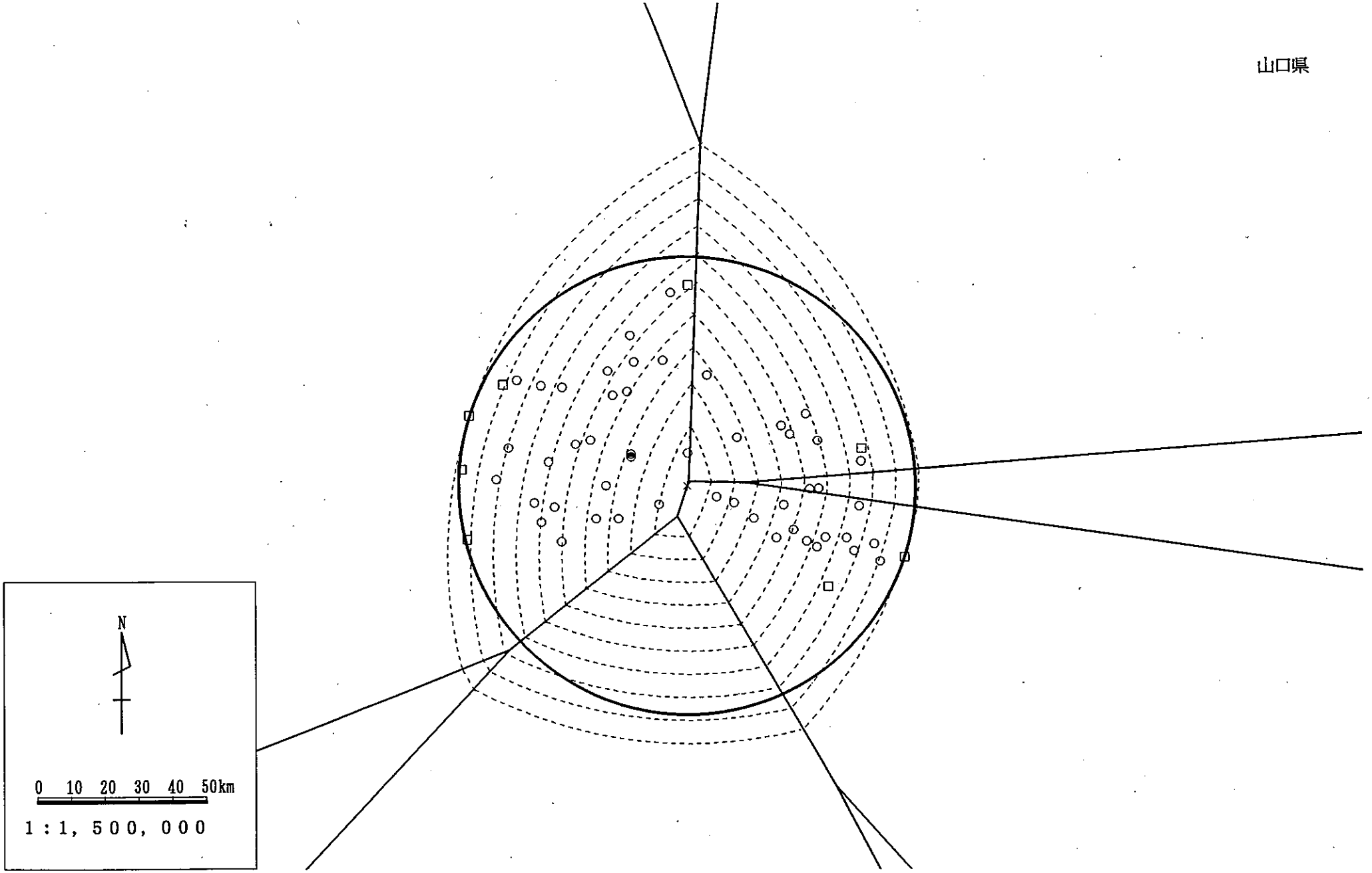

Figure B35. Contour map of the Yamaguchi Prefecture

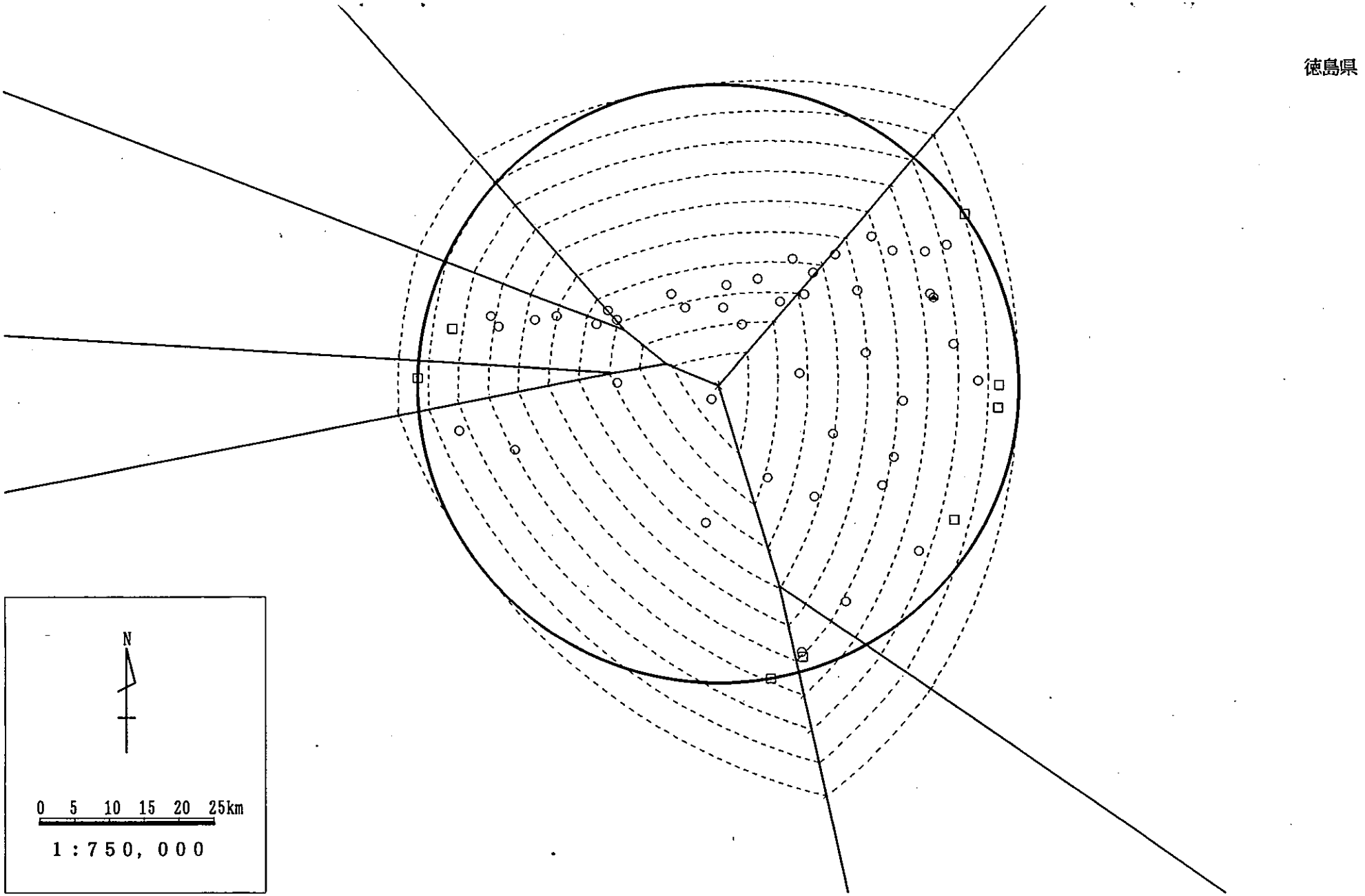

Figure B36. Contour map of the Tokushima Prefecture

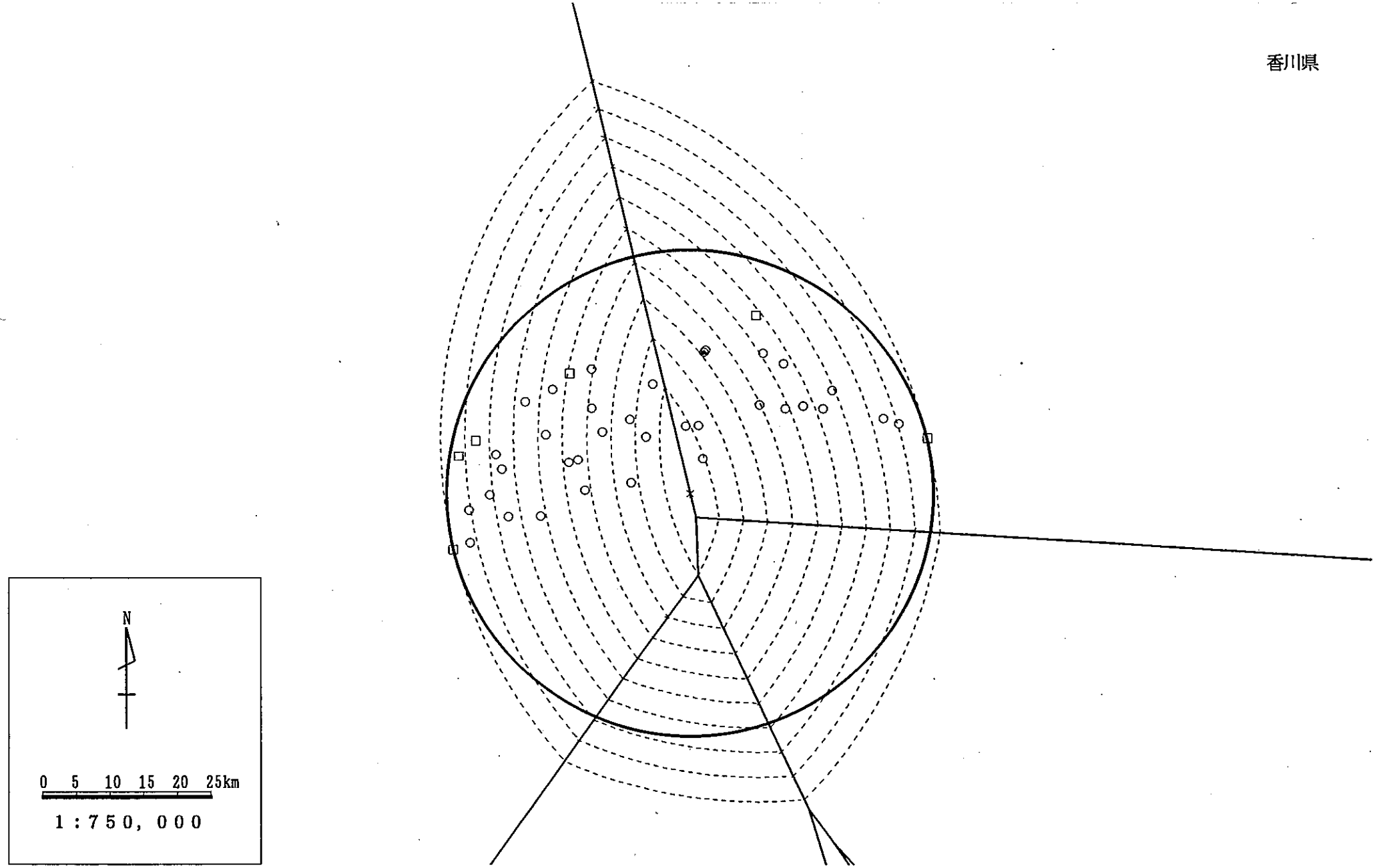

Figure B37. Contour map of the Kagawa Prefecture

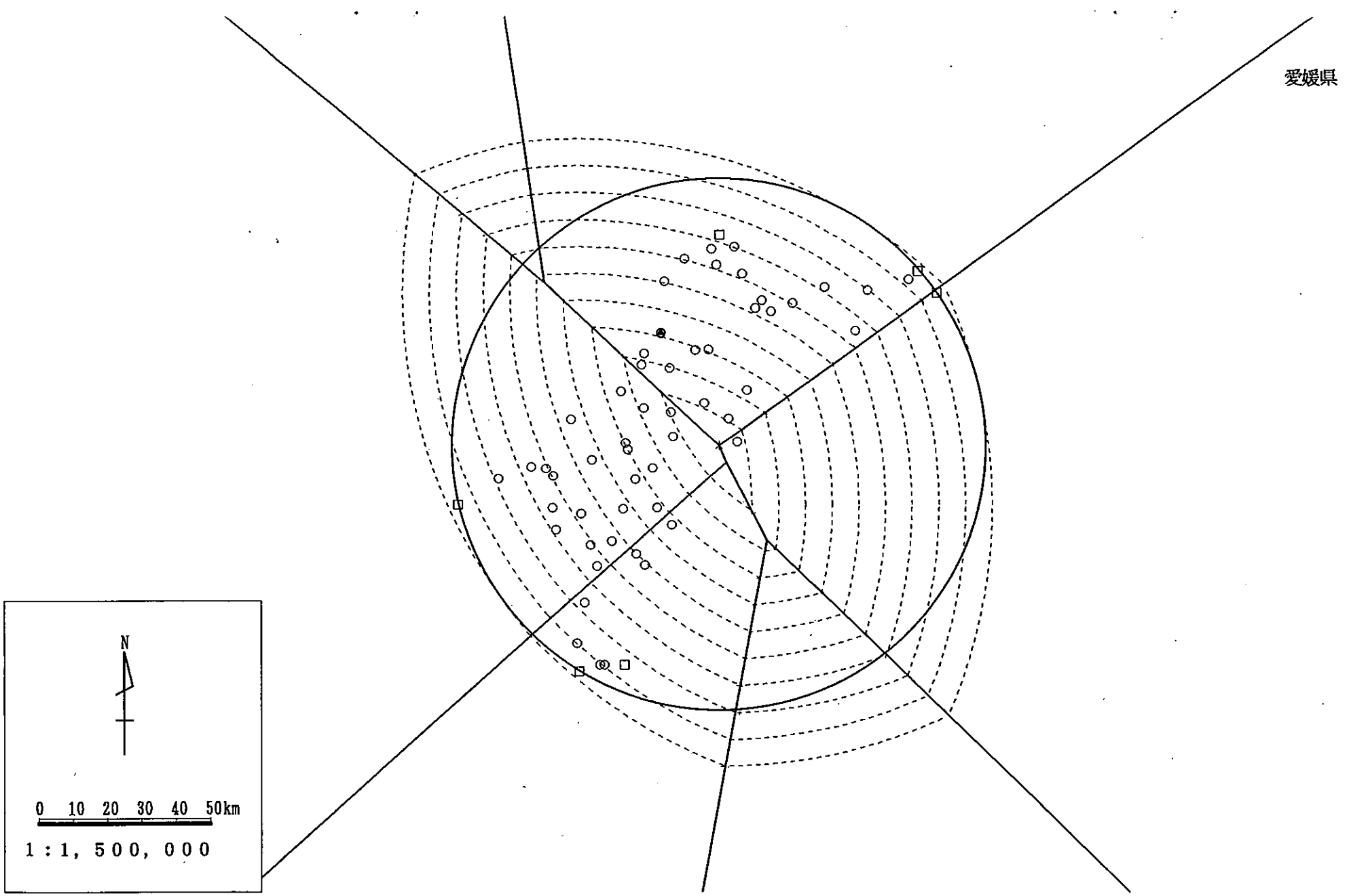

Figure B38. Contour map of the Ehime Prefecture

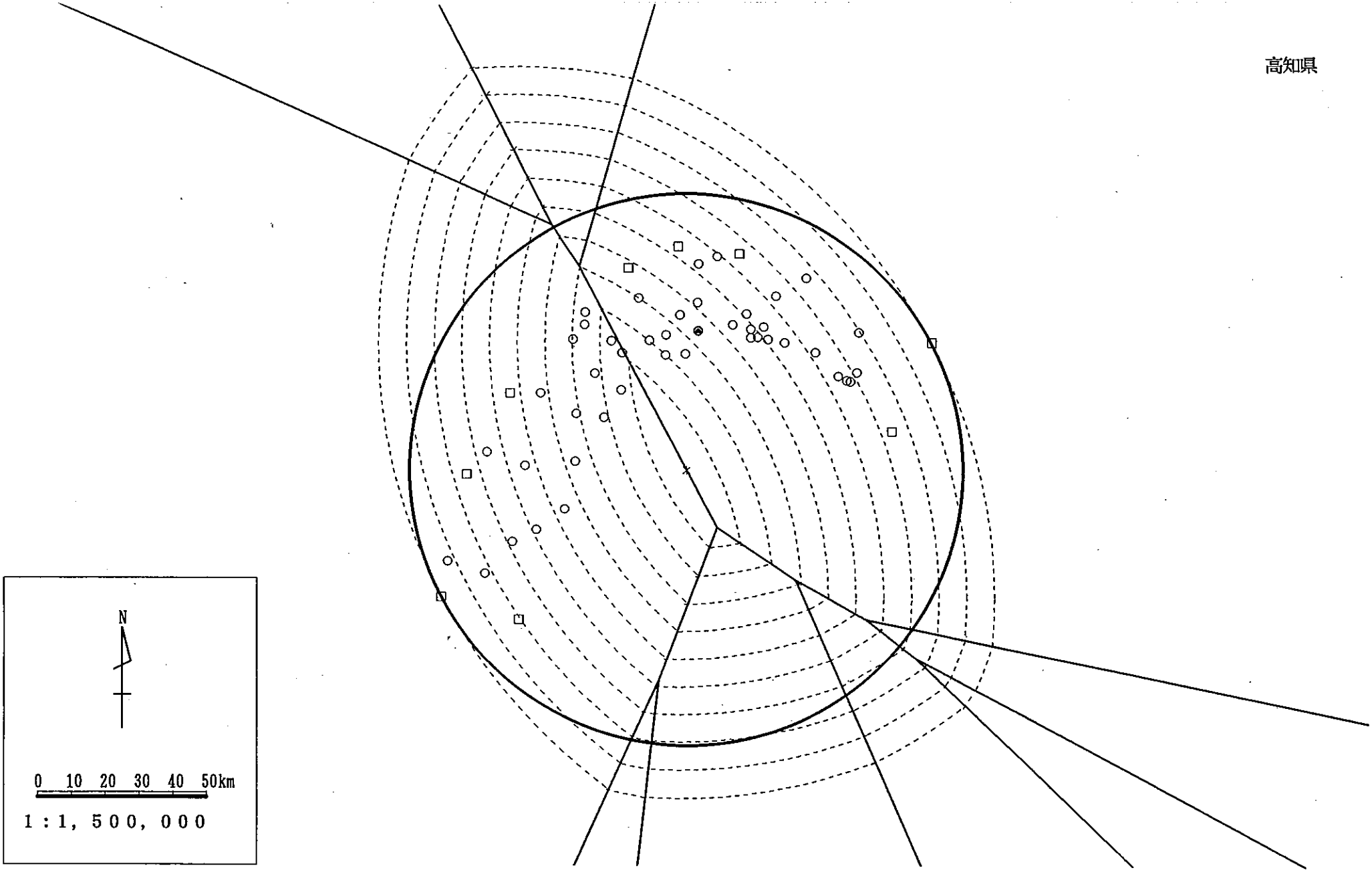

Figure B39. Contour map of the Kouchi Prefecture

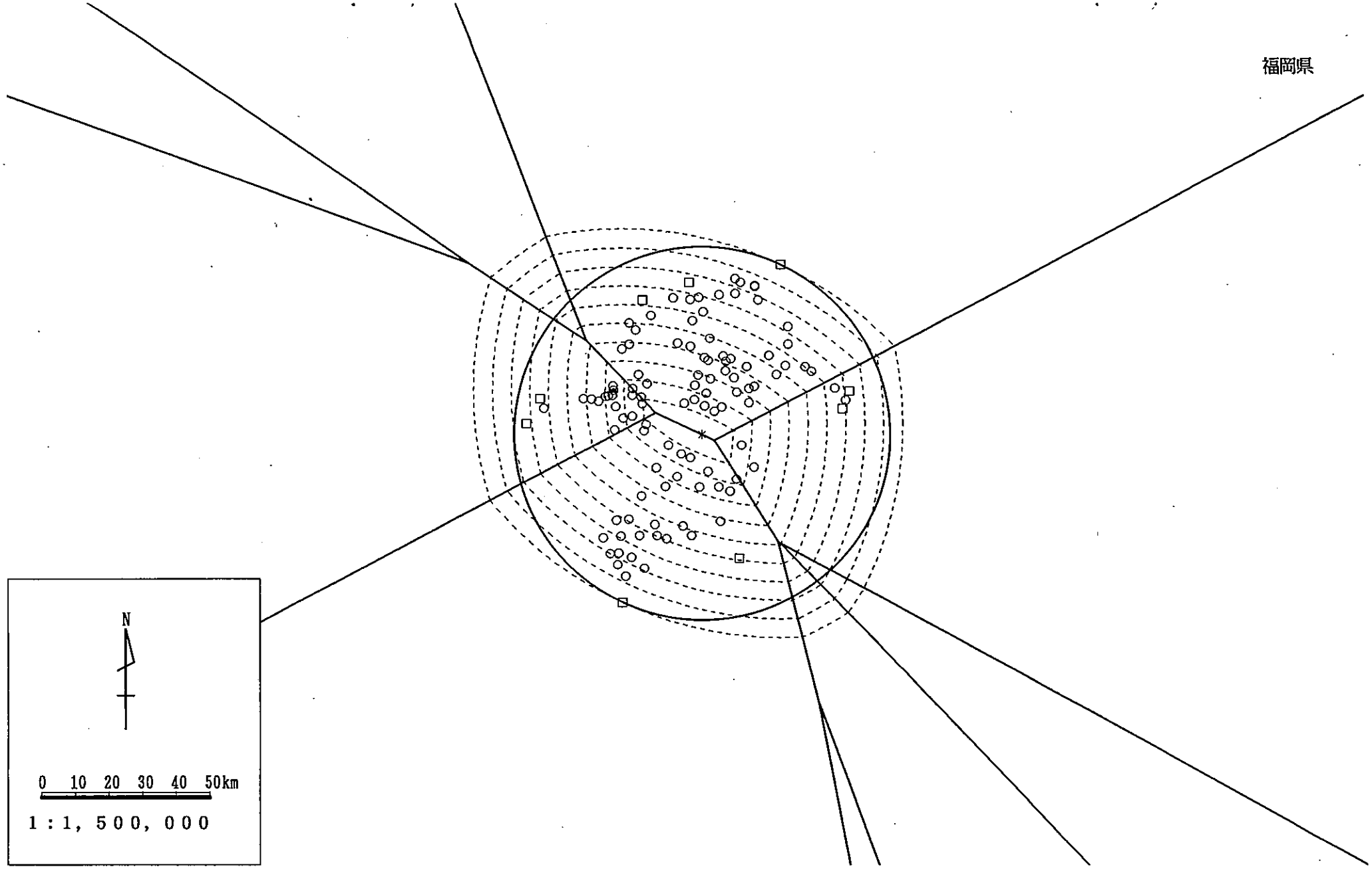

Figure B40. Contour map of the Fukuoka Prefecture

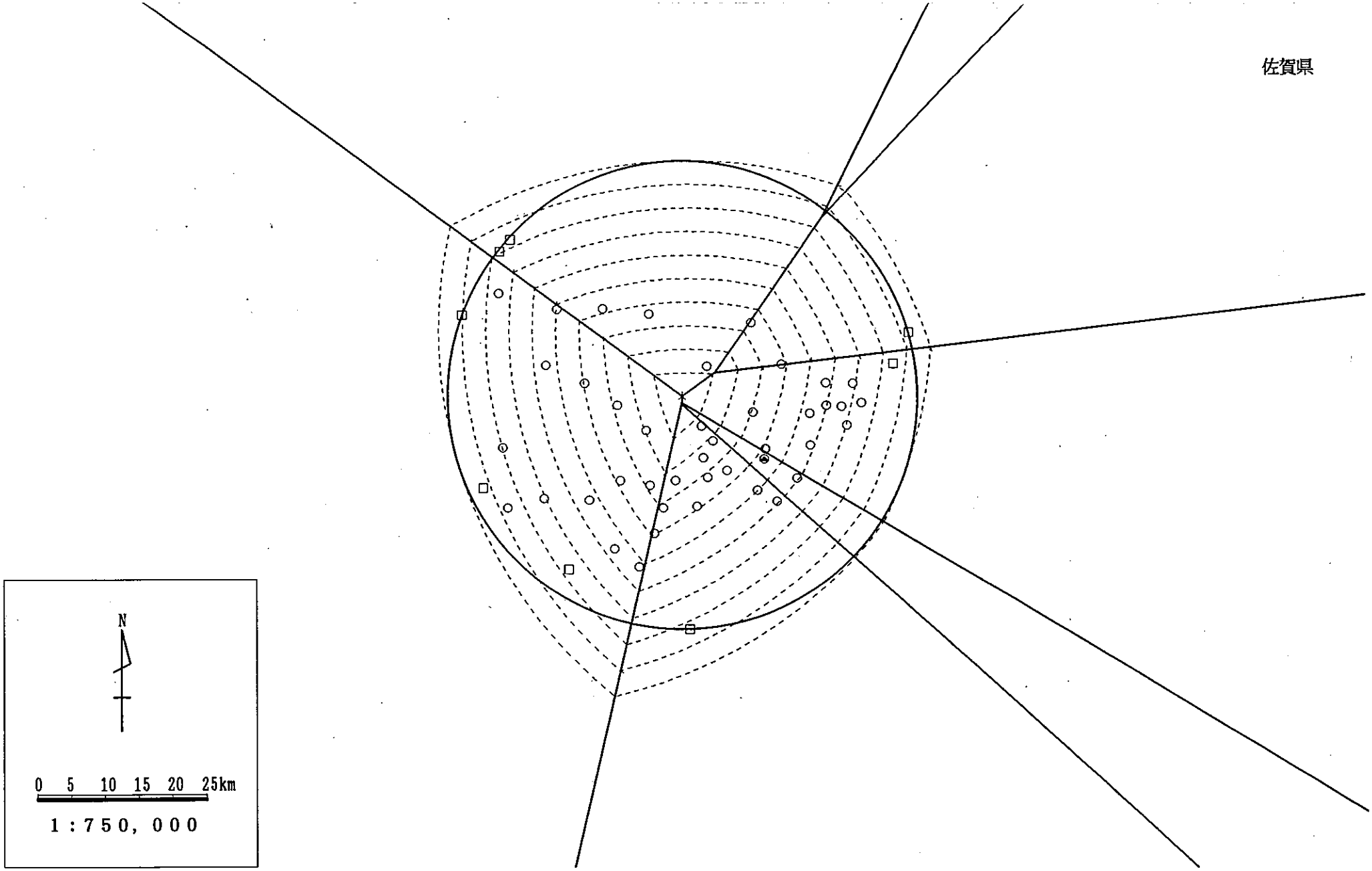

Figure B41. Contour map of the Saga Prefecture

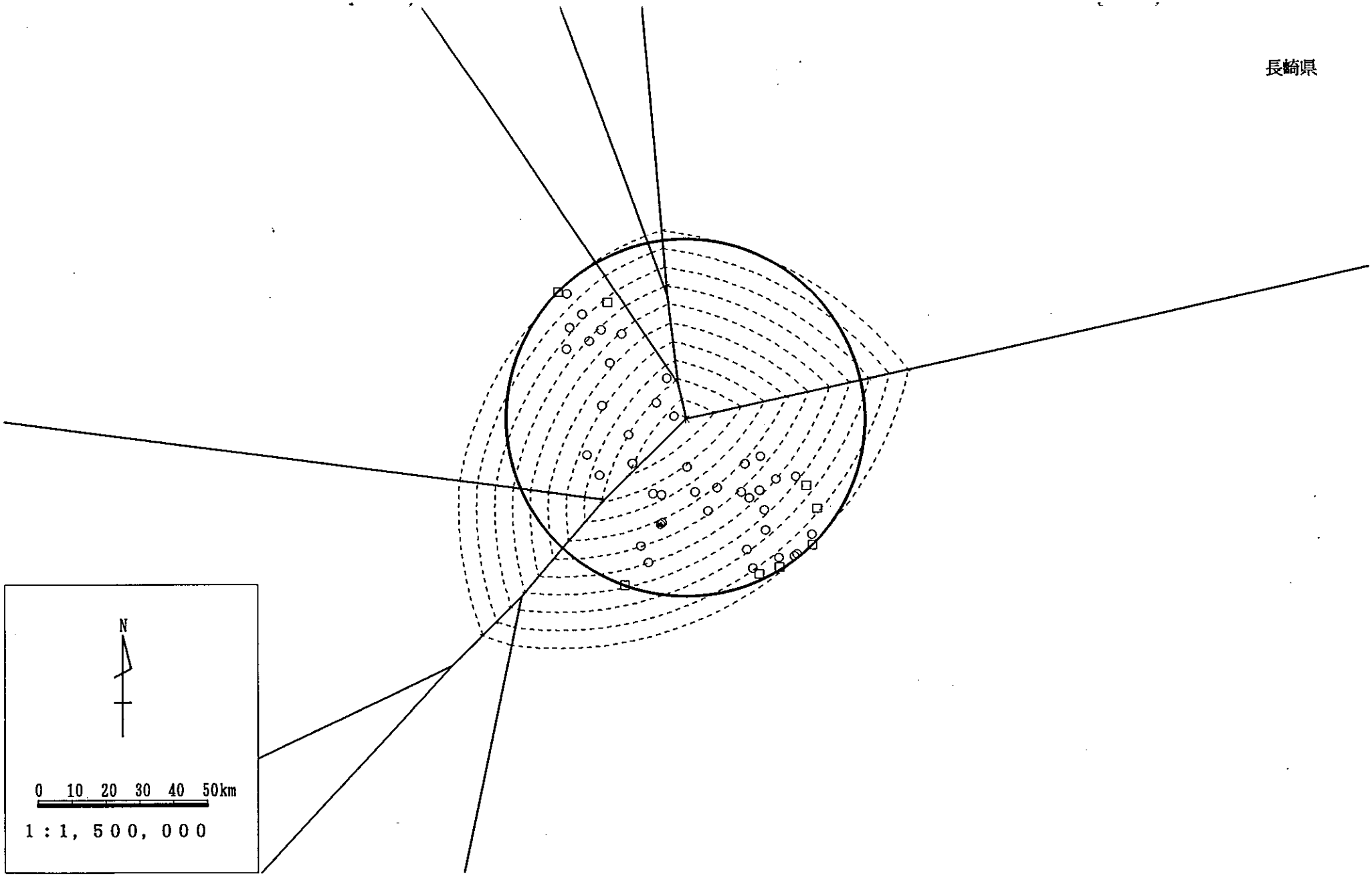

Figure B42. Contour map of the Nagasaki Prefecture

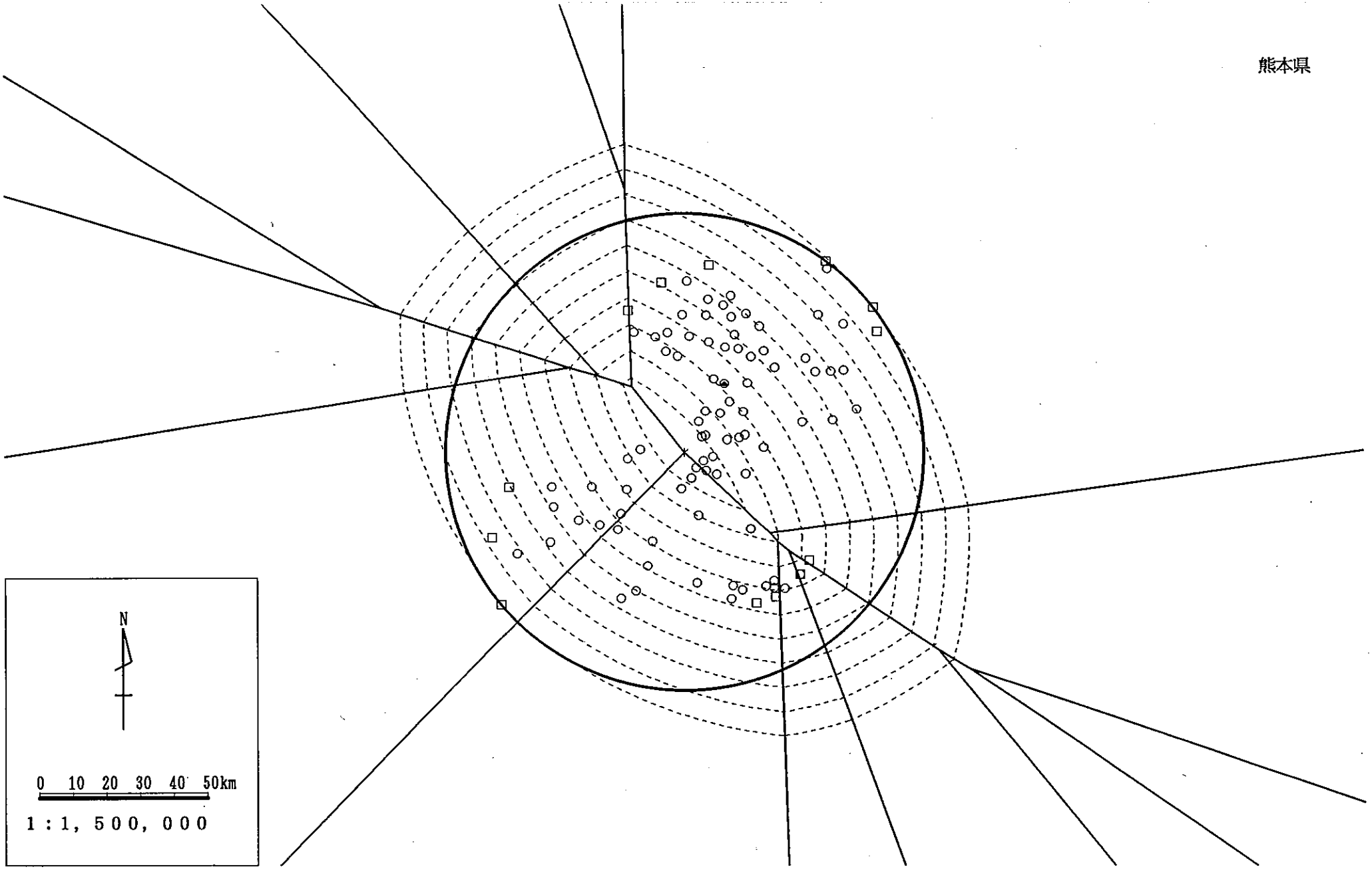

Figure B43. Contour map of the Kumamoto Prefecture

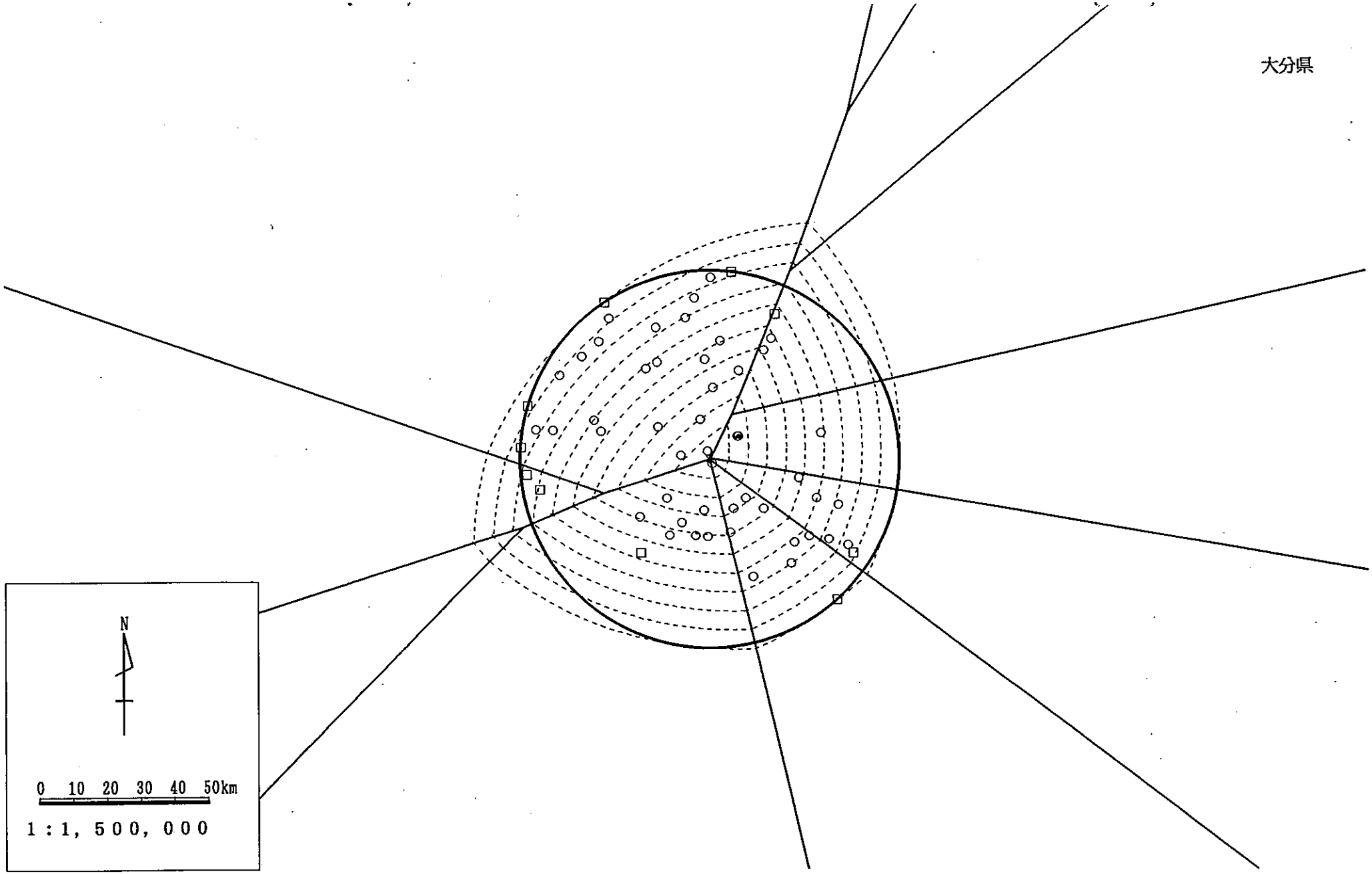

Figure B44. Contour map of the Oita Prefecture

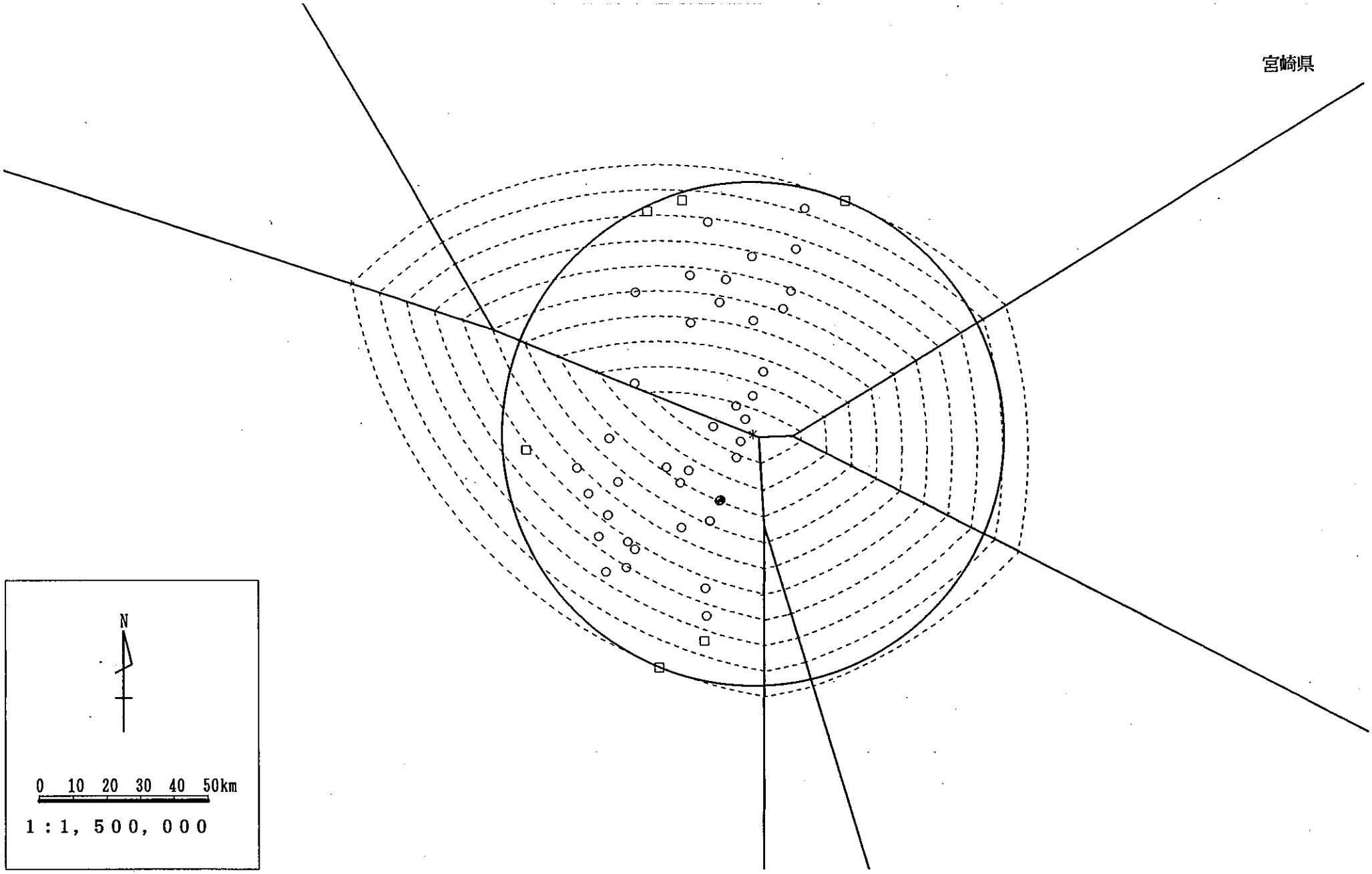

Figure B45. Contour map of the Miyazaki Prefecture

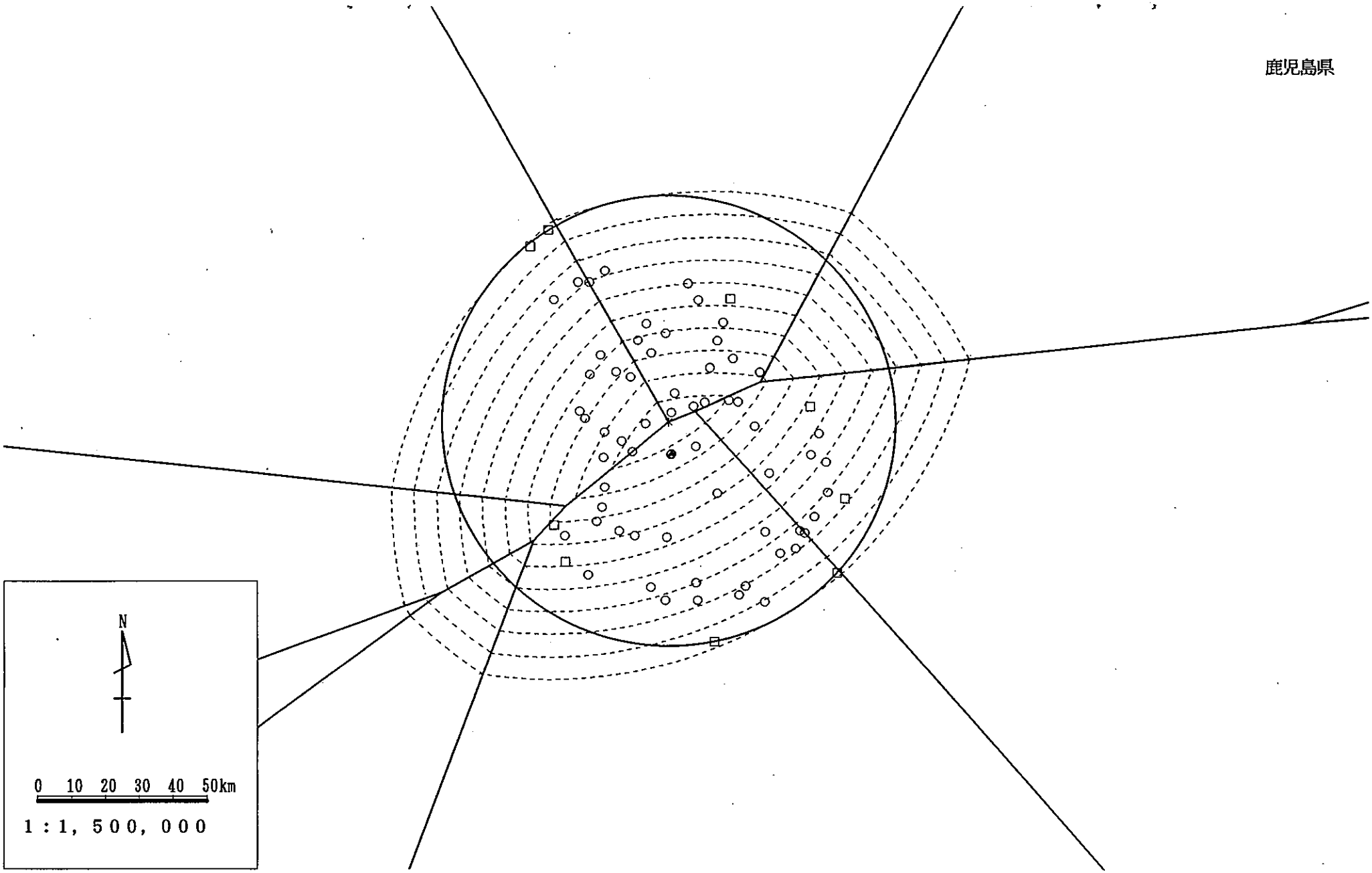

Figure B46. Contour map of the Kagoshima Prefecture

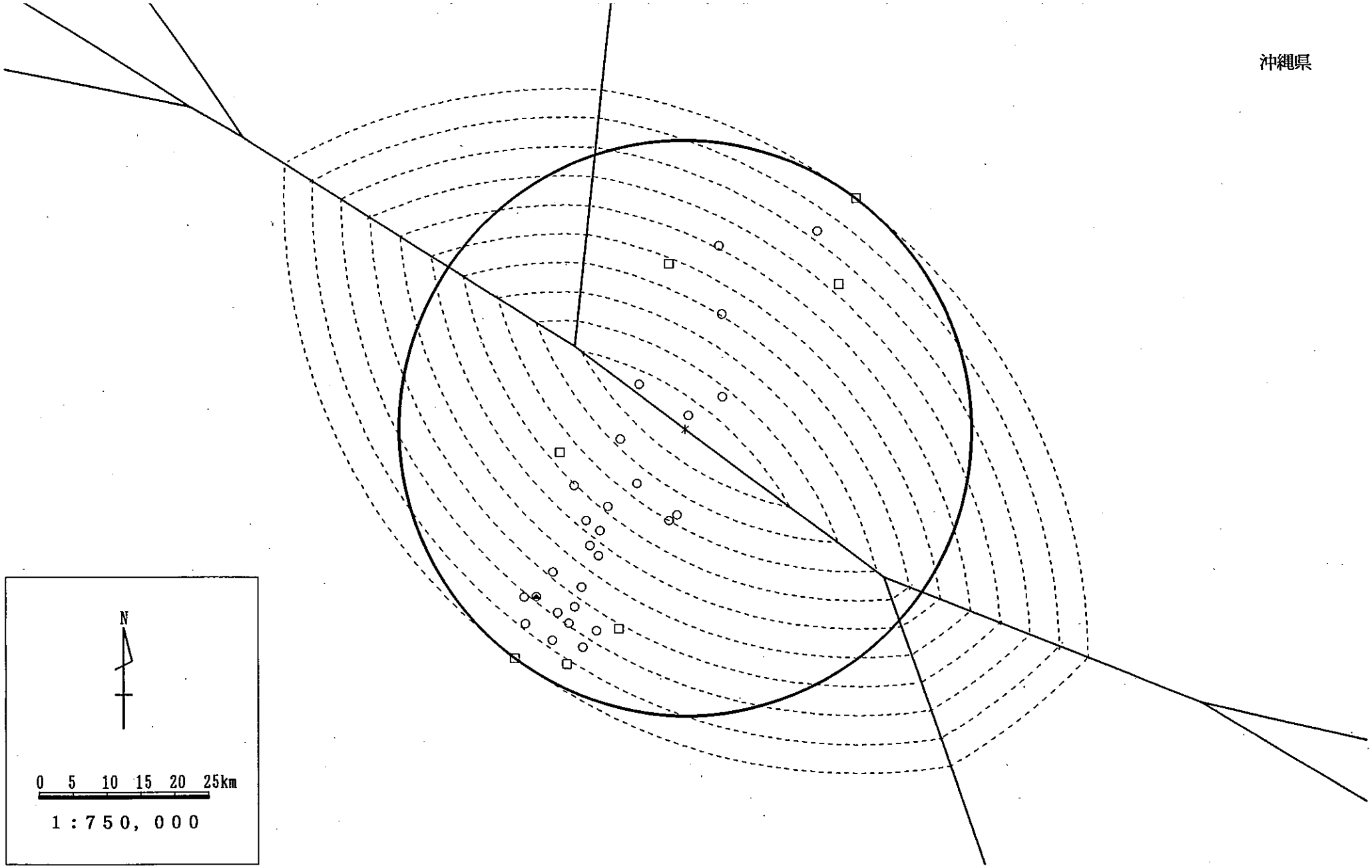

Figure B47. Contour map of the Okinawa Prefecture